Effect of rooibos treatment on inflammatory and oxidative stress genes in *in vitro* and *in vivo* models of NAFLD

By

Thendo Innocent Mabuda

Manuscript presented in fulfilment of the requirements for the degree Master of Science (Medical Physiology) in the Faculty of Medicine and Health Sciences at Stellenbosch University

Supervisor: Dr. K. B. Gabuza

Co-Supervisors: Dr. S. Windvogel
Prof. C.J.F. Muller
Dr. R. Johnson

March 2021

Declaration

By submitting this thesis electronically, I declare that the entirety of the work contained therein is my own, original work, that I am the sole author thereof (save to the extent explicitly otherwise stated), that reproduction and publication thereof by Stellenbosch University will not infringe any third-party rights and that I have not previously in its entirety or in part submitted it for obtaining any qualification.

March 2021

Abstract

Background: Non-alcoholic fatty liver disease (NAFLD) and non-alcoholic steatohepatitis (NASH) have been associated with the rise in metabolic diseases. Inflammation and oxidative stress are key mediators in NAFLD development. Current therapeutics used to treat NAFLD include insulin sensitisers and vitamin E. Afriplex GRT extract was previously showed to decrease inflammation and oxidative stress in cardiac cells. The study aimed to assess if Afriplex GRT extract could protect against hepatic oxidative stress, apoptosis and inflammation in *in vitro* and *in vivo* NAFLD models. **Methods**: Liver steatosis was induced *in vitro* by exposing HepG2/C3A human liver cells to 1 mM oleic acid for 24 h. Anti-steatotic effects of Afriplex GRT [1, 10 and 100 µg/mL] and/or Pioglitazone [30 µM] were determined in mono- and co-treatments for 24 hrs post induction of steatosis. The 3-[4,5-dimethylthiazol-2-yl]-2,5-diphenyl tetrazolium bromide (MTT) assay was performed to determine cell metabolic activity and viability. An Oil red O assay was used to quantify the intracellular lipid content of the treated C3A cells *in vitro*. Liver samples were obtained from a previous study, which used C57BL/6 mice with hepatosteatosis treated with or without Afriplex GRT [74 and 740 mg/kg] and pioglitazone [15 mg/kg] for ten weeks. Both *in vitro* and *in vivo* models were analysed for the expression of genes and proteins associated with the development of NAFLD (AKT, AMPK-α, TNF-α, SOD2, IRS1, PPAR-α, SREBF1, ChREBP and FASN) using qRT-PCR and Western blot analysis. **Results**: Treatment with oleic acid experimentally induced steatosis in C3A cells ($p < 0.01$), as confirmed by Oil red O staining. Afriplex GRT treated cells showed a reduction in fat accumulation in a dose-dependent manner. Furthermore, co-treatment with pioglitazone was shown to be effective ($p < 0.05$). Genes involved in lipid metabolism (*SREBF1*, *ChREBP* and *FASN*) were suppressed by treatment with Afriplex GRT, contributing to reduced lipid content in both models. Afriplex GRT also induced a reduction in the expression of *SOD2* and the inflammatory cytokine (TNF-α). **Conclusion**: Afriplex GRT reduces hepatic steatosis in C3A cells and C57BL/6 mouse liver by modulating *SREBF1*, *ChREBP* and *FASN* gene expression. The extract also affected the expression of oxidative stress and inflammation related genes in both models, through the reduced gene expression of *SOD2* and *TNF-α,* suggesting that Afriplex GRT has potential as a therapeutic for NAFLD.

Opsomming

Agtergrond: Nie-alkoholiese vetterige lewersiekte (NAFLD) en nie-alkoholiese steatohepatitis (NASH) word geassosieer met die toename in metaboliese siektes. Inflammasie en oksidatiewe stres is van die hoof oorsake in die ontwikkeling van NAFLD. Huidige terapieë wat gebruik word vir die behandeling van NAFLD sluit insulien-sensitiseerders en vitamien E in. Voorheen is getoon dat Afriplex GRT inflammasie en oksidatiewe stres in hartselle verminder. Hierdie studie het ten doel gehad om te bepaal of Afriplex GRT ekstrak en pioglitazone, lewerselle kan beskerm teen oksidatiewe stress, apoptose en inflammasie in modelle van NAFLD. **Metodes**: Lewersteatose is in HepG2/C3A menslike lewerselle geïnduseer deur hulle met 1 mM oliesuur vir 24 uur te behandel. Anti-steatotiese effekte van Afriplex GRT [1, 10 en 100 µg/mL] en / of pioglitazone [30 µM] is bepaal 24 uur na steatose-induksie, beide as mono- en kombinasie behandelings. Lewermonsters afkomstig van 'n vorige studie waarin C57BL/6-muise vir tien weke lank behandel is met Afriplex GRT [74 en 740 mg/kg] en pioglitazone [15 mg/kg] is gebruik om die ekspressie van gene en proteïene wat verband hou met die ontwikkeling van NAFLD (AKT, AMPK-α, TNF-α, SOD2, IRS1, PPAR-α, SREBF1, ChREBP en FASN) deur qRT-PCR en Western blot te ondersoek. **Resultate**: *In vitro* veroorsaak oleïensuur steatose in C3A-selle ($p < 0.01$). Afriplex GRT-behandelde selle het 'n konsentrasie-afhanklike afname van vet akkumulasie getoon. Verder is getoon dat die kombinasie van pioglitazone en Afriplex GRT ($p < 0.05$) meer effektief was. Gene wat betrokke is by lipiedmetabolisme (*SREBF1*, *ChREBP* en *FASN*) was deur Afriplex GRT in beide modelle verlaag. Afriplex GRT het ook oksidatiewe stres (*SOD2*) en inflammasie (TNF-α) verminder. **Gevolgtrekking**: Afriplex GRT verminder hepatiese steatose in C3A-selle en in C57BL/6-muise se lewers deur die modulering van *SREBF1*, *ChREBP* en *FASN* geenuitdrukking. Die ekstrak beskerm ook teen oksidatiewe stres en inflammasie deur die geenekspressie van *SOD2* en *TNF-α* te verlaag, wat daarop dui dat Afriplex GRT 'n terapeutiese potensiaal toon om NAFLD te behandel.

Acknowledgements

I would like to begin by acknowledging my family and friends for motivating me through this fruitful period. To my mother Mrs E. M. Singo-Mashila**,** I thank you for the continued support throughout this journey, your guidance through all that I have went through is highly appreciated. Thank you for helping me achieve my dreams.

I would like to thank my supervisor Dr. Kwazikwakhe Gabuza, and co-supervisors, Prof. Christo Muller, Dr. Shantal Windvogel and Dr. Rabia Johnson for giving me the opportunity to showcase my eagerness in advancing within this research field and for always supporting me throughout the duration of my project. Dr. Gabuza, I thank you for always being the voice of reason, and for pushing me to where I am today. Prof. Muller, thank you for putting things into perspective and for supporting my work, I'm honoured to have worked in your laboratory. Dr. Windvogel, I extend the highest appreciation to you for taking me on as your student and for being patient with me. Dr. Johnson, thank you for your guidance, you have an incredible work ethic and I'm truly honoured to have worked with you and your team.

I am grateful to the South African Medical Research Council (SAMRC) "Biomedical Research and Innovation Platform" (BRIP) for their support and training; it was a pleasure to work with this great team of scientists. A special thanks to all senior students at BRIP with a special mention to Dr. Ntamo, Dr. Hlengwa, Ms. Malemela, Ms. Viraragavan, Ms. Sangweni and Ms. Shabalala, who urged me to never quit. I extend my appreciation to all senior staff members at BRIP with a special thanks to Prof. Louw, Dr. Riedel-van Heerden, Dr. Mabasa, Dr. Patel, Mrs. van Aarde, and Mrs. Obonye, who guided me through the operations of the workplace.

I would like to give thanks to the National Research Foundation and the SAMRC for their financial support.

Table of Contents

List of Figures

List of Tables

List of Abbreviations

ACC 1/2	Acetyl-CoA carboxylase 1/2
ADIPOR 1/2	Adiponectin receptor 1/2
ADME	Absorption, distribution, metabolism and excretion
ALT	Alanine aminotransferase
AMPK-α	5' adenosine monophosphate-activated protein kinase-*α*
ANOVA	Analysis of variance
AP-1	Activator protein-1
Apaf-1	Apoptotic protease activating factor 1
APES	Aminopropyltriethoxysilane
AST	Aspartate aminotransferase
ATCC	America Type Culture Collection
ATP	Adenosine triphosphate
AUC	Area under the curve
BAX	Bcl-2 associated X protein
BCA	Bicinchoninic acid
BCL-2	B-cell lymphoma 2
bHLH-Zip	Basic helix-loop-helix-leucine zipper
BSA	Bovine serum albumin
CAT	Catalase
CASP3	Caspase-3
CD95	Cluster of differentiation 95
cDNA	Complementary deoxyribonucleic acid

ChREBP	Carbohydrate-response element-binding protein
CO_2	Carbon dioxide
CoA	Co-enzyme A
CV	Crystal violet
CVD	Cardiovascular disease
CYP450	Cytochromes P450
DISC	Death-inducing signalling complex
DMSO	Dimethyl sulfoxide
DNA	Deoxyribonucleic acid
DNase	Deoxyribonuclease
DPP-4	Dipeptidyl peptidase-4
EMEM	Eagle's essential minimal medium
EtOH	Ethanol
FasL	Fas Ligand
FASN	Fatty acid synthase
FBS	Foetal bovine serum
FFA	Free fatty acids
G6PC	Glucose-6-phosphatase
GLP-1	Glucagon-like peptide 1
GLUT-4	Insulin-dependent glucose transporter 4
GLUT-2	Glucose transporter 2
GPX2	Glutathione peroxidase 2
GRT	Afriplex GRT extract

GST	Glutathione s-transferases
GSTZ1	Glutathione S-transferase Zeta 1
HDL	High-density lipoproteins
HMG-CoA	β-Hydroxy β-methylglutaryl-CoA
HPRT	hypoxanthine-guanine phosphoribosyltransferase
HRP	Horseradish peroxidase
HSL	Hormone-sensitive lipase
IκK	Inhibitor kappa B kinase
IgG	Immunoglobulin G
IL-6	Interleukin 6
IRS1	Insulin receptor substrate 1
JC-1	5,5',6,6'-Tetrachloro-1,1',3,3' tetraethylbenzimidazolylcarbocyanine iodide
JNK	c-Jun N-terminal kinase
LDH	Lactate dehydrogenase
LDL	Low-density lipoprotein
Leprdb	Leptin receptor deficient
LPS	Lipopolysaccharide
MCD	Methionine-choline deficient
MLYCD	Malonyl-CoA Decarboxylase
mRNA	Messenger ribonucleic acid
MTT	3-[4,5-dimethylthiazol-2-yl]-2,5-diphenyl tetrazolium bromide
NADPH	Nicotinamide adenine dinucleotide phosphate

NAFLD	Non-alcoholic fatty liver disease
NASH	Non-alcoholic steatohepatitis
NF-κB	Nuclear factor-kappa beta
OD	Optical density
OGTT	Oral glucose tolerance test
ORO	Oil Red O
PAGE	Polyacrylamide gel electrophoresis
PBS	Phosphate-buffered saline
PCK1	Phosphoenolpyruvate carboxykinase 1
PCR	Polymerase chain reaction
PI	Propidium iodide
Pi3K	Phosphoinositide 3-kinases
PPAG	Z-2-(β-D-glucopyranosyloxy)-3 phenylpropenoic acid
PPAR- γ	Peroxisome proliferator-activated receptor gamma
PS	Phosphatidylserine
PVDF	Polyvinylidene fluoride
qRT-PCR	Quantitative real-time polymerase chain reaction
RIPA	Radioimmunoprecipitation assay
RNA	Ribonucleic acid
RNase	Ribonuclease
ROS	Reactive oxygen species
SDS	Sodium dodecyl sulphate
SGLT2	Sodium-glucose co-transporter-2

SOD2	Superoxidase dismutase 2
SREBP-1c	Sterol regulatory element-binding protein-1c
SREBF1	Sterol regulatory element-binding factor-1
T1DM	Type 1 diabetes mellitus
T2DM	Type 2 diabetes mellitus
TBS	Tris buffered saline
TBST	Tris-Buffered Saline and Tween 20
TNF-α	Tumour necrosis factor alpha
TZD	Thiazolidinedione
VLDL	Very low-density lipoprotein
α	Alpha
β	Beta
γ	Gamma

List of Units of Measurements

%	Percentage
°C	Degrees Celsius
amp	Ampere
cm	Centimetre
cm^2	Squared centimetres
g/L	Grams per litre
h	Hour
Hz	Hertz
kb	Kilobase
kDa	Kilo Dalton
m/s	Meters per second
mg	Milligram
mg/g	Milligrams per gram
mg/kg	Milligram per kilogram
mg/mL	Milligram per millilitre
min	Minute
mL	Millilitre
mL	Millilitres
mm	Millimetre
mM	Millimolar
nm	Nanometre
nM	Nanomolar

pH	Potential of hydrogen
rpm	Revolutions per minute
sec	Second
V	Volts
x *g*	Times gravity
µg	Microgram
µg/mL	Microgram per millilitre
µL	Microliter
µm	Micrometre
µM	Micromolar

Outputs of the study

- Mabuda T.I, Windvogel S., Johnson R., Muller C., Gabuza K. Effect of Rooibos treatment on inflammatory and oxidative stress genes in *in vivo* and *in vitro* models of NAFLD. **Poster presentation**, Biomedical Research and Innovation Platform Annual Research Symposium, South African Medical Research Council, Cape Town, South Africa, October 2019.
- Mabuda T.I, Windvogel S., Johnson R., Muller C., Gabuza K. Effect of green rooibos tea extract (Afriplex GRT) on inflammatory and oxidative stress genes in an *in vitro* and *in vivo* model of NAFLD. **Poster presentation**, Biomedical Research and Innovation Platform Annual Research Symposium, South African Medical Research Council, Cape Town, South Africa, October 2020.
- Mabuda T.I, Windvogel S., Johnson R., Muller C., Gabuza K. Effect of green rooibos tea extract (Afriplex GRT) on inflammatory and oxidative stress genes in an *in vitro* and *in vivo* model of NAFLD. **Virtual oral presentation**, Early Career Scientists Convention, South African Medical Research Council, Cape Town, South Africa, October 2020.

1. Introduction

Non-alcoholic fatty liver or hepatic steatosis refers to the excessive cumulative influx of free fatty acids (FFAs) into hepatocytes [1]. FFAs play a pivotal role in many cellular processes which include cellular membrane synthesis, storage of energy in adipocytes, as well as intracellular signalling pathways. An uncontrolled build-up of FFAs disrupts the efficiency of metabolic pathways and may cause organs such as liver to become resistant to insulin [2]. As hepatocytes become inflated with fatty acids, the surface area of those hepatocytes become bigger, leading to compression of nearby hepatocytes. The compression of hepatocytes may lead to inflammatory response that lead to tissue damage comparable with what is observed with secondary causes of liver fat accumulation such as excessive consumption of alcohol or side effects related to the consumption of modern therapeutics [3, 4].

Only when the fat accumulation of the liver exceeds 5% of the total organ mass, it can be defined as a "fatty liver" [5]. A number of pathophysiological mechanisms trigger hepatic steatosis. These include reduced fatty acid β-oxidation by the mitochondria, endogenous fatty acid synthesis, increased delivery of fatty acids to the liver as well as indigent exporting and integrating lipids within hepatocytes [6]. Furthermore, constant accumulation of FFAs in the liver results in lipoperoxidative stress and hepatic damage [2]. The two pathways involved in the metabolism of FFAs that are processed by the liver to generate energy in the form of ATP or produce triglycerides are known as oxidation and esterification. These pathways are essentially responsible for the genesis of very low-density lipoprotein (VLDL) particles [7].

Hostile and long-term consequences of the metabolism arise from physiologically unregulated overall rate of hepatic FFA uptake, which is linked directly to FFA concentrations in the liver. Along with being one of the largest internal organs in the body, the liver also plays a vital role in metabolising lipids by importing and exporting FFAs. The liver regulates FFAs by synthesizing lipids when there is a shortage and storing lipids when in abundance, however the burden laid upon the hepatic system through the increased flux of FFAs in the system may cause/lead to severe and/or complex complications beyond hepatic steatosis such as non-alcoholic fatty liver disease (NAFLD) [8].

The increase in the number of diabetes and obesity diagnosis contributes to the increase in NAFLD cases to about 1.8 billion of the global population [9]. Effects brought upon by hepatic FFA induced insulin resistance causes inflammation and apoptosis, as the disease progresses

[10]. NAFLD-associated insulin resistance is linked to hyperlipidaemia, due to the restriction of the anti-lipolytic action of insulin [11,12]. The imbalance of adiponectin and tumour necrosis factor α (TNF-α), secreted by the adipose tissues has been linked to the development of insulin resistance-associated NAFLD. This alters the insulin signalling pathway leading to the increased flux of FFAs into the liver [13]. Of concern is the progressive nature of NAFLD to a recurrent liver disorder around the globe as the disease may ultimately progress into non-alcoholic steatohepatitis (NASH), which is an even more severe condition [9]. Hepatic oxidative stress contributes to the "second hit" of NAFLD progression. Microsomal and peroxisomal fatty acid oxidation is a key component in the progression of the disease through oxidative stress. This coupled with mitochondrial dysfunction and lipid peroxidation has been regarded as major contributors of reactive oxygen species (ROS) generation in the liver [14]. Furthermore, without treatment and diet change, these conditions are likely to manifest into progressive chronic hepatic injury, for instance, liver fibrosis (cirrhosis) and at the worst hepatocellular carcinoma [15].

Thiazolidinediones (TZDs) exhibit anti-inflammatory properties in patients with steatohepatitis by the suppression of pro-inflammatory pathways [16]. As such, these are responsible for the reversal of these abnormalities by resolving effects of insulin resistance in adipose tissues, the liver and skeletal muscles. A TZD derivative, known as pioglitazone, functions as a peroxisome proliferator-activated receptor-gamma (PPAR-γ) agonist and insulin sensitizer. Pioglitazone is currently used to treat patients diagnosed with type-2 diabetes mellitus (T2DM). A placebo-controlled trial study has shown that this drug improves the metabolism of glucose and lipids in diabetic patients by counteracting the effects of insulin resistance [17]. Pioglitazone reduces blood sugar and lipid levels in hepatic steatosis, which makes it appropriate to treat T2DM patients as well as those with hepatic steatosis [18]. Unfortunately, pioglitazone is known to contribute to tumours of the bladder and its use has since been withdrawn as a form of treatment in some countries [17,19].

Pioglitazone is a synthetic ligand for peroxisome proliferator-activated receptors (PPARs). These are transcription factors responsible for altering the transcription of genes and therefore influencing the metabolism of lipids and carbohydrates [20]. This, therefore allows a change in the amount of proteins that are synthesised, which then leads to metabolic changes in the presence of the drug [21]. Moreover, pioglitazone improves glycaemic control in patients with diabetes by its action on receptors PPAR-γ-1 and PPAR-γ-2, which enhances the body's sensitivity towards insulin. Other action of pioglitazone is exerted on PPAR-α and this is

associated with improved lipid metabolism. The interaction of ligands such as pioglitazone to respective receptors has shown to cause an increase in the uptake of glucose and its utilisation in surrounding organs, thereby decreasing gluconeogenesis effects in the liver and eventually reducing insulin resistance [21].

Aspalathus linearis, commonly referred to as rooibos, naturally grows in the Western Cape's greater Cederberg region in South Africa. The fynbos biome hosts this flowering shrub in abundance and locals have used this plant as a herbal tea by crushing the plants stems and leaves. This now commercialized herbal tea has been a research subject over the years for its use in traditional regiments [22] and research has identified the crops constituents, as significant quantities of polyphenolic compounds and antioxidants have been identified [23]. Rooibos is of interest to phytochemical research as it hosts numerous antioxidant-associated health benefits such as anti-viral properties as well as anti-mutagenic and anti-inflammatory effects [24]. In addition, rooibos has been previously reported to have hypolipidemic, anti-diabetic and anti-inflammatory activities attributed to bioactive compounds such as; aspalathin (a *C*-linked dihydrochalcone glucoside) and Z-2-(β-D-glucopyranosyloxy)-3-phenylpropenoic acid (PPAG) [25]. Globally, the use of herbal products such as rooibos and traditional medicines as a natural form of health care, is also becoming prevalent in developing countries [26].

Current pharmaceuticals are costly and harbour a number of unpleasant side effects. Although some anti-diabetic drugs are used to treat NAFLD, plant-derived polyphenols are gaining recognition as potential therapies, which harbour less side effects, with their use complementary to current therapies being an option [27]. The potential that rooibos possesses by its action on lipid metabolism, amongst a host of other antioxidant related benefits, may modulate the abnormal hepatic lipid influx and potentially ameliorate hepatic steatosis and NAFLD.

2. Literature Review

2.1 The metabolic syndrome and hepatic steatosis

The metabolic syndrome is described as a cluster of metabolic derangements that, ultimately increase the risk of heart disease, T2DM, stroke and liver dysfunction [28,29]. These metabolic derangements include hyperglycaemia, dyslipidaemia, inflammation, obesity and increased blood pressure [28]. The metabolic syndrome is linked to obesity and insulin resistance, which increase liver dysfunction through the increased flux of lipids in the body [29]. Fatty liver or hepatic steatosis is identified as the most common type of liver disease, caused by the abnormal retention of FFAs in hepatocytes, leading to moderate to severe hepatocellular injury [30]. The occurrence of this disorder has revealed that metabolic syndrome, more specifically, insulin resistance associated with T2DM and obesity are the major causes of the NAFLD [31]. Physiological changes observed in patients with NAFLD have been reported to be the result of insulin resistance and obesity [32]. Obese patients challenged with insulin resistance are therefore faced with the inability to process increased blood glucose and triglyceride levels [33]. This further deteriorates the hepatic system, contributing to the pathogenesis of simple steatosis to NAFLD, as increased adipose tissue lipolysis causes the release of FFAs into circulation [34].

2.1.1 *The effect of dyslipidaemia in NAFLD development*

Patients plagued with NAFLD often have other features of the metabolic syndrome, in this case, dyslipidaemia, insulin resistance, diabetes and obesity are highlighted as risk factors associated with NAFLD [3135]. Dyslipidaemia in NAFLD is characterised by the increase in serum triglycerides and increased low-density lipoprotein (LDL) coupled with the decreased levels of high-density lipoproteins (HDL) [36].

The pathogenesis of dyslipidaemia in NAFLD has not yet been fully elucidated, although the imbalance in cholesterol concentrations has shown to increase the likelihood of the development of cardiovascular disease and steatohepatitis [37]. NAFLD is also characterised by atherogenic dyslipidaemia, postprandial lipidemic and HDL-dysfunction [38]. It was reported that, although HDL exerts beneficial pleiotropic properties, in the presence of dysglycaemia, oxidative stress and/or inflammation, HDL particles may be transformed into dysfunctional molecules exerting pro-atherogenic effects [39].

A study consisting of sixteen patients with NAFLD and twenty four control subjects demonstrated that patients with fatty liver disease have significant abnormal imbalance of body cholesterols, that results in atherogenic traits, mainly caused by the hepatic overproduction of very low-density lipoprotein (VLDL) particles into the circulation [40]. Dietary cholesterol intake constantly exposes the liver to free cholesterols. Therefore, the liver contributes directly to cholesterol homeostasis. The dysregulation of cholesterol homeostasis has been previously reported in patients with NAFLD [41,42]. Hepatocytes mainly acquire cholesterol through mitochondrial and/or cytoplasmic oxidation reactions, where acetyl-CoA and acetoacetyl-CoA are converted to 3-hydroxy- 3-methylglutaryl-CoA (HMG-CoA) by HMG-CoA synthase, contributing to cholesterol biosynthesis [43].

2.1.2 *Insulin resistance-associated NAFLD and diabetes mellitus*

Insulin resistance occurs when the body is unable to respond to insulin, which is secreted by the pancreas in response to increased blood glucose levels. Previous studies have highlighted how NAFLD is associated with the increase in insulin resistance when compared to controls, as the findings showed how insulin resistance increases with an increased degree of steatosis [44,45]. Insulin resistance-associated NAFLD has also been associated with hyperlipidaemia, as the body's inability to effectively utilise insulin restricts the hormones' anti-lipolytic action [11,12]. Due to insulin resistance, the liver reportedly experiences an increase in glycolysis, subsequently decreasing apolipoprotein B-100 which inhibits the exportation of VLDL particles [7]. The development of insulin resistance-associated NAFLD has been linked to the imbalance of adiponectin and tumour necrosis factor α (TNF-α) cytokines secreted by the adipose tissues. Through the inhibition of insulin-stimulated glucose uptake and glycogen synthesis in the liver, an alteration in the insulin signalling pathway to fatty acid stimulated insulin signalling as a compensation is observed, which favours increased flux of free fatty acids (FFAs) thus owing to insulin resistance [13].

Patients that suffer from NAFLD without any risk factors associated with the metabolic syndrome, account for 16% of the NAFLD prevalence [35,46,47]. On the contrary, the prevalence is higher in high-risk patients such as obese patients (91%), individuals with hyperlipidaemia accounting for 90% and diabetics accounting for 60% [7]. Diabetes mellitus is a major risk factor in the obesity endemic, with obese diabetics facing the risk of developing microvascular and macrovascular complications, that may eventually contribute to hepatic insulin resistance [12].

There are two known types of diabetes mellitus, type 1 diabetes mellitus (T1DM) and T2DM. T1DM patients are unable to produce insulin, whereas T2DM patients are affected by body's inability to respond to increased levels of blood glucose, either by producing insufficient insulin or the action of insulin is impeded [48]. It is reported that approximately 10% of all diabetes cases are T1DM, and the remaining 90% of the cases are classified as T2DM [48]. NAFLD development and progression may be associated with insulin resistance and diseases such as diabetes and obesity, but not all NAFLD patients are diabetic or obese. In fact, there is evidence in literature that indicates that NAFLD occurs in non-diabetic patients, therefore there may be other factors contributing to NAFLD development suggesting that insulin resistance may not be the determining factor of NAFLD severity [49].

2.1.3 *The role of obesity in hepatic steatosis*

The imbalance in energy intake and energy expenditure results in a pathological white adipose tissue remodelling, characterized by adipocyte hypertrophy, chronic inflammation, and fibrosis leading to obesity. Obesity is mainly caused by a high caloric diet, as studies have shown that a lack of exercise coupled with a poor diet leads to excessive weight gain [50]. In some cases, a genetic mutation may be the cause of a poor metabolism, owing to the cause. FFAs are absorbed into specialised connective tissues known as white adipose tissues, a mechanism which allows the body to transport excess FFAs away from vital organs such as the liver [51]. In an obese state, this mechanism is altered therefore leading to an abnormal retention of FFAs in vital organs and their peripheral tissues.

Implications that lead to the development of hepatic steatosis stem from the abnormal accumulation of FFAs in circulation. In obese patients, metabolic disturbances such as reduced insulin sensitivity and increased glycogen storage favour the development of NAFLD [52]. The conversion of glucose to glycogen as a storage mechanism is used by the liver to compensate for increased or decreased blood glucose levels. Glucose is also converted to FFAs by the liver and the adipose tissues for long/short-term storage [51–53]. In the liver, excessive storage of FFAs causes hypertrophy of the hepatocyte and ultimately steatosis.

Steatosis of the liver may be instigated by a number of other pathophysiological mechanisms that include reduced β-oxidation by the mitochondria due to mitochondrial dysfunction, an enhanced flux of dietary FFAs into hepatocytes, as well as the poor exportation of FFAs from hepatocytes and *de novo* lipogenesis [54]. This hepatic manifestation is concerning as the global burden has spiked due to the constant rise in metabolic related diseases. An assessment was

published as early as 2018, where they reported the estimated global prevalence of NAFLD to a 25% incidence in the global population [55]. Their findings highlighted a few regional differences, with the most cases reported in the South American continent as well as countries in the Middle East and the least cases reported in Africa [55,56]. This has therefore made NAFLD the most common chronic liver disease worldwide, predicted to become the main cause of cirrhosis and denoting this disease as the hepatic manifestation of the metabolic syndrome [57].

2.2 Pathogenesis of non-alcoholic fatty liver disease

NAFLD is induced by simple steatosis and is regarded as the manifestation of physiological processes that cause a build-up of lipids in the hepatic tissue, which is not related to excessive alcohol consumption. Its pathogenesis is a result of numerous factors, which are highlighted by an interplay of metabolic pathways involved in *de novo* lipogenesis, gluconeogenesis, β-oxidation, the secretion of cytokines and poor sensitivity by a host of receptors. The exact mechanism by which NAFLD develops or progresses still remains a topic in research, with no definitive mechanism elucidated [58]. NAFLD underlies more severe conditions such as NASH [59], and without effective intervention it may progress into irreversible hepatic injury such as liver fibrosis (cirrhosis) and potentially hepatocellular carcinoma (Fig. 2.1) [15].

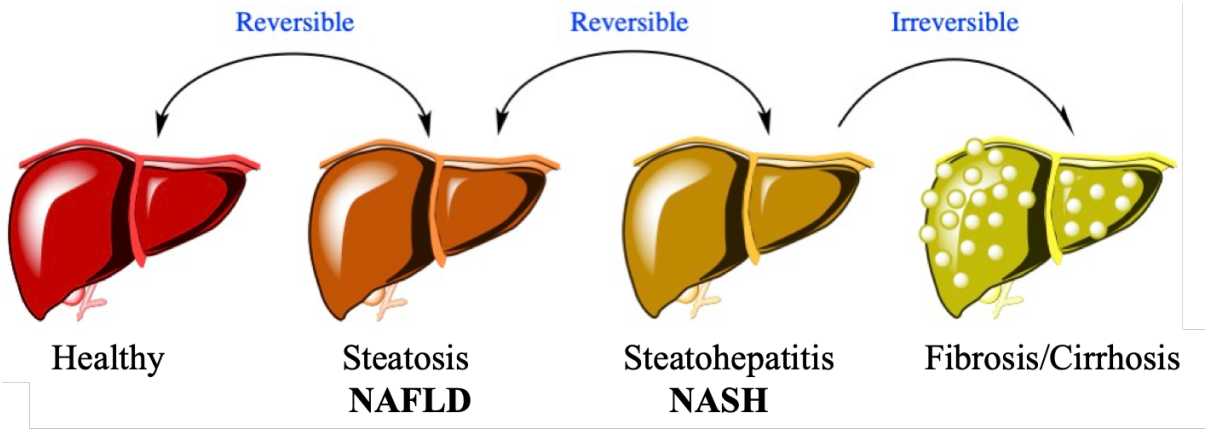

Figure 2.1 Progression of hepatic steatosis (adapted from, Chalasani *et al*. [10]).

2.2.1 *Steatohepatitis*

Seventy five to a hundred million American individuals were reportedly affected by NAFLD in 2017, making up to an estimated 40% of the adult population in the United States, with 12% accounting for individuals living with NASH [56]. Limited data on the prevalence of NAFLD is available in Africa. In 2019 Paruk *et al*., reported that amongst patients with T2DM the prevalence of NAFLD by non-invasive ultrasound, was 10% to 69% in Nigeria, 50% in Sudan and 73% in Ethiopia [60]. In South Africa a study conducted on obese patients in the Western Cape, reported a prevalence of NAFLD (48%) [61]. NASH is described as condition more severe than hepatic steatosis, where studies show an intense build-up of FFAs in the liver, leading to the hypertrophy and inflammation of hepatocytes [15]. The main cause of NASH, like in NAFLD, is not related to the excessive consumption of alcohol. In fact evidence has substantiated the severity of the condition with increased absorption of FFAs into hepatocytes, substantial inflammation of the hepatic tissue with increased scarring, contributing to the reduction of liver functionality [15].

According to the "two-hit" theory of NAFLD pathogenesis, increased FFAs into the portal system along with increased lipogenesis and decreased β-oxidation are the initial steps to hepatic steatosis induction [62]. The "second hit" occurs as a result of increased cytokines, endotoxins as well as reactive oxygen species (ROS), contributing to the progression of NAFLD to NASH [63]. Most patients take years to develop NASH from hepatic steatosis. Evidence therefore, demonstrates that NAFLD is indeed a multisystem disease, affecting extra-hepatic organs through the regulation of metabolic pathways involved in hepatocellular homeostasis [64].

2.2.2 *Liver fibrosis*

Liver fibrosis is the end-stage of a spectrum of chronic liver conditions, sharing features of necroinflammation and altered regenerative nodules, all of which reduce the normal structure of the liver to reduced functional mass and the degradation in vascular architecture [65]. Currently, the most common aetiologies for liver fibrosis are, alcoholic-related liver disease (ALRD) and NAFLD, steatohepatitis as well as chronic hepatitis-B and hepatitis-C [66].

In a group of individuals with NASH, forty-fifty percent of these individuals will reportedly develop hepatic fibrosis [64]. An increased risk in liver related deaths were reported to be 5-10 fold depending on the severity of the condition in a meta-analysis of 40 studies, owing to the

rate at which each patient develops fibrosis [64]. In 2009, patients with steatohepatitis accounted for 10% of the average patients listed for liver transplantation in developed countries [67].

Substantial evidence has shown that liver fibrosis and cirrhosis are the common causes of the development of hepatic carcinoma. Individuals with NAFLD-induced liver fibrosis have increased chances of developing hepatic carcinoma compared to patients with other aetiologies of liver fibrosis [68]. NAFLD is fast becoming one of the leading causes of cirrhosis and hepatic carcinoma, whilst the prognosis of NAFLD-related cirrhosis is poor, the treatment of NAFLD should be highly emphasised well before the condition progresses to hepatic carcinoma. NAFLD pathogenesis elaborates on how severe and complex the disease may develop when left untreated.

2.3 Effect of metabolic perturbations on NAFLD pathogenesis

Fatigue is the most commonly experienced symptom in patients living with liver disease, partly due to the nature of the liver condition but more specifically as a result of changes in neurotransmission in the brain [69,70]. NAFLD usually shows no symptoms however, fatigue and abdominal pain may be experienced by patients suffering from the disease. Patients with diabetes experience high blood glucose levels and in order to process this excess energy the body stores it in the liver as glycogen and as FFAs in adipose tissues [69,70]. For the body to utilise this energy, the cell must first convert it to ATP (adenosine triphosphate) by converting pyruvate through the Krebs cycle to acetyl-CoA [69]. A series of processes in the Krebs cycle leads to the production of palmitic acid, where acetyl-CoA is carboxylated to malonyl-CoA facilitated by acetyl-CoA carboxylase 1 (ACC1) catalysis, resulting in palmitic acid production through the enzyme fatty acid synthase (FASN) [71]. The elongation and desaturation of the palmitic acid molecule leads to the synthesis of stearic acid, and further desaturation of the stearic acid molecule results in the production of oleic acid [69,71]. Therefore, during hepatic steatosis there is an unparalleled surplus of FFA molecules, mainly the product of *de novo* fatty acid synthesis of oleic acid. Although there is a definitive pathway, which describes the synthesis of FFA molecules, the rate of this mechanism has been reported to be amplified by lack of hepatic insulin sensitivity, adding to the increased flux of intrahepatocellular lipid accumulation [71,72].

2.3.1 The role of lipogenesis in NAFLD

Lipotoxicity is a major risk factor for patients with NAFLD due to ectopic lipid accumulation [73]. Mechanisms that are responsible for cellular homeostasis include the elimination of the overflow of lipids to prevent further liver functional complications. Dietary factors and *de novo* fatty acid synthesis are highly associated with the influx of FFAs into the circulation and the overall increased plasma fatty acid levels [72]. This, along with the metabolic syndrome, contributes to the progression or worsening of the disease as the mechanisms involved in lipid degradation are ineffective in controlling the pathogenesis of NAFLD.

Organelles involved in regulating the lipid overflow include the mitochondria and functional peroxisomes, which have a central role in lipid degradation, counteractively managing the abnormal accumulation of FFAs in hepatocytes during metabolic stress [74]. Peroxisomes are specialised organelles involved in fatty acid oxidation, as substrate specificity of very long-chain fatty acids and branched-chain fatty acids are directed to β-oxidation and alpha-oxidation, respectively [75].

Increased insulin and blood glucose in circulation triggers *de novo* lipogenesis, leading to the abnormal retention of FFAs in hepatocytes. Sterol regulatory element-binding transcription factor-1 (*SREBF1*), has been reported to have a role in the development of hepatic steatosis [76]. *SREBF1* encodes for sterol regulatory element-binding protein-1c (SREBP-1c) in humans and is an isomer in a family of transcription factors which include, carbohydrate-response element-binding protein (ChREBP) and PPAR-γ [76]. SREBP-1c is a membrane-bound transcription factor responsible for lipogenesis, and as a result the increased triglyceride levels during steatosis is due to the modulation of genes involved in the triglycerides synthesis [77].

Acetyl-CoA carboxylase 2 (ACC2) activation, an isomer of acetyl-CoA carboxylase (ACC), is regarded as a mode where SREBP-1c initiates FFA production [78]. ACC is responsible for malonyl CoA production in the mitochondrial membrane, thereby contributing to the increase in malonyl CoA levels and leading to β-oxidation reduction [79]. β-oxidation is strongly dependent on carnitine palmitoyl transferase-1, which is responsible for translocating FFAs into the mitochondria, therefore, carnitine palmitoyl transferase-1 inhibition prevents this action and lipid degradation by β-oxidation is reduced, enabling the accumulation of FFA molecules.

By consequence of the increased FFAs, the inhibition or reduction of the above mentioned regulatory responses results in the rise of plasma FFA levels [78,79]. Furthermore, SREBP-1c overexpression is highly associated with NAFLD development, by the amplification of hepatic fatty acid synthesis [76,77].

2.3.2 Hepatic oxidative stress

Hepatic oxidative stress is represented as a "second hit" in the pathogenesis of NASH. In NAFLD, microsomal and peroxisomal fatty acid oxidation, mitochondrial dysfunction as well as lipid peroxidation are regarded as major contributors to increased ROS production [14]. Hepatic oxidative stress is reported as the major cause of NAFLD progression to steatohepatitis, (Fig. 2.2).

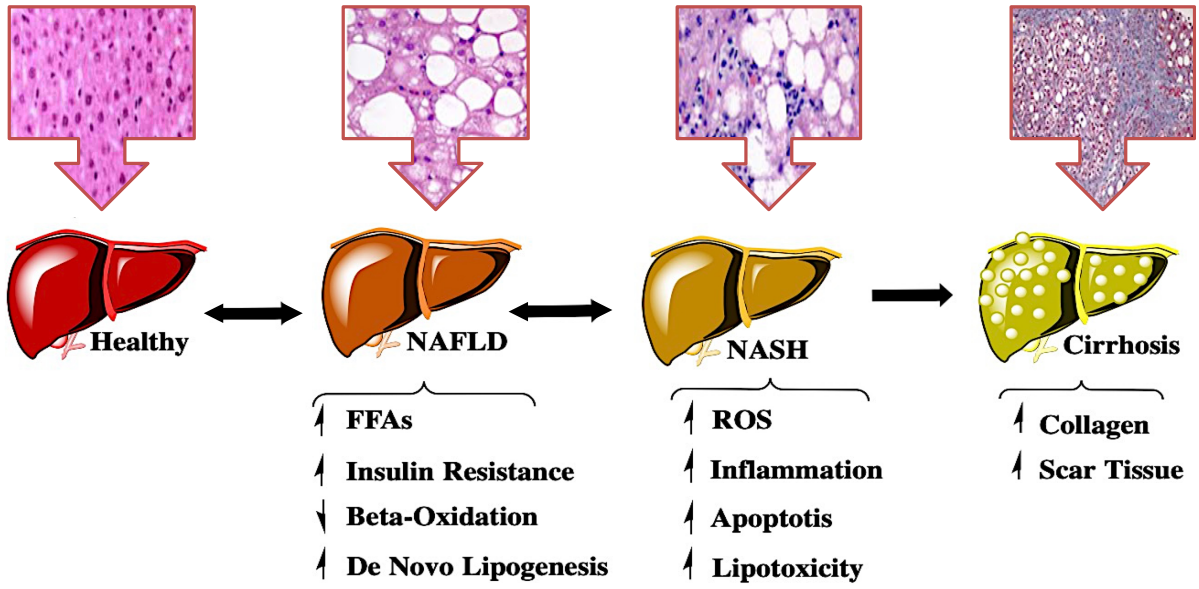

Figure 2.2 Multiple hit model of NAFLD, illustrative of the response mechanisms of the pathogenesis, as NAFLD progresses to NASH (adapted from, James and Day [1]).

Homeostasis of lipid and glucose metabolism is regulated mainly by activities in the mitochondria, including β-oxidation, electron transfer and ATP production [80]. The abnormalities in the mitochondria are primary causes for the altered balance between pro-oxidant and anti-oxidant mechanisms, leading to the induction of ROS production [81]. Under normal physiological conditions, the rate at which ROS and anti-oxidants are generated is balanced but in NAFLD and NASH this balance is disrupted [14]. This is supported by evidence that suggests that mitochondrial dysfunction, through mitochondrial DNA damage, might be the instigator of the increased lipid accumulation and oxidative stress in the liver, progressing

NAFLD into steatohepatitis [82]. Mitochondrial DNA damage has been analysed in previous studies, and the results show that the damaged nucleic genes are ultimately responsible for encoding mitochondrial proteins involved in the progressive increase of oxidative stress levels [83].

The endogenous antioxidant defences such as the enzymes catalase (CAT) and superoxidase dismutase 2 (SOD2) are responsible for the detoxification of ROS, by converting the superoxides and hydrogen peroxide into less toxic species [84]. Clinical data show that this trait is deficient in patients with NASH along with the activity of glutathione s-transferases (GST), an enzyme involved in xenobiotic detoxification and the protection of hepatocytes against exogenous derived oxidative stress [85].

Regulated expression levels of anti-oxidants, through hepatic oxidative stress, have been reported to contribute to the inflammation observed in NASH [57]. A study by Nobili *et al*, showed that lipid oxidation produces signalling modulators during the progression of the disease to NASH, linking hepatic steatosis to necroinflammation by mechanisms of lipid peroxidation [86]. The study used a methionine-choline deficient (MCD) diet on eight week-old male C57BL/6J mice to induce and characterise the possible involvement of adaptive immunity in NASH [57]. Extensive liver injury and lobular inflammation were observed, and the results indicated that hepatic oxidative stress contributes to the progression of NAFLD to NASH by stimulating cellular immune responses, thus providing evidence of the possible role of adaptive immunity in the pathogenesis of the disease [86,87].

2.3.3 Inflammatory response

The systemic inflammatory response observed in NASH has supported evidence that the clinical burden of NAFLD is not only confined to liver-related morbidity and mortality but that NAFLD is a multisystem disease, affecting several extra-hepatic organs and regulatory pathways [64]. Studying the pathophysiology of NAFLD has led to the discovery of various genomic aspects involved in the mild disease state and the pathogenesis into NASH, through the activation of inflammatory pathways [85]. The cascade of events highlighted in the progression of the disease is linked to the nuclear factor-kappa B (NF-κB), TNF-α and interleukin 6 (IL-6), that are referred to as three of the major pro-inflammatory cytokines, that regulate innate and adaptive immune responses [85,88].

Reports in the literature have shown that TNF-α has a vital role in the initiation of hepatic insulin resistance, where the expansion of visceral adipose tissue stimulates its release [89]. This activates a cascade of downstream inflammatory signalling kinases, namely, inhibitor kappa B kinase (IκK) and C-Jun-N-terminal kinase (JNK) [89]. These events lead to the recruitment of downstream molecules, NF-κB and activator protein-1 (AP-1) resulting in the inhibition in the phosphorylation of insulin receptor substrate (IRS), which in turn impairs insulin signalling and leads to peripheral insulin resistance, (Fig. 2.3) [14].

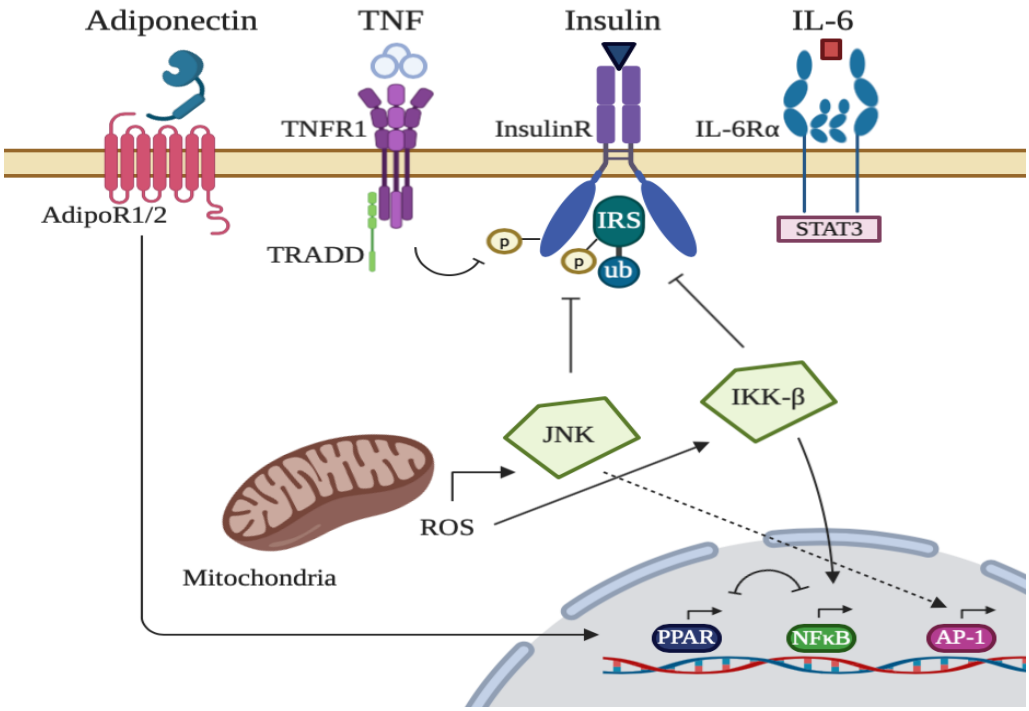

Figure 2.3 Inflammatory pathway involved in the regulation of insulin resistance (adapted from, Tilg and Moschen [14]). **TNF-**Tumour necrosis factor**, TNFR1-** Tumour necrosis factor receptor 1**, IL-6-** Interleukin 6**, IL-6Rα-** Interleukin 6 receptor alpha**, AdipoR1/2-** Adiponectin receptor 1/2**, TRADD-** Tumor necrosis factor receptor type 1-associated DEATH domain protein**, InsulinR-** Insulin receptor**, IRS-** insulin receptor substrate**, P-** phosphorylated**, ub-** ubiquitin**, STAT3-** Signal transducer and activator of transcription 3**, ROS-** Reactive oxygen species**, JNK-** c-Jun N-terminal kinase**, IKK-β-** Inhibitor Of Nuclear Factor Kappa B Kinase Subunit Beta**, PPAR-** Peroxisome proliferator-activated receptor**, NFkB-** Nuclear factor kappa B**, AP-1-** Activator protein 1.

In addition, TNF-α decreases hepatocyte insulin sensitivity by reducing the overall expression of insulin-dependent glucose transporter (GLUT-4), along with the reduction in phosphorylation of IRS resulting to hepatic insulin resistance. Insulin resistance is also associated with an overall increase in the amount of FFAs circulating within the blood system [11,90]. The modulation of the increased FFAs in hepatocytes is led by lipogenic and lipolytic

genes FASN and SREBP-1c respectively [63]. FASN, in response to hormone signalling is responsible for *de novo* lipogenesis, whereas SREBP-1c is a transcription factor that plays a major role in maintaining lipid homeostasis and regulating fatty acid metabolism [63]. The transcriptional control of the genes involved in glycolysis and lipogenesis is altered with the increased expression of the TNF receptor, as there is an increased expression of SREBP-1c, impairing insulin sensitivity and contributing to the progression of NAFLD to NASH [91].

Research has shown that the increased secretion of the hormone adiponectin by adipocytes acts as an anti-inflammatory substrate. Adiponectin is a hormone that is involved in regulating glucose levels and is a major product of adipocytes, which binds to its receptors adiponectin receptor 1 (ADIPOR1) and adiponectin receptor 2 (ADIPOR2). ADIPOR2 is located mainly in the liver and as adiponectin binds to ADIPOR2, it stimulates the secretion of anti-inflammatory cytokines (IL-10), blocking NF-κB activation thereby inhibiting the release of TNF-α and IL-6 [63]. Findings show that adiponectin plays an important role in preventing liver steatosis, as it was observed to cause an upregulation of PPAR-α expression, resulting in further fatty acid oxidation [92]. However, its hepatoprotective effects are not yet fully elucidated as the results demonstrate that TNF-α and adiponectin suppress and antagonise each other's production and action in the target organ [92].

2.3.4 Pro-apoptotic pathways

NAFLD is caused by the increased flux of lipids into hepatocytes. Hepatocytes initially adapt to these increased levels by utilisation and storage mechanisms. However, through the progressive manifestation of the disease, cells develop inflammation and undergo lipid-induced cell death driven by activation of pro-apoptotic pathways [93]

Apoptosis is a mode of cell suicide essential for tissue homeostasis and removal of damaged cells from the body [94]. It is characterised by morphological and biochemical features [95]. During early apoptosis, phosphatidylserine (PS), a component of the cell membrane found within the inner leaflet of the cell's lipid bilayer, becomes externalised by the flipping of the membrane, making the cell a target to scavenger receptors. This serves as an effective apoptosis marker identified by the binding of annexin-V [96]. Furthermore, there is a formation of blebs within the cell's mitochondrial membrane which causes a depolarisation of the mitochondrial membrane [97]. In the later stages, the cell loses its membrane integrity and chromosomal DNA is cleaved into oligonucleosomal sized fragments [95,97].

Apoptosis may occur in either of the two common pathways, the extrinsic and intrinsic pathway [97]. The extrinsic pathway of apoptosis is characterised by external stimuli which cause binding of death ligand (FasL) to a related cell surface receptor (CD95) [98]. Once a ligand binds to its receptor, there is formation of a death-inducing signalling complex (DISC) that recruits initiator caspase-8 which upon activation, initiates activation of the executioner caspase, caspase-3 [99]. The intrinsic pathway is mediated by intrinsic stimuli which cause a decrease in mitochondrial membrane potential leading to a release of pro-apoptotic proteins such as cytochrome-c into the cytosol thereby triggering cell death [95,97]. Cytochrome-c then binds to apoptotic protease activating factor 1 (Apaf-1) and activates the initiator caspase, caspase-9. Once activated, caspase-9 activates executioner caspase, caspase-3 [99].

An abnormal increase in FFAs modulates the extrinsic and intrinsic pathways of apoptosis. Unsaturated fats such as oleic acid, impart sensitivity to the death receptor-mediated apoptotic pathway by inducing CD95 and initiating the extrinsic pathway of apoptosis [98]. Saturated FFAs such as palmitic and stearic acid, lead to c-jun N-terminal kinase (JNK) dependant activation of the intrinsic apoptosis pathway. This is related to mitochondrial oxidative stress and the interaction with members of the B-cell lymphoma 2 (Bcl-2) family of regulatory proteins bound to the mitochondrial membrane, including Bax (pro-apoptotic) and Bcl-2 (anti-apoptotic) proteins [100].

Impaired mitochondrial function is a central abnormality responsible for the progression of hepatic steatosis to steatohepatitis [101]. Malhi *et al*., conducted a study that highlighted how hepatic lipoapoptosis was exhibited throughout the pathogenesis of NAFLD in several models of NAFLD, using monounsaturated and saturated fatty acids as a mode of induction in multiple hepatocyte cell lines and primary mouse hepatocytes [100]. Equal cellular steatosis was observed regardless of the class of FFA used, however, the activation of apoptosis and JNK was greater during exposure to saturated FFAs as opposed to unsaturated FFAs [100].

2.4 Current therapeutic intervention of NAFLD

The past decades have provided us with evidence that shows how lipid droplet accumulation in the liver can decrease the efficiency of insulin and eventually full blown insulin resistance [102]. As ectopic lipid accumulation and insulin resistance occur there are complications in glucose and lipid homeostasis, which increase the risk for cardiovascular disease (CVD). Therefore, to understand the underlying mechanisms caused by the hepatic manifestation of

the metabolic syndrome, current therapeutic interventions that help alleviate the rise in CVD risk factors mainly caused by the pathogenesis of NAFLD will be discussed below.

In insulin-resistant states such as NAFLD and NASH, marked depletion in circulating levels of adiponectin are observed [103]. Several prospective studies have thus investigated how adiponectin levels change in the pathogenesis of NAFLD [104,105]. Whereas a meta-analysis study showed that the progression from simple steatosis to NASH is resultant of a decrease in circulating adiponectin levels, and when NASH progresses to cirrhosis, an increase in adiponectin levels are observed [106]. Furthermore, PPAR agonists have led to an increase in circulating adiponectin in conjunction with histological improvements in patients living with NASH. Treating patients with metformin for one year reduced aspartate aminotransferase (AST) and alanine aminotransferase (ALT) levels, and also increased serum adiponectin levels in patients that have developed NAFLD [107]. Several studies have shown that TZDs; pioglitazone and rosiglitazone, improve adiponectin levels [17]. Similarly, statins increase adiponectin levels and have been speculated to effectively manage NAFLD through its action on regulating dyslipidaemia [108]. Therapeutic agents that have potential benefits to the liver, and insulin-sensitizing agents for T2DM are promising, although lipid-lowering medications are used for conventional indications instead of directly affecting NAFLD. The effect of direct replacement of adiponectin or other adipokines on NAFLD still needs to be investigated as there are no licensed pharmacological drugs that are currently approved by the U.S Food and Drug Administration [102]. However, current recommendations for NAFLD therapy are limited to the treatment of individual characteristics of the metabolic syndrome such as type two diabetes, as summarised in Table 2.1 [102].

Table 2.1 Summary of recommended pharmacotherapies for NAFLD and NASH [102].

Drug	Mode Of Action	AASLD Guidance (2017)	Side Effects
Pioglitazone	PPAR-ϒ agonist, anti-diabetic drug that helps restore insulin response thus lowering blood glucose levels	Recommended for NASH patients, with insulin resistance	Muscle pain Weight gain Bladder cancer
Metformin	Biguanide, anti-diabetic drug, prevents production of glucose in the liver, lowering blood glucose	Not Recommended as treatment for NASH due to lack of evidence	Irregular bowel movements Hypoglycemia Lactic acidosis
Exenatide	GLP-1 agonists, promoting the action of GLP-1 and insulin biosynthesis by pancreatic beta cells	Premature as a treatment for NASH	Hypoglycemia Kidney failure Pancreatitis
Sitagliptin	DPP-4 inhibitors, promoting the action of GLP-1 and insulin biosynthesis by pancreatic beta cells	Premature as a treatment for NASH	Joint pain Pancreatitis Heart failure
Statins	HMG-CoA reductase inhibitors, a class of cholesterol lowering drugs	Recommended for dyslipidemia, but avoid use in decompensated cirrhosis	Irregular bowel movements Muscle inflammation (Myositis) Kidney failure

Anti-diabetic drugs include insulin sensitisers (biguanides; metformin and thiazolidinediones; pioglitazone), stimulating insulin secretagogues (sulfonylureas, glucagon-like peptide 1 (GLP-1) receptor agonists (GLP-1 analogues and dipeptidyl peptidase-4 (DPP-4) inhibitors), as well as suppressors of postprandial glucose uptake in the digestive tract (α-glucosidase inhibitors, acarbose) and inhibitors of renal reabsorption of glucose (sodium-glucose co-transporter-2 (SGLT2), dapagliflozin) [109]. Primary factors in selecting any of these glucose-lowering agents include efficacy in reducing hyperglycaemia, as seen with pioglitazone, and to reduce the progression of NAFLD. Alternatively, cholesterol-lowering drugs such as statins are also considered as possible therapeutic agents for NAFLD, through the inhibition of 3-hydroxy-3-methylglutaryl-CoA (HMG-CoA) reductase [10]. However, the most extensively evaluated intervention for NAFLD are weight loss through lifestyle and dietary changes, as well as the use of antioxidants and natural medications [110].

Pioglitazone is a synthetic ligand for PPARs and acts as a PPAR-γ agonist and insulin sensitiser [111]. Mechanistically, pioglitazone activates and translocates PPAR-γ to the nucleus which then forms a complex with the retinoid x receptor alpha, modulating several gluconeogenic genes in the liver. The transcription of the insulin-sensitive glucose transporter, GLUT4, is induced in adipose tissue [112,113]; enhancing glycaemia, glucose transport and utilisation, as well as suppressing hepatic glucose production [114]. Pioglitazone is classified as a weak ligand for PPAR-α, and as such reduces insulin resistance, suppresses inflammation and infers a role in increasing β-oxidation whilst improving hepatic steatosis and non-alcoholic fatty liver disease [115]. Pioglitazone alters the transcription of genes, which influence lipid and carbohydrate metabolism whilst exhibiting anti-inflammatory effects in patients with NASH, due to its modulation of signalling pathways that are involved with intracellular pro-inflammation [17].

Furthermore, pioglitazone improves NAFLD by suppressing steatohepatitis markers. However, side effects highlight the disadvantage of using pioglitazone, as it leads to significant weight gain [110]. Despite this increase in weight, thiazolidinediones have the best evidence-based data for efficacy in NAFLD/NASH, but long-term adverse cardiovascular and other related side effects attributed to these drugs are a serious issue and are likely to prevent licensing of thiazolidinediones as treatment for NAFLD [102].

2.5 Rooibos

Given the need for therapeutics that offer long-term efficacy, with reduced side effects and cost, there is a growing interest for natural or plant-based therapies to help prevent or manage chronic metabolic conditions [27]. *Aspalathus linearis* (Brum.f) Dahlg., also known as rooibos, is a South African fynbos shrub that belongs to the family Leguminosae and it is indigenous to the Cederberg region of the Western Cape Province, (Fig. 2.4). Rooibos is known for producing a mild-tasting herbal tea from freshly harvested leaves, which are sundried to oxidise (ferment) the harvested leaves and stalks for a richer taste and strong aroma. In South Africa, rooibos is ranked the most commonly consumed herbal tea as reported in 2011, by the South African Rooibos Council (SARC), with an estimated 10.9 million households actively consuming rooibos tea [23]. The commercialised tea is mainly oxidised, producing a distinctive red colour, the tea is low in tannins, has no caffeine but is rich in unique bioactive polyphenolic compounds [24]. Compared to the traditional fermented rooibos tea, unfermented/green rooibos contains higher amounts of polyphenols, more specifically *C*-glucosyl dihydrochalcones, flavones and flavanols [24,25]. Therefore, green rooibos has the potential as a therapeutic, by its high phenolic content.

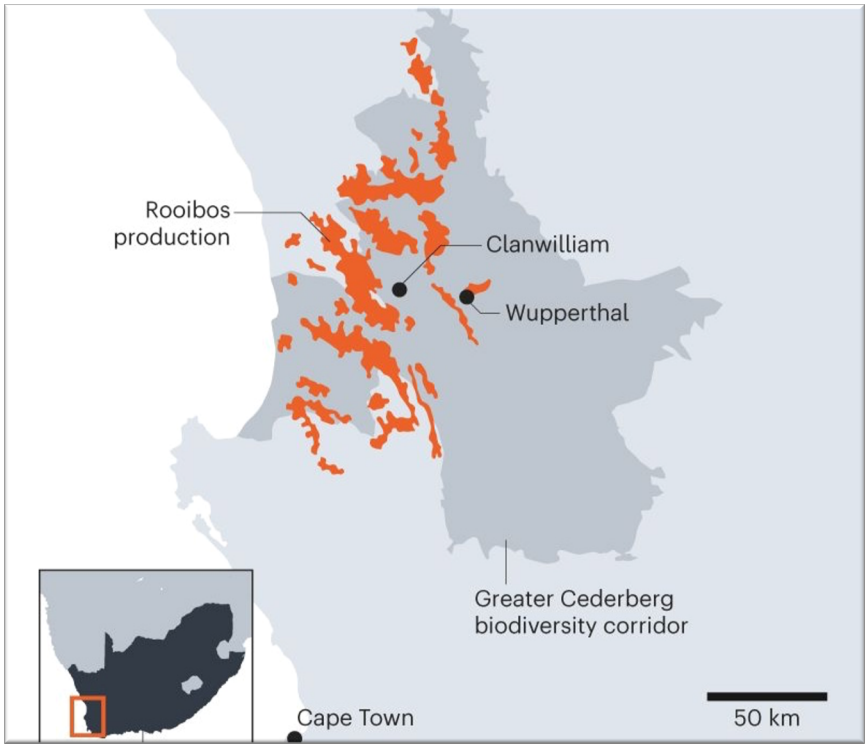

Figure 2.4 Greater Cederberg Biodiversity Corridor, production areas of *Aspalathus linearis* (Brum.f) Dahlg. (adopted from, Nordling [116]).

2.5.1 Biochemical characteristics and bioavailability of rooibos

Several health benefits, that involve anti-inflammatory responses [117], glucose modulating [118,119], anti-diabetic [120] and lipid-lowering effects [121], have been attributed to the use of rooibos as an alternative therapeutic [25]. Rooibos contains some rare polyphenolic compounds and compounds of interest such as phenyl pyruvic acid glucoside (PPAG; Z-2-(b-D-glucopyranosyloxy)-3-phenylpropenoic acid), as listed in Table 2.2 [25,122]. The major flavonoid found in rooibos is aspalathin, and to date aspalathin (a dihydrochalcone *C*-glucosyl) is uniquely found in *Aspalathus* species. During processing, oxidative changes to the phenolic composition of the plant forms part of the traditional fermented rooibos tea, which is rich in flavour, colour and aroma [23]. In unfermented (green) rooibos the flavonoid content is higher. Extracts produced from unfermented/green rooibos, as per Table 2.2, is higher than the "traditional" fermented rooibos extract.

Table 2.2 Flavonoid content of unfermented rooibos extracts compared to fermented rooibos extracts [25,122].

		Extract (g/100g)	
	COMPOUND	**UNFERMENTED**	**FERMENTED**
C-Glucosyl dihydrochalcones	Aspalathin	11,95	0,59
	Nothofagin	1,40	0,03
C-Glucosyl flavones	Orientin	1,10	1,01
	Isoorientin	1,43	1,07
	Vitexin	0,15	0,07
	Isovitexin	0,18	0,15
O-Glycosyl flavonols	Quercetin-3-O-rutinoside (rutin)	0,36	0,19
	Quercetin-3-O-robinobioside	0,70	0,45
	Quercetin-3-O-galactoside (hyperoside)	0,12	0,09
	Quercetin-3-O-glucoside (isoquercitrin)	0,16	0,06
Phenylpropenoic acid glucoside	PPAG	0,27	0,57

The absorption, distribution, metabolism and excretion (ADME bioavailability) determines the bioactivity of bioactive food compounds, as they should reach the site of action, to execute their health benefits [123]. Plenty of factors limit or enhance the bioavailability of any compound, from ingestion, digestion in the digestive tract and its interactions with other dietary sources to name a few [124]. An *in vitro* study using a Caco-2 monolayer cell model demonstrated, that the absorption of aspalathin improved when present in an unfermented green rooibos extract as opposed to a pure aspalathin compound [125]. The study critically highlighted how the other plant components in the extract may assist in the transport of aspalathin across the membrane.

In an *in vivo* study by Kreuz *et al*., pigs which were fed an aspalathin-enriched, unfermented "green" rooibos extract equalling, 157–167 mg/kg body weight per day for eleven days, reported no aspalathin and metabolites detected in the plasma of the treated animals [126]. Several metabolites, aglycones of aspalathin, dihydro-(iso)orientin and aspalathin conjugated with a methyl group and/or glucuronic acid were found in the pigs' urine, suggesting that the absorption of aspalathin could have been attributed to the liberation of the aglycones by colonic microflora [126]. The study by Kreuz *et al*., along with a study on non-human primates [127], also revealed that with a single dose of the aspalathin-enriched unfermented "green" rooibos extract about three times higher, trace amounts of aspalathin were detected in the blood plasma of the treated animals [126].

2.5.2 Hepatoprotective effects

Patients presenting with glucose intolerance and dyslipidaemia are progressively considering natural products as an alternative or adjunctive therapy as opposed to conventional medications due to their perceived health benefits and efficacy [128]. Several of these natural products contain phenolic compounds such as flavonoids known to be largely responsible for the biological activity, including beneficial effects on glucose and lipid metabolism [129]. Within this context, several studies have alluded to the glucose and lipid modulating effects of rooibos [130], as aspalathin was demonstrated to stimulate insulin release from pancreatic beta cells and a subsequent increase in glucose uptake in muscle tissues, thus benefiting glucose homeostasis in various models of T2DM [25]. In addition, rooibos has also been shown to have LDL-C lowering [131], and cardioprotective effects [130]. A study by Patel *et al.*, demonstrated, the safety and pharmacological effects of an aspalathin-rich unfermented "green" rooibos extract in combination with pioglitazone and atorvastatin *in vivo* using a Wistar rat model [132]. The *in vivo* study showed a significant pharmacokinetic interaction, where "GRT" moderately inhibits cytochrome P450-3A4 (CYP3A4) activity, affecting the bioavailability of drugs metabolised by the CYP iso-enzyme [132].

Literature has demonstrated the association between the consumption of foods rich in flavonoids and cellular damage, through radical scavenging of ROS and enzymatic processes responsible for free radical production [133]. A study conducted by Ajuwon *et al*., investigated the effects of a fermented rooibos extract on a Wistar rat model and assessed the hepatic markers of oxidative stress, as well as the release of pro-inflammatory cytokines in lipopolysaccharide (LPS)-induced liver injury [22]. LPS treatment significantly increased serum levels of ALT, AST and LDH, resulting in the induction of liver injury, attributed to toxic mediators produced by activated macrophages [134]. The study concluded that treatment with a fermented rooibos extract attenuated LPS-induced liver injury, by suppressing the formation of pro-inflammatory cytokines and modulating oxidative stress levels [22]. This is interesting, however the efficacy of an aspalathin-rich unfermented "green" rooibos extract is yet to be determined in experimentally induced models of NAFLD.

The use of rooibos as a potential therapeutic will not only benefit the local market because the herbal tea is indigenous to South Africa but will also have a huge impact on markets globally. This is because the United Kingdom together with Germany, the Netherlands, Japan, and the United States of America are some of the top importers of rooibos, representing more than 80% of the export market (data supplied by South African Rooibos Council, 2013) [135].

2.6 Models used to study the pathogenesis of non-alcoholic fatty liver disease

To study the pathogenesis of NAFLD, researchers have used various animal models incorporating pathological patterns and histological alterations found in the different stages of the disease in humans. Rodents have been the leading *in vivo* model used in biomedical research, with genetically modified and dietary induced rodent models employed to mimic the pathogenesis of the disease [136]. Other animal models for example, Ossabaw pigs and primates are larger animal models and are much related to humans than rodents but are also expensive options to use in a laboratory [137].

In vitro models for NAFLD are considered an alternative approach to elucidate the molecular mechanisms involved in the progression of the disease. Previously, researchers were investigating signalling cascades and mechanisms of action using *in vivo* models of NAFLD and confirmed the findings through clinical studies [138]. However, recent studies have employed the use of primary cell cultures and immortalised cell lines to widely improve *in vitro* models of NAFLD [139]. Human or model organism cells are cultured in various conditions to induce pathological patterns observed in humans suffering from the disease. Various culturing techniques are utilised such as mono-culture, co-culture and three-dimensional cell culture models, where the complex architecture, interaction and physiological setting of the hepatic tissue of one, two or more cell types is commonly present in the human body (Figure 2.5) [137,139].

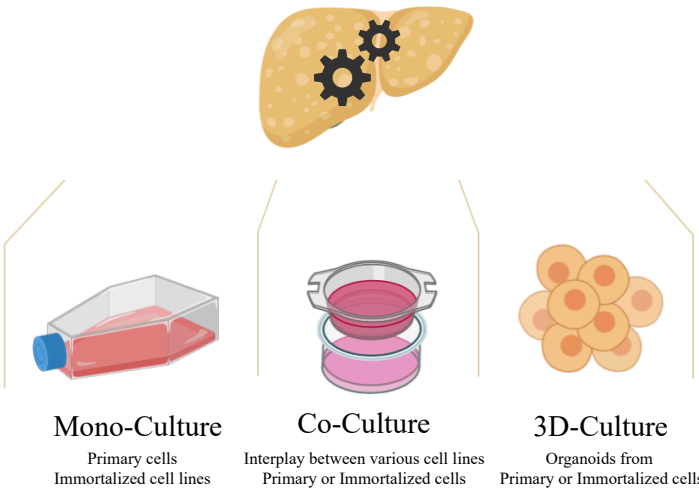

Figure 2.5 Various *in vitro* models of NAFLD (adapted from, Kanuri and Bergheim [137]).

The most abundant dietary FFAs are unsaturated oleic acid as well as saturated palmitic acid [140]. These free fatty acids have been identified in liver steatosis, and literature has confirmed steatosis induction using both FFA's *in vitro* and *in vivo* using various liver cell lines and rodent models [141,142]. Palmitic acid has shown to be cytotoxic at concentrations higher than 0,75 mM, thus NAFLD experimental induction methods would ideally lean towards the use of oleic acid to avoid cytotoxicity [143]. Genetic rodent models serve well as *in vivo* models of NAFLD due to the low variability caused by dietary models.

The study was therefore aimed at investigating the potential of a aspalathin-rich green rooibos extract (Afriplex GRT) as a therapeutic intervention to protect against hepatic oxidative stress, inflammation and apoptosis in experimentally induced cell (*in vitro*) and animal (*in vivo*) models of NAFLD.

The objectives of the study were (**i**) to establish an *in vitro* model of steatosis using C3A cells treated with oleic acid, (**ii**) to treat the oleic acid-induced cells with pioglitazone and Afriplex GRT as mono-therapies and in combination, (**iii**) to perform histological analysis of mouse liver sections obtained from a previous study to confirm hepatic steatosis and assess the effects of treatment, as well as (**iv**) an expression analysis of target genes and proteins using qRT-PCR and Western blotting on both the C3A cells and mouse liver samples.

3. Methodology

3.1 Experimental Design:

In vitro and *in vivo* models of NAFLD:

An immortalised liver cell line, a derivative of HepG2 (HepG2/C3A) hepatocytes, was utilised in the *in vitro* study as a representative liver cell line to experimentally induce hepatic steatosis using oleic acid to assess the potential therapeutic intervention by treating with Afriplex GRT, (Figure 3.1).

The *in vivo* study used liver tissue samples from leptin receptor-deficient non-diabetic db^+ (lean) and obese diabetic *db/db* (obese) male mice from a previous study. The *db/db* mice are leptin receptor-deficient ($Lepr^{db}$) and have persistent hyperphagia, become obese and spontaneously develop diabetes that is associated with hepatic steatosis. This provided a rodent model that mimicked NAFLD in human patients, (Figure 3.2).

3.2 Cell culture:

Sub-culture of C3A liver cells:

Vials containing C3A liver cells (ATCC CRL-10741) which were stored at -196 °C, were thawed at room temperature in a laminar flow hood (*Labtech™, Ortenberg, Germany*) at 23 °C with a windspeed of 0.53 m/s, to ensure sterility for subsequent culturing in 17 mL of Eagle's essential minimal medium (EMEM) that was pre-warmed to 37 °C and supplemented with non-essential amino acids, sodium pyruvate (1 mM), foetal bovine serum (FBS) (10%), L-glutamine (1%) and glucose (19.5 mM). Inoculation of the cell suspension into a 75 cm^2 cell culture flask was performed. The flask was then incubated at 37 °C and humidified with 5% CO_2 overnight. Passage numbers were recorded (restricted to below 30 passages) to avoid phenotypic drift from the number of times the cells were trypsinised and reseeded. The medium was refreshed (every second day) until the cells reached the targeted 80 % confluency to resume the experimentation.

The cells were sub-cultured using the standardised protocol until they reach 75-80% confluence to be used for further experimentation. The spent media was aspirated, and the remaining cells were washed with 8 mL of [1x] phosphate-buffered saline (PBS). To retrieve the cells, 3 mL of trypsin was added to each 75 cm^2 flask, and the cells incubated, as above, for 3-7 min. Standardised cell culture growth medium (7 mL) was added to the cells to inactivate trypsin

and a single cell suspension was obtained by pipetting the cell suspension with a 10 mL serological pipette. A 15 mL centrifuge tube was then used to centrifuge the transferred cell suspension at 800 x g using *SL16R* centrifuge (*ThermoFischer Scientific™, Massachusetts, USA*) for 5 min. Depending on the size of the cell pellet, the pellet was then re-suspended in 5-10 mL cell culture growth medium and 0.5 mL of the suspension transferred into a centrifuge tube (2 mL) for cell counting.

Counting of the cells was done by pipetting the cell suspension (10 µL) into a centrifuge tube (2 mL), which contained 10 µL of trypan blue solution at 0.4% and mixed by pipetting up and down. The mixture (10 µL) was then pipetted onto a haemocytometer and live cells were manually counted in each quadrant using phase contrast on an inverted light microscope at 10x magnification (*Olympus CK x31, Tokyo, Japan*). The 5-10 mL cell suspension was subsequently seeded using a standardised cell density for C3A cells (10 x 10^5, 1.0 x 10^5 cells per well for 96 and 24/6 well plates, respectively), as previously determined by Mazibuko [144]. For quantitation of cell viability and the determination of lipid accumulation, 96 well cell culture plates were used. For mitochondrial depolarisation assays, 24 well cell culture plates were used and finally, 6 well cell culture plates were used for cell harvesting for genomic and proteomic analysis.

3.2.1 Treatment conditions:

Induction and anti-steatosis treatment of HepG2/C3A liver cells:

HepG2/C3A liver cells were sub-cultured for three consecutive passages before treatment with an optimised concentration of oleic acid [1 mM] (*Sigma-Aldrich, St. Louis, USA*) for 24 h, to induce hepatic steatosis, as previously reported by Alkhatatbeh *et al.* [145]. A 24 h treatment assessment on the anti-steatosis effects of Afriplex GRT and/or pioglitazone was determined through the use of monotherapies and co-treatments, at various concentrations, following a 24 h steatosis induction period.

Stock concentrations at [100, 10 and 1 mg/mL] of Afriplex GRT extract were prepared by weighing 10 mg of the pure extract and dissolving it in 0.1 mL of 100% DMSO and serial diluting the solution (1:100) in supplemented EMEM growth media to obtain the desired stock concentrations. A stock concentration at [30 mM] of pioglitazone (*Sigma-Aldrich, St. Louis, USA*) was prepared by weighing [11.787 mg] of the pure compound and dissolving it in 1 mL of 100% DMSO. Induction media was prepared fresh each day and the cells were grouped and

induced as per table 3.1 below, using oleic acid for 24 h. Treatment media for the various concentrations was prepared fresh the next day and the treatments were grouped as per table 3.1 below; including a 0.1% DMSO vehicle control as the stock treatments were dissolved in 100% DMSO and finally obtained a final concentration of 0.1% DMSO as well as the desired treatment concentrations.

Table 3.1 *In vitro* steatosis induction and anti-steatosis treatment layout.

	(24h) Oleic Acid Induction	**(24h) Treatment**
Normal Control	None	None
Induced Control	1 mM	None
DMSO Vehicle Control	1 mM	0.1%
Pioglitazone	1 mM	30 µM
Afriplex GRT	1 mM	1 µg/mL
	1 mM	10 µg/mL
	1 mM	100 µg/mL
Pioglitazone + Afriplex GRT	1 mM	30 µM + 1 µg/mL
	1 mM	30 µM + 10 µg/mL
	1 mM	30 µM + 100 µg/mL

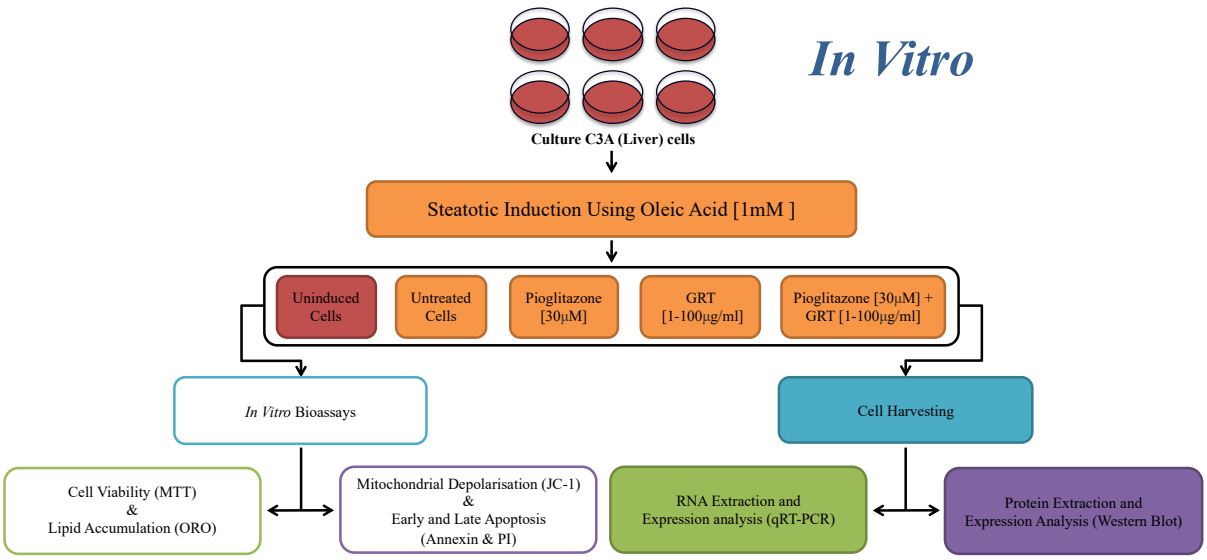

Figure 3.1 C3A liver steatosis study design.

3.3 *In vitro* biochemical assays, staining techniques and harvesting:

3.3.1 Cell viability testing of C3A liver cells:

In vitro mitochondrial dehydrogenase activity:

The mitochondrial succinate dehydrogenase activity of the cells exposed to steatosis induction and anti-steatosis treatment was analysed using a 3-[4,5-dimethylthiazol-2-yl]-2,5-diphenyltetrazolium (MTT) assay. The colorimetric assay measured the cell metabolic activity following induction and treatment of the cells. The MTT assay determines the relative viability of the cells by assessing the cell metabolic activity in each treatment condition along with its controls. The assay is based on the ability of NADPH-dependent cellular oxidoreductase enzymes to reduce the MTT dye to a purple formazan [146].

Therefore, following treatment of the C3A liver cells an MTT assay was conducted on the 96 well cell culture plate by incubating the treated cells with an MTT reagent (2 mg/mL) at 37 °C for 30 min. After incubation, 200 µL DMSO and 25 µL Sorenson's buffer was added into each well, and the plate was kept at room temperature, and wrapped in aluminium foil to block out light. The plate was subsequently read using a plate reader *ELx800* (*BioTek®, Winooski, VT, USA*) at an absorbance reading of 570 nm.

3.3.2 Lipid analysis:

Lipid accumulation assay of C3A liver cells:

Following steatosis induction with oleic acid and the anti-steatosis effects of Afriplex GRT and pioglitazone, free fatty acids within the cultured cells and the lipid content were evaluated using an oil red O (ORO) based colorimetric and cell staining assay. Oil red O is described as a hydrophobic dye that is substantially more soluble in neutral triglycerides and lipids than its solvent alcohol [147].

Briefly, following treatment, the C3A liver cells were fixed using 10% formalin onto the 96 well tissue culture plates for 15 min at room temperature. Once fixed the cells were rinsed with 100 µL PBS to get rid of formalin. A 0.7% working solution of ORO was then added to the cells and were incubated for 30 min at room temperature. The ORO stain was aspirated, and the stained cells were rinsed several times with distilled water followed by visualisation at 20x and 40x magnification under an inverted light microscope (*Olympus CK x31, Tokyo, Japan*). After visualisation, the distilled water was aspirated, and absolute isopropanol was added to

the cells to extract the dye from the stained fatty acids. The extracted stain was therefore transferred into a fresh 96 well assay plate and the absorbance (490 nm) was read on a plate reader *ELx800* (*BioTek®, Winooski, VT, USA*).

After extraction of ORO, the cells were rinsed with 70% ethanol and the ethanol was then aspirated. The nuclei of the cells were subsequently stained with 0.5% crystal violet (CV) working solution and incubated for 5 min at room temperature, to account for the viability of the cells during the experiment. The CV stain was then aspirated completely and after rinsing the cells a few times with PBS, 70% ethanol was added into each well and the CV stain was extracted from the cells. The CV stain was then transferred to a fresh 96 well assay plate, and the CV absorbance (570 nm) intensity was read on a plate reader *ELx800* (*BioTek®, Winooski, VT, USA*).

3.3.3 Mitochondrial membrane potential:

The 5, 5', 6, 6'-Tetrachloro-1, 1', 3, 3'-tetraethylbenzimidazolylcarbocyanine iodide (JC-1) is a lipophilic cationic fluorescent dye, which through mitochondrial membrane potential, serves as an indicator of cell health. The JC-1 dye fluoresces green (λ_{ex} 520 nm) in its monomeric form when exposed to unhealthy cells due to a low membrane potential and in healthy cells the JC-1 dye fluoresces red (λ_{em} 596 nm) by the formation of J-aggregates due to a high membrane potential. Based on the green to red fluorescence ratio of the dye in the mitochondria an assessment of mitochondrial depolarisation can be considered as the higher the green/red fluorescence ratio the higher the depolarisation of the mitochondrial membrane, as previously reported [148].

Thus, the anti-steatosis potential of Afriplex GRT and pioglitazone on oleic acid-induced steatosis were determined by assessing the mitochondrial membrane potential using a JC-1 stain (cat. no.: T3168; *Sigma, Stanheim, Germany*) [149]. Following the 24 h treatment, the media was discarded, and cells washed with 500 µL PBS and stained with 500 µL of 2 µM JC-1 stain and the cells incubated at 37 °C for 30 min. Following incubation the cells were washed once again with 500 µL PBS and mitochondrial membrane potential was imaged using a *Nikon Eclipse Ti/S Fluorescence Microscope* with digital camera (*Nikon, Minato City, Tokyo, Japan*) at 200x magnification [149]. The intensity of the red fluorescence was then quantified using the ImageJ32 software application (imagej.nih.gov/ij/list.html) through densitometric analysis.

3.3.4 Cell harvesting:

Following a 24 h stress induction and a further 24 h of treatment with Afriplex GRT and pioglitazone in 6-well cell culture plates (as shown in section 3.2 above), cell culture medium was aspirated, and the attached cells were washed with 1 mL ice-cold PBS. After the wash step, 0.3 mL Buffer RLT (*Qiagen™, Hilden, Germany*) [for mRNA extraction] or 0.3 mL *Invitrogen™ Tissue Extraction Reagent I* (*ThermoFischer Scientific™, Massachusetts, USA*) [for protein extraction] was added into each well and the cells were detached from the tissue culture plates using a cell scraper. The cells were then pooled per treatment sample to make up a total volume of 0.9 mL of each cell suspension. The collected samples per treatment were transferred from the plates into 2 mL centrifuge tubes and kept on ice throughout the sample harvest period.

3.4 Animal handling:

Ethical approval and growth parameters:

The study made use of 40 C57BL/6 Lepr *db/db and db/*$^{+}$ mice from Jacksons laboratory, which were housed at the SAMRC Primate Unit and Delft Animal Centre (PUDAC). The SAMRC-Ethics Committee for Research in Animals (SAMRC-ERCA) and the University of Zululand Committee on Animal Research and Ethics (UZREC), approved the animal study, with reference numbers (SAMRC-ERCA REF.05/17) and (UZREC 171110-030) respectively, see appendices (subsection 9.1 and 9.2). Additional ethical clearance was requested and granted from Stellenbosch University (ACU-2020-14382) (subsection 9.3 of appendix).

The mice model presents with obesity traits at four weeks of age, as the mice actively express the (*Leprdb*) mutation. These mice were housed in pairs, with free access to food (standard chow diet) and water, in a relative humidity of 50%, controlled temperature of 23-24 ^{o}C and 12 h light and dark cycles. For six weeks, the mice were acclimatised to the experimental environment, with body weights assessed weekly.

The mice were then randomised into four *db/db* treatment groups (n = 8 per group), with the lean *db/*$^{+}$ (n = 8 per group) littermates included as controls. Food intake data were recorded weekly by weighing the food given to the mice in the feeder and weighing the food left and the spillage to work out the food consumed. Body weights were also measured weekly throughout the ten-week treatment period.

3.4.1 Treatment conditions and tissue harvesting:

Anti-diabetes treatment of genetically induced diabetic mice:

The mice were randomly grouped into Control (*db/+*), Untreated (*db/db*), Pioglitazone [15 mg/kg] treated (*db/db*), GRT 1 [74 mg/kg] treated (*db/db*) and GRT 2 [740 mg/kg] treated (*db/db*) groups, where the animals were given treatment mixed with powdered standard chow diet daily for ten weeks. The Afriplex GRT extract was used for treatments (GRT 1 and GRT 2). The control and untreated groups were fed the same food equivalent but with treatment excluded. Daily treatment dosages were administered in proportion to the average daily food intake. The treatment doses of pioglitazone and Afriplex GRT were both selected based on previous animal studies [120,150] with the mouse equivalent dosages converted using the conversion formula described by Reagan-Shaw *et al.* [151].

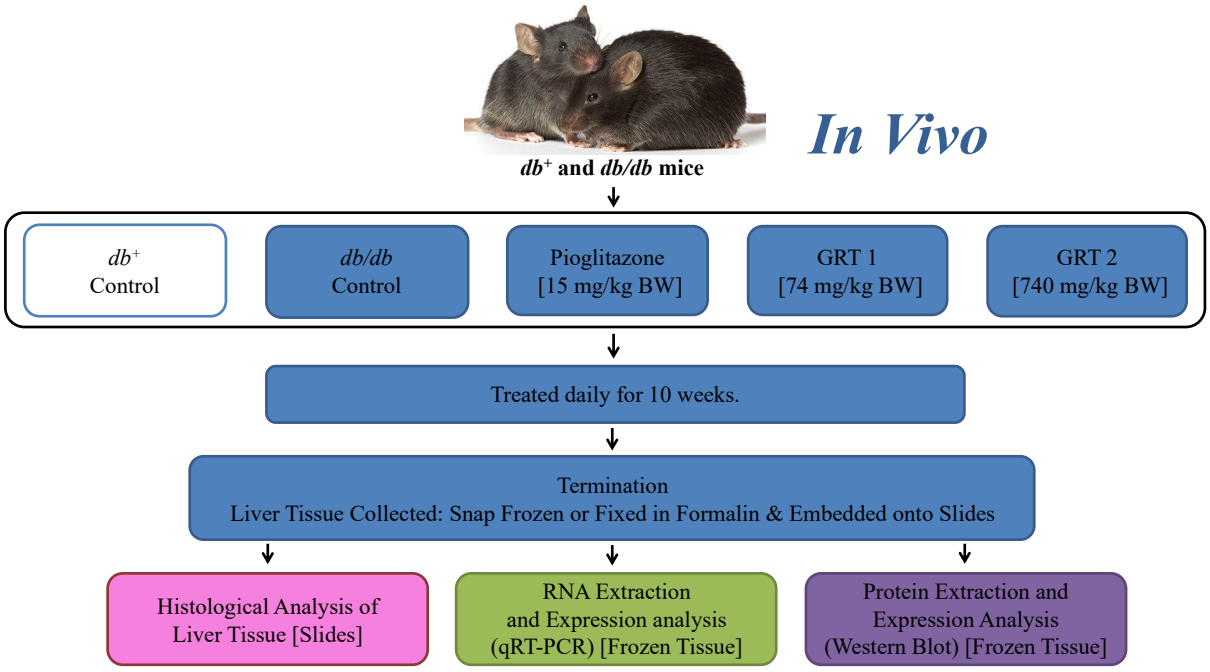

Figure 3.2 *In vivo db/db* mouse study outline and study design.

Animal terminations and tissue collection:

After 10 weeks of treatment, the mice were anaesthetised with 2% fluothane and 98% oxygen gas inhalation. Deep anaesthesia was tested by the pinch of the toe, and once established, animals were euthanised by exsanguination with blood drawn from the vena cava and the liver collected and weighed. The harvested organs were either snap-frozen (for protein expression),

preserved in *RNAlater®* (*Applied Biosystems, CA, USA*) [for mRNA extraction] or fixed overnight in 10% phosphate-buffered formalin, pH 7.4 [for histology].

3.5 Biochemical assays and staining techniques:

Haematoxylin and Eosin staining of liver sections:

A histological examination of the harvested liver tissue samples was performed to assess abnormalities related to hepatic steatosis and NAFLD, across the treatment groups. Liver samples were fixed overnight in 10% phosphate-buffered formalin (pH 7.4), thereafter processed on a *TP 1020* automatic tissue processor (*Leica, Wetzlar, Germany*) through increasing concentrations of ethanol (70% EtOH for 1.5 h, 90% EtOH for 2 h and absolute EtOH for 3 h). The tissue was also processed through xylene before being impregnated with heated paraffin wax. Once processed, the tissue embedded in paraffin wax was cut in 5 µm sections using a *RM 2125 RTS* rotary microtome (*Leica, Wetzlar, Germany*).

The cut sections were then floated out in a water bath (± 40 °C) and mounted onto 3-aminopropyltriethoxysilane (APES) coated slides. The slides were heated at 60 °C for 45 min, adhering the sections to the melted wax. Before rehydrating the sections with decreasing concentrations of ethanol (absolute and 95%), the slides were dewaxed with two ten-minute changes of xylene. The rehydrated and dewaxed slides were rinsed with distilled water and subsequently stained with haematoxylin (Mayer's) stain for 12 min. The stained slides were washed with distilled water and then counterstained with 1% eosin stain (aqueous solution) for 2 min. Stained slides were dehydrated with increasing ethanol concentrations (95% and absolute) and cleaned with xylene, prior to mounting. The slides were mounted with Entellan® mounting medium and 24 x 40 mm coverslips were used. Slides were left to air dry at room temperature and the slides were visualised and images captured under a *Nikon Eclipse Ti/S Inverted Microscope* with digital camera (*Nikon, Minato City, Tokyo, Japan*) at 200x magnification.

The mounted liver sections, were assessed for their hepatic steatosis severity using the NAFLD severity scoring method defined in a study by Trak-Smayra *et al.* [152]. The method scores the intensity, distribution and lipid content accumulated in the mice liver lobules. Thus, the intensity of hepatic steatosis was assessed as the percentage of hepatocytes which contained lipid vacuoles analysed at 200x magnification in ten randomly selected non-overlapping fields. The zonal distribution within the lobules was also used to further score the lipid accumulation

in the liver sections. The size of the lipid vacuoles identified in the hepatocytes classifies the type of steatosis observed in the liver sections.

Blood glucose and oral glucose tolerance test:

Fasted blood glucose levels were measured weekly using *OneTouch Select*® glucometer, by loading a blood sample obtained from a tail prick. A week prior to terminations, the animals were subjected to an oral glucose tolerance test (OGTT). The mice were fasted for 16 h and a baseline glucose level was determined, thereafter the mice were given 1 g/kg glucose via oral gavage. The blood glucose levels were measured from a tail prick at various time points (0, 15, 30, 60 and 120 min). The area under the curve (AUC) was subsequently calculated with the trapezoidal rule on *GraphPad Prism version 7.00 for Macintosh*.

3.6 mRNA extraction and quantification from cells and liver tissue:

Cell lysates were prepared from harvested C3A cells on ice using Buffer RLT (*Qiagen™, Hilden, Germany*) and the total mRNA was extracted from the harvested C3A liver cells using an *RNeasy* mini kit (*ThermoFischer Scientific™, Massachusetts, USA*). The extracted mRNA was subsequently used for cDNA synthesis for use in qRT-PCR analysis, with the aim to detect genes involved in; insulin signalling (*IRS1*) and glucose transport (*GLUT2*), lipid and glucose metabolism (*AMPK-α*), (*PPAR-γ*), (*PPAR-α*), Fatty acid synthase (*FASN*), Glucose-6-phosphatase (*G6PC*), Phosphoenolpyruvate carboxykinase 1 (*PCK1*), (*SREBF1*) and carbohydrate-response element-binding protein (*CHREBP*) and oxidative stress response, Glutathione peroxidase 2 (*GPX2*) and superoxide dismutase 2 (*SOD2*) respectively.

Liver tissue lysates were prepared from 50 mg of harvested liver tissue on ice using Buffer RLT (*Qiagen™, Hilden, Germany*) and the total mRNA was extracted from the harvested liver tissue using a *RNeasy* mini kit (*ThermoFischer Scientific™, Massachusetts, USA*). mRNA was subsequently converted into cDNA for qRT-PCR analysis, with the aim to detect genes involved in; apoptosis (*Casp3*), insulin signalling (*Irs1*), glucose transport (*Glut2*), lipid and glucose metabolism (*Ppar-γ*, *Ppar-α*, *Fasn*, *Srebf1* and *Chrebp*) and oxidative stress response (*Sod2*) respectively.

Following cell or tissue harvesting, a stainless-steel bead (*Qiagen™, Hilden, Germany*) was added to each 2 mL centrifuge tube containing the cell suspension or liver tissue. The samples were then homogenised using a *TissueLyser* (*Qiagen™, Hilden, Germany*) *at* 25 Hz for sixty seconds, and this was repeated four or five times for C3A liver cells, with 1 min intervals on

ice. The homogenised suspension was then centrifuged at 15000 x *g* for 15 min at 4 °C. The supernatant was carefully removed and transferred to a 2 mL Eppendorf tube, where one volume of 50 % ethanol was added to the lysate and mixed by pipetting up and down. Thereafter, 550 µL of the homogenate sample was transferred to a RNeasy spin column placed in a 2 mL collection tube which is supplied by the manufacturer in the kit. The samples were then centrifuged at 15000 x *g* for 15 sec at room temperature, and the flow-through was discarded.

The spin columns were centrifuged at 15000 x *g* for 15 sec at room temperature, with 700 µL of the RW1 buffer, and the flow-through was discarded. Thereafter, 500 µL of the RPE buffer was added to the spin columns, which were then centrifuged at 15000 x *g* for 15 sec at room temperature with the flow-through discarded and the step repeated. The spin columns were placed in fresh 2 mL centrifuge tubes and then centrifuged at full speed for one minute. Following centrifugation, the spin columns were placed in fresh 1.5 mL centrifuge tubes, which were supplied by the manufacturer. RNase-free water (50 µL) was added directly to the spin column membrane, which were then left to stand for a minute and then centrifuged at 15000 x *g* for one minute to elute the RNA.

The eluted RNA samples were thus placed on ice for the quantification step using the Nanodrop ND-100 spectrophotometer (*Nanodrop Technologies, Wilmington, DE, USA*). The samples were measured by blanking initially with 1 µL of the RNase-free water, thereafter 1 µL of the sample was loaded onto the pedestal and the absorbance was measured. The purity of the RNA samples was determined from the 260/280 nm ratio reading of the Nanodrop system. The value ranging from 1.8 to 2 suggested a pure RNA sample measured in duplicates to account for pipetting errors.

3.6.1 DNAse treatment and cDNA synthesis:

Genomic DNA contamination was eliminated from RNA samples by DNase treatment using the *Turbo DNase kit* according to the manufacturer's protocol (*ThermoFischer Scientific™, Massachusetts, USA*). Briefly, RNase-free water was added to 20 µg of RNA, to a final volume of 50 µL. Thereafter 5 µL of DNase buffer and 1 µL of DNase were added to the RNA samples and incubated at 37 °C for 30 min. An additional 1 µL of DNase was added to the RNA and incubated at 37 °C for another 30 min. Thereafter, 10 µL of the *DNase Inactivation Reagent* was added to the RNA samples. The samples were then placed in an orbital shaker for 5 min at room temperature and then centrifuged at 15000 x *g* for a minute and a half. The RNA was

transferred to a fresh tube and the RNA concentrations were read using NanoDrop™ OneC spectrophotometer (*ThermoFischer Scientific™, Massachusetts, USA*).

Nuclease-free water was added to the DNase treated samples to a volume of 10 µL. Total RNA (2 µg) was thereafter reverse transcribed into a single-stranded complementary DNA (cDNA) using the *High-Capacity cDNA reverse transcription kit* (*Applied Biosystems, Foster City, CA, USA*), according to the manufacturer's instructions (Cat. no.: 4368814). A PCR reaction mix was prepared containing 12.5 µL SYBR Green master mix, 1 µL ActB primers (10 µM) and 9.5 µL nuclease-free water to a total volume of 24 µL per reaction. To test the cDNA for genomic DNA contamination, 1 µL cDNA was pipetted into a 96-well PCR plate and 24 µL of the PCR reaction mix was added to a total reaction volume of 25 µL, per well. The plate containing the reaction mix with cDNA was then mix and centrifuged on a benchtop centrifuge and the reaction was run at standard PCR conditions (Table 3.2) using *ABI 7500 Sequence Detection System* (*Applied Biosystems, Foster City, CA, USA*).

Table 3.2 Thermal Cycler Running Conditions.

Stage	Cycle Repetitions	Temperature	Time
1 (Hold)	1	50.0 °C	02:00 min
2 (Hold)	1	95.0 °C	10:00 min
3 (Amplification)	40	95.0 °C	00:15 min
		60.0 °C	01:00 min

3.6.2 qRT-PCR Analysis:

TaqMan® gene expression assay probes (*ThermoFischer Scientific™, Massachusetts, USA*) were used to assess the mRNA expression of both *in vitro* (Table 3.3) and *in vivo* (Table 3.4) studies. A PCR master mix was prepared by adding 5 µL TaqMan® universal master mix to 0.5 µL of the TaqMan® gene expression assay probe and 3.5 µL nuclease-free water. The made-up PCR master mix was pipetted into a 96-well PCR plate (9 µL per well) with 1 µL cDNA per well.

Treatment plates were measured using the standard curve method, a 10-fold serial dilution was constructed using a combination of control and treatment samples. Housekeeping genes were used to normalise the relative expression across the various genes tested. *β-Actin* was used to normalise samples of the *in vitro* model and *Hprt* was used to normalise the samples of the *in vivo* model, as *β-Actin* was regulated in the mouse liver samples. The fold change was

calculated using the equation: fold change = $\left(\frac{\text{treatment - normal control}}{\text{normal control}}\right)$ and the treatments were compared to the control which was set at 1. Real time qPCR was analysed in duplicate and once prepared the plates were then shaken and centrifuged on a benchtop centrifuge and the reaction was run at standard PCR conditions (Table 3.2) using *ABI 7500 Real-Time PCR System,* (*Applied Biosystems, Foster City, CA, USA*).

Table 3.3 List of *in vitro* TaqMan® gene expression assay probes.

TaqMan® gene expression symbol:	**TaqMan® gene expression name:**	**Target species:**	**Gene name:**
PRKAA1	Hs01562307_mH	Human	*AMPK-α*
MLXIPL	Hs00975714_m1	Human	*ChREBP*
FASN	Hs01005622_m1	Human	*FASN*
G6PC	Hs02802676_m1	Human	*G6PC*
SLC2A2	Hs01096906_g1	Human	*GLUT2*
GPX2	Hs01591589_m1	Human	*GPX2*
IRS1	Hs00178563_m1	Human	*IRS-1*
PCK1	Hs00159918_m1	Human	*PCK1*
PPARA	Hs00947536_m1	Human	*PPAR-α*
PPARG	Hs01115513_m1	Human	*PPAR-γ*
SOD2	Hs00167309_m1	Human	*SOD2*
SREBF1	Hs02561944_s1	Human	*SREBF1*
ACTB	Hs03023943_g1	Human	*β-ACTIN* (Housekeeping)

Table 3.4 List of *in vivo* TaqMan® gene expression assay probes.

TaqMan® gene expression symbol:	**TaqMan® gene expression name:**	**Target species:**	**Gene name:**
Mlxipl	Mm02342723_m1	Mouse	*Chrebp*
Casp3	Mm01195085_m1	Mouse	*Caspase-3*
Fasn	Mm00662319_m1	Mouse	*Fasn*
Slc2a2	Mm00446229_m1	Mouse	*Glut2*
Irs1	Mm01278327_m1	Mouse	*Irs-1*
Ppara	Mm00440939_m1	Mouse	*Ppar-α*
Pparg	Mm00440940_m1	Mouse	*Ppar-γ*
Sod2	Mm01313000_m1	Mouse	*Sod2*
Srebf1	Mm00550338_m1	Mouse	*Srebf1*
Hprt	Mm03024075_m1	Mouse	*Hprt* (Housekeeping)

3.7 Protein expression and quantification:

Cell lysates were prepared from harvested C3A cells on ice using *Invitrogen™ Tissue Extraction Reagent I* (*ThermoFischer Scientific™, Massachusetts, USA*). The total protein was harvested from the lysates and Western blot analysis was then conducted using methods previously described by Johnson *et al.* [153]. Protein concentrations were determined using a *Pierce™ BCA Protein Assay Kit* (*ThermoFischer Scientific™, Massachusetts, USA*) and equal amounts of proteins were separated on a 12% SDS PAGE and electro-transferred onto polyvinylidene fluoride (PVDF) membrane, to detect proteins involved in; insulin signalling (IRS1 and PI3K), lipid and glucose metabolism (AKT, AMPK-α, PPAR-γ and MLYCD) oxidative stress (GSTZ1), inflammatory response (TNF-α) and apoptotic pathways (Caspase-3), respectively.

Liver tissue lysates were prepared from 50 mg of harvested liver tissue kept on ice using *Invitrogen™ Tissue Extraction Reagent I* (*ThermoFischer Scientific™, Massachusetts, USA*). Western blot analysis was then carried out according to established methods at the SAMRC (South African Medical Research Council) BRIP (Biomedical Research and Innovations Platform) [153]. Protein concentrations were determined using a *Pierce™ BCA Protein Assay Kit* (*ThermoFischer Scientific™, Massachusetts, USA*) and equal amounts of proteins were separated on a 12% SDS PAGE and electro-transferred onto polyvinylidene fluoride (PVDF) membrane, to detect proteins involved in; lipid and glucose metabolism (AKT, AMPK-α, PPAR-α and MLYCD) oxidative stress (GSTZ1), inflammatory response (TNF-α) and apoptotic pathways (Caspase-3), respectively.

Following cell or tissue harvesting, a stainless-steel bead (*Qiagen™, Hilden, Germany*) was added to each 2 mL centrifuge tube containing the cell suspension or liver tissue. The samples were then homogenised using *TissueLyser* (*Qiagen™, Hilden, Germany*) at 25 Hz for sixty seconds, this was repeated 5-6 times, with 1 min intervals on ice. The homogenised samples were then centrifuged at 15000 x *g* for 15 min at 4 °C using. The supernatant containing the total protein was carefully removed and transferred into 1.5 mL centrifuge tube for storage at -20 °C.

Total protein concentrations were determined using *Pierce™ BCA Protein Assay kit* (*ThermoFischer Scientific™, Massachusetts, USA*). The BCA working reagent was prepared by adding 50 parts of solution A with 1 part of solution B, as per manufacturer's instructions. A 10 µL volume of BSA standards (0.125 µg/mL to 2 µg/mL) was pipetted into a 96-well flat-

bottom assay plate. The same volume of the experimental samples was pipetted into the assay plate and 200 µL of the working reagent was added to each well containing 10 µL of the sample or standard. The assay plate containing the samples and reagents was placed onto a plate shaker and generously mixed by shaking for 10 sec. The assay plate was then incubated at 37 °C for 30 min before the absorbances (570 nm) of the samples were read on a plate reader *ELx800* (*BioTek®, Winooski, VT, USA*). The absorbance readings from the BCA assay was used to calculate the concentrations of the experimental samples by extrapolating the data from the standard curve.

3.7.1 Casting and running sodium dodecyl sulphate polyacrylamide gel electrophoresis (SDS-PAGE):

The protein samples were separated using a 12% SDS PAGE prepared using *TGX Stain-free FastCast Acrylamide kit* (*Bio-Rad, Hercules, USA*). The gels were prepared based on the number of gels needed, in a glass beaker. The resolver gel was poured into 1.5 mm Bio-Rad (*Bio-Rad, Hercules, USA*) spacer plates, leaving 1.5 cm for the stacking gel, and the gel was allowed to polymerise over 30 min. The stacking gel was then prepared and poured over the polymerised resolver gel and based on the number of samples, an appropriate well-forming comb was added without trapping any bubbles, while the gel polymerised over 30 min.

Once the gels have set the glass plates were removed from the casting tray and were installed into the mini cell buffer dam. A 1x running buffer was made up and poured into the inner chamber until an overflow was reached. Protein samples were allowed to thaw on ice and were then diluted (1:1) with 2x Laemmli sample buffer [154]. The samples were heated at 95 °C for 5 min on the *AccuBlock* digital dry bath (*Labnet™, Edison, NJ, USA*), then immediately put back on ice.

A *Precision Plus Protein All Blue* ladder (5 µL) and the protein samples (30 µg) were loaded into each well of the 12% polyacrylamide gel for a total protein profiling gel, which was then electrophoresed at 150 V for 1 h. Following electrophoresis, the total protein profiling gels were then stained in 0.1% (w/v) *Coomassie Brilliant Blue* stain overnight before destaining in a destaining solution and an image was then processed on a *ChemiDoc MP* (*Bio-Rad, Hercules, USA*). The same methodology was followed when running gels for Western Blot analysis, however, a *Precision Protein Western C Standard* ladder was used as a molecular weight marker instead.

3.7.2 PVDF membrane equilibration and protein transfer:

Immuno-Blot Polyvinylidene fluoride (*PVDF*) *membranes* (*Bio-Rad, Hercules, USA*) and *Whatman* filter paper were cut to fit the size of the gels (8 x 6 cm) and (9 x 7 cm) respectively. The membranes were soaked in absolute methanol for a minute to activate the membranes. The membranes, the filter paper as well as the SDS PAGE gels were then soaked in transfer buffer for 10 min to equilibrate them for the protein transfer step. The transfer sandwich cassette was thus assembled by order; three layers of filter paper, a PVDF membrane, an SDS PAGE gel and three layers of filter paper. The sandwich was placed in the *Trans-Blot Turbo Transfer System* (*Bio-Rad, Hercules, USA*) cassette and the lid was locked. The transfer was set to a 1.5 mm gel transfer for 10 min at 25 V.

Following the transfer step, the PVDF membrane was carefully removed from the sandwich and submerged in Ponceau S stain, on a *Stuart Gyro-Rocker SSL3* (*Sigma-Aldrich, St. Louis, USA*) orbital shaker at 50 rpm for 10 min. The membrane was then removed from the stain and washed in distilled water until the background was clear of the red stain, an image was captured on a *ChemiDoc MP* (*Bio-Rad, Hercules, USA*), and the membrane was cut to size avoiding contact with the protein bands before submerging the blot into 1x tris buffered saline – *tween20*® (TBST) to reverse the red stain.

3.7.3 Western blot analysis:

In order to detect the protein of interest, the blot was incubated in 5% fat-free milk prepared in 1x TBST to block the non-specific binding of proteins for 2 h on an orbital shaker. After blocking the blots were then washed with 1x TBST and incubated overnight with the specific primary antibody in 1x TBST, as per table 3.5 below, on an orbital shaker at 4 °C. The morning after, the blot was washed three times in 1x TBST in ten-minute intervals on an orbital shaker. The blot was then incubated in the secondary antibody (Table 3.6), specific to the primary antibody, with 2.5% fat-free milk made up in 1x TBST and 2 µL StrepTactin horseradish peroxidase (HRP) on an orbital shaker for 1.5 h at room temperature.

Following incubation with the secondary antibody (Table 3.6) the proteins of interest were detected using a *LumiGLO Chemiluminescent Substrate Kit* (*ThermoFischer Scientific™, Massachusetts, USA*). A working solution was prepared from the detection kit, with 1-part peroxide solution and 1-part Luminol/enhancer solution. The membrane was therefore

submerged in the working solution for 5 min in a dark place, as the substrate is light sensitive, and the blots were imaged on a *ChemiDoc MP* (*Bio-Rad, Hercules, USA*).

Once the blots were imaged and the proteins were detected, they were washed in 1x TBST for 2 min before the membranes were stripped. Thereafter, the blots were submerged in stripping buffer and incubated for 8 min at room temperature on an orbital shaker. The blots were then removed from the stripping buffer and washed twice in five-minute intervals with PBS, and washed twice more with 1x TBS in five-minute intervals. The stripped membranes were then blocked in 5% fat-free milk for 2 h and incubated overnight with another primary antibody. The next morning the blots were incubated for 1.5 h with the respective secondary antibody in 2.5% fat-free milk at room temperature. β-Actin was used to normalise samples of the *in vitro* model and β-Tubulin was used to normalise the samples of the *in vivo* model, as β-Actin was regulated in the mouse liver samples. The blots were detected and imaged, the stripping was repeated for a maximum of three antibodies per blot (two stripping sessions per blot). The band intensity of the blots was quantified using an ImageLab™ software v6.0.1 (Bio-Rad.com). The fold change was calculated using the equation: $\text{fold change} = \left(\frac{\text{treatment - normal control}}{\text{normal control}}\right)$ and the treatments were compared to the control which was set at 1.

Table 3.5 List of western blot primary antibodies.

Antibody	**Supplier**	**Source**	**Cat. no.**	**Pathway**	**Mwt**
[AKT] Protein Kinase B	Cell Signalling Technology (Danvers, MA, USA)	Rabbit	9272	Adipokine signalling	60 kDa
[phospho-AKT]	Cell Signalling Technology (Danvers, MA, USA)	Rabbit	4060	Adipokine signalling	60 kDa
[ampkα] AMP-Activated Protein Kinase alpha	Cell Signalling Technology (Danvers, MA, USA)	Rabbit	2532	Adipokine/ Insulin signalling	62 kDa
[phospho-AMPKα]	Cell Signalling Technology (Danvers, MA, USA)	Rabbit	2535	Adipokine/ Insulin signalling	62 kDa
Caspase 3	Cell Signalling Technology (Danvers, MA, USA)	Rabbit	9962	Apoptosis	35 kDa

[gstz1] Glutathione Transferase Zeta 1	Abcam (Cambridge, UK)	Rabbit	ab153995	Oxidative Stress	24 kDa
[irs-1] Insulin Receptor Substrate 1	Cell Signalling Technology (Danvers, MA, USA)	Rabbit	3407	Insulin signalling	180 kDa
[mlycd] Malonyl-CoA Decarboxylase	Abcam (Cambridge, UK)	Rabbit	ab95945	Acetyl-CoA Biosynthesis	52 kDa
[pi3k] Phosphoinositide 3-Kinase	Cell Signalling Technology (Danvers, MA, USA)	Rabbit	4257	Insulin signalling	85 kDa
β-Actin	Santa Cruz Biotechnology (Dallas, TX, USA)	Mouse	sc-47778	Loading Control Protein	43 kDa
β-Tubulin	Cell Signalling Technology (Danvers, MA, USA)	Rabbit	2146	Loading Control Protein	55 kDa
[ppar-γ] Peroxisome Proliferator-Activated Receptor gamma	Cell Signalling Technology (Danvers, MA, USA)	Rabbit	2435	Adipokine/ Insulin signalling	57 kDa
[tnf-α] Tumour Necrosis Factor alpha	Cell Signalling Technology (Danvers, MA, USA)	Rabbit	11948	Inflammatory Response	28 kDa
[ppar-α] Peroxisome Proliferator-Activated Receptor alpha	Abcam (Cambridge, UK)	Rabbit	ab8934	Adipokine/ Insulin signalling	52 kDa

Table 3.6 List of western blot secondary antibodies.

Antibody	**Reference/Supplier**	**Source**	**Cat. no.**
IgG Anti-Rabbit HRP-Linked	Cell Signalling Technology (Danvers, MA, USA)	Rabbit	7074
IgG Anti-Mouse HRP-Linked	Cell Signalling Technology (Danvers, MA, USA)	Mouse	7076

3.8 Statistical analysis:

The data is presented as mean ± standard error of the mean (SEM) ($n \geq 3$, unless stated otherwise). The comparison among the groups of the raw data from the biochemical assays, Western blots and mRNA expression were analysed using one-way ANOVA followed by Tukey's multiple comparisons test, Using *GraphPad Prism version 7.00 for Macintosh, GraphPad Software, La Jolla California USA,* www.graphpad.com. The differences were considered to be significantly different when $p < 0.05$.

4. Results

4.1 *In vitro* biochemical assays and staining techniques

4.1.1 *Cell viability (MTT) and lipid analysis (ORO)*

The MTT assay data (Figure 4.1) illustrates a significant reduction in cell mitochondrial activity with the oleic acid-induced control ($p < 0.05$). This reduction was also seen with the various treatments when compared to the normal control, except for pioglitazone 30 µM, Afriplex GRT 10 and 100 µg/mL treatments. No significant changes were observed when comparing the various treatments to the induced control. Barring the significant decrease in mitochondrial activity, the cells still expressed over 70% mitochondrial activity, suggesting that both the induction period with oleic acid and subsequent treatment with Afriplex GRT and pioglitazone was not cytotoxic.

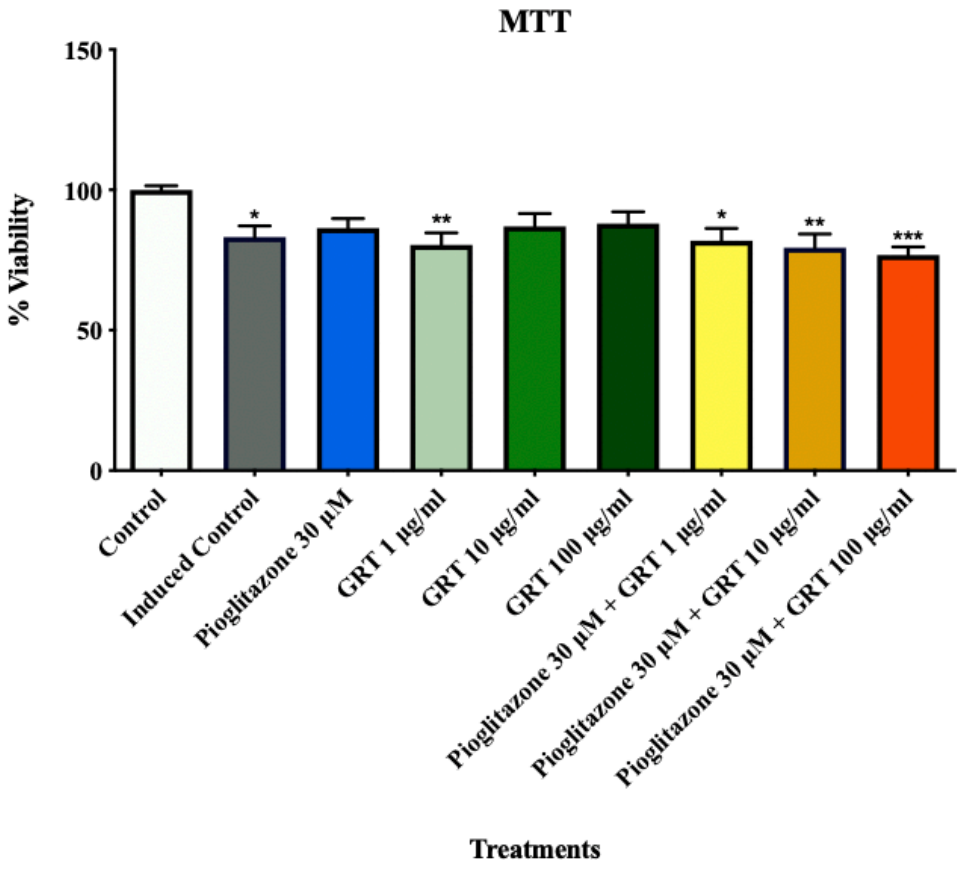

Figure 4.1 MTT assay, showing the effects of steatosis induction [1 mM oleic acid] along with the effects of anti-steatotic effects of various treatments with pioglitazone and/or Afriplex GRT (GRT), on cell viability. Data represented as mean ± SEM (n = 3), where *P < 0.05, **P < 0.01 and ***P < 0.001 when compared to the normal control.

Oil red O data (Figure 4.2) illustrates a significant increase in lipid content for the induced control ($p < 0.01$) when compared to the normal control. Subsequent treatment with pioglitazone showed a slight decrease in lipid content when compared to the induced control. Treatment with Afriplex GRT induced a slight but dose-dependent reduction in lipid content when compared to the induced control. A significant reduction in lipid content was observed following two of the combination treatments (pioglitazone 30 µM + Afriplex GRT 1 µg/ml and pioglitazone 30 µM + Afriplex GRT 10 µg/ml) ($p < 0.05$) when compared to the induced control.

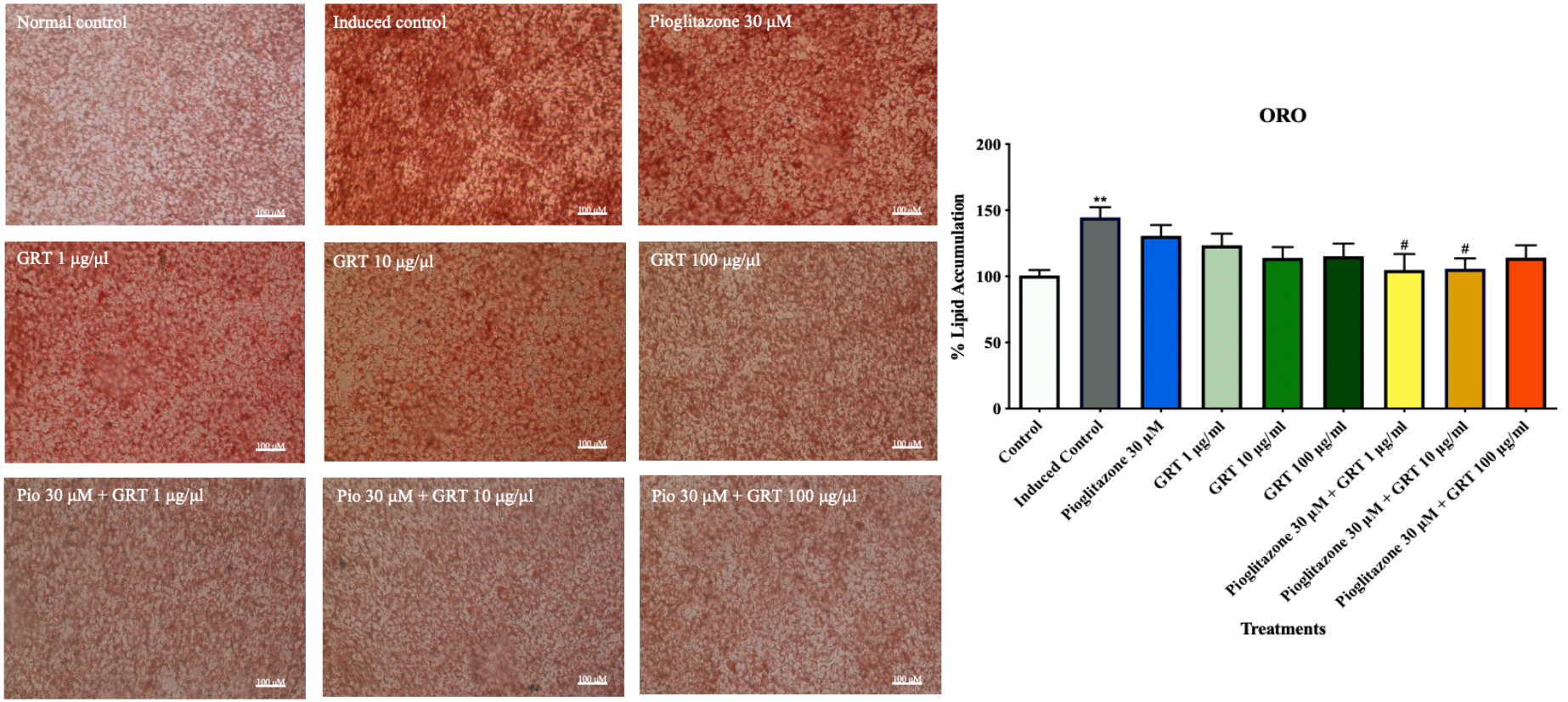

Figure 4.2 Oil red O assay, showing the effects of steatosis induction [1 mM oleic acid] along with the anti-steatotic effects of various treatments with pioglitazone and/or Afriplex GRT (GRT), on lipid accumulation. Images are a representation of one experiment, captured at 200x magnification using a Nikon Eclipse Ti/S light microscope (scale represents: 100µm). Histogram illustrates spectrophotometric data of three independent repeats of the destained section oil red O assay. Data represented as mean ± SEM (n = 3), where **P < 0.01 when compared to the normal control and $^{\#}$P < 0.05, when compared to the induced control respectively.

4.1.2 *Mitochondrial depolarisation (JC-1)*

Figure 4.3 illustrates data generated from exposing the treated cells to a lipophilic cationic fluorescent dye; 5,5,6,6'-tetrachloro- 1,1',3,3'-tetraethylbenzimi-dazoylcarbocyanine iodide (JC-1), which serves as an indicator of mitochondrial membrane potential (mitochondrial depolarisation). Healthy cells such as the normal control in this study showed an intense red fluorescence, this is expected as the dye enters the mitochondria and forms J-aggregates that change the fluorescent property of the JC-1 dye. Unhealthy cells such as the induced control in the study show an intense green fluorescence, as the dye does not form J-aggregates due to its low mitochondrial membrane potential and the dye remains in its monomeric form. Therefore, the higher the ratio of green to red fluorescence the higher the depolarisation of mitochondrial membrane. Densitometric data shown by the histogram shows a significant reduction in red fluorescence when comparing the induced control to the normal control ($p < 0.0001$). This reduction was also seen across the various treatments, whereas Afriplex GRT 100 µg/mL and the highest dose of the combination treatment (pioglitazone 30 µM + Afriplex GRT 100 µg/mL) slightly improved the condition when compared to the normal control ($p < 0.001$). Interestingly, treatment with Afriplex GRT 100 µg/mL and the highest dose of the combination treatment (pioglitazone 30 µM + Afriplex GRT 100 µg/mL) showed a significant increase in red fluorescence when compared to the induced control ($p < 0.0001$), suggesting that the treatment with Afriplex GRT 100 µg/mL restored the mitochondrial membrane potential when compared to the induced control with no additive effects from pioglitazone 30 µM. However, the increase in fluorescence was still not enough to match the level observed from the normal control.

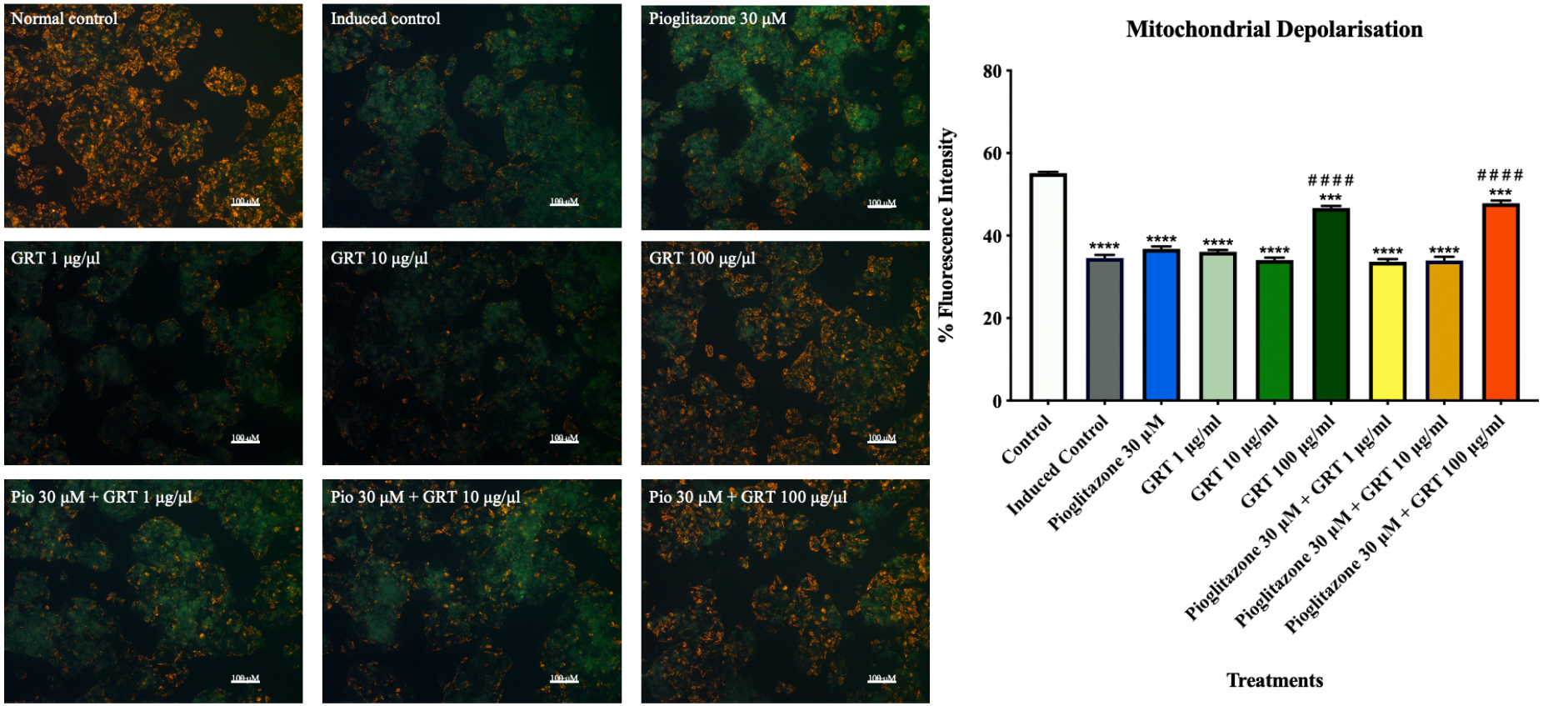

Figure 4.3 JC-1 assay, showing the effects of steatosis induction [1 mM oleic acid] along with the anti-steatotic effects of various treatments with pioglitazone and/or Afriplex GRT (GRT), on mitochondrial depolarisation. Images are a representation of one experiment, captured at 200x magnification using a Nikon Eclipse Ti/S Fluorescence Microscope (scale represents: 100µm). Histogram illustrates densitometric quantification data from the images captured following the JC-1 assay. The red fluorescence shown in the images was quantified using ImageJ32.app software. Data represented as mean ± SEM (n = 3), where ***P < 0.001 and ****P < 0.0001 when compared to the normal control and $^{\#\#\#\#}$P < 0.0001, when compared to the induced control respectively.

4.2 *In vitro* mRNA expression (qRT-PCR)

Figure 4.4 illustrates differences in the mRNA expression data of genes involved in lipid metabolism, fold change was calculated using the equation: fold change = $\left(\frac{\text{treatment - normal control}}{\text{normal control}}\right)$ and the treatments were compared to the control which was set at 1. Figure 4.4 (**a**) *AMPK-α* is shown to be significantly down-regulated by Afriplex GRT 100 µg/mL treatment ($p < 0.05$), when compared to the induced control, and no other significant differences were observed. *ChREBP* in Figure 4.4 (**b**) showed a significant upregulation with the induced control ($p < 0.05$), when compared to the normal control, and treatment with pioglitazone 30 µM ($p < 0.05$), Afriplex GRT 10 µg/mL ($p < 0.01$) as well as the highest concentration of the combination treatment (pioglitazone 30 µM + Afriplex GRT 100 µg/mL) ($p < 0.01$) showed a significant down-regulation when compared to the induced control. *FASN* in Figure 4.4 (**c**) also showed a significant upregulation with the induced control when compared to the normal control ($p < 0.05$), however, no other significant differences were observed. *SREBF1* in Figure 4.4 (**d**) showed a slight upregulation with the induced control when compared to the normal control, but the difference was insignificant. Treatment with pioglitazone 30 µM and Afriplex GRT 100 µg/mL showed a significant down-regulation when compared to the induced control ($p < 0.05$).

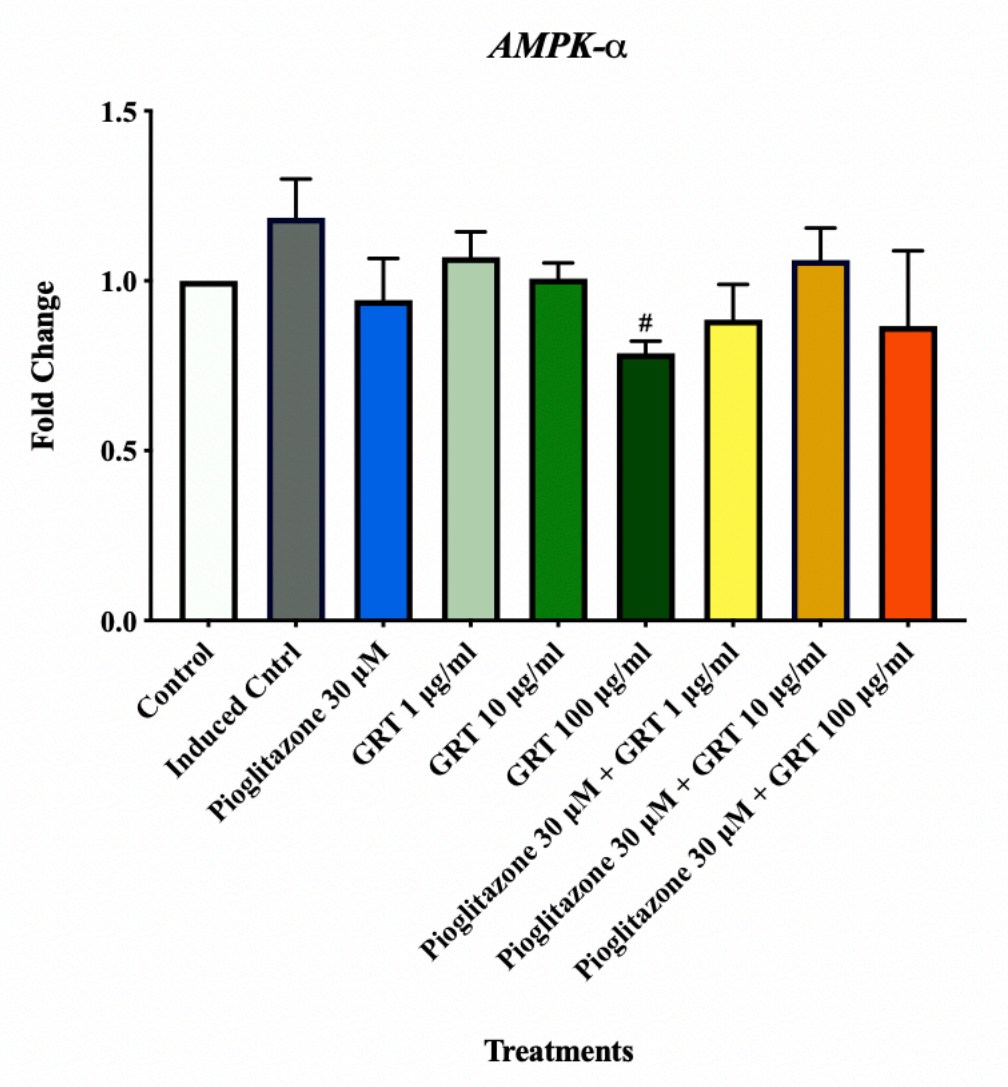

Figure 4.4 (a) *AMPK-α* mRNA expression of C3A cell-lysates normalised to *β-actin*, showing the effects of 24 h steatosis induction [1 mM oleic acid] along with the anti-steatotic effects of various treatments with pioglitazone and/or Afriplex GRT (GRT). Data represented as mean ± SEM (n = 3), where $^{\#}P < 0.05$ when compared to the induced control.

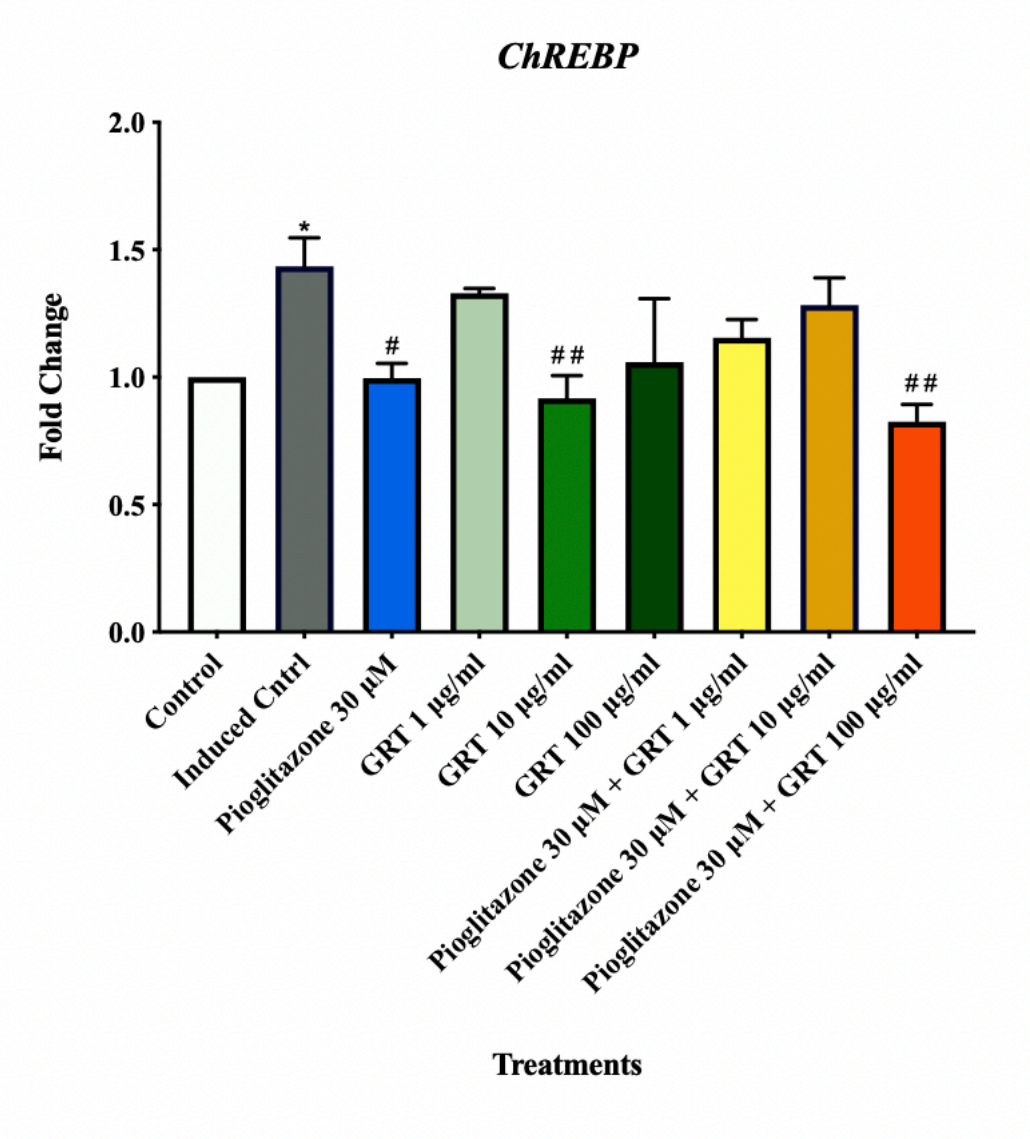

Figure 4.4 (b) *ChREBP* mRNA expression of C3A cell-lysates normalised to *β-actin*, showing the effects of 24 h steatosis induction [1 mM oleic acid] along with the anti-steatotic effects of various treatments with pioglitazone and/or Afriplex GRT (GRT). Data represented as mean ± SEM (n = 3), where *P < 0.05, when compared to the normal control and $^{\#}P < 0.05$, $^{\#\#}P < 0.01$ when compared to the induced control.

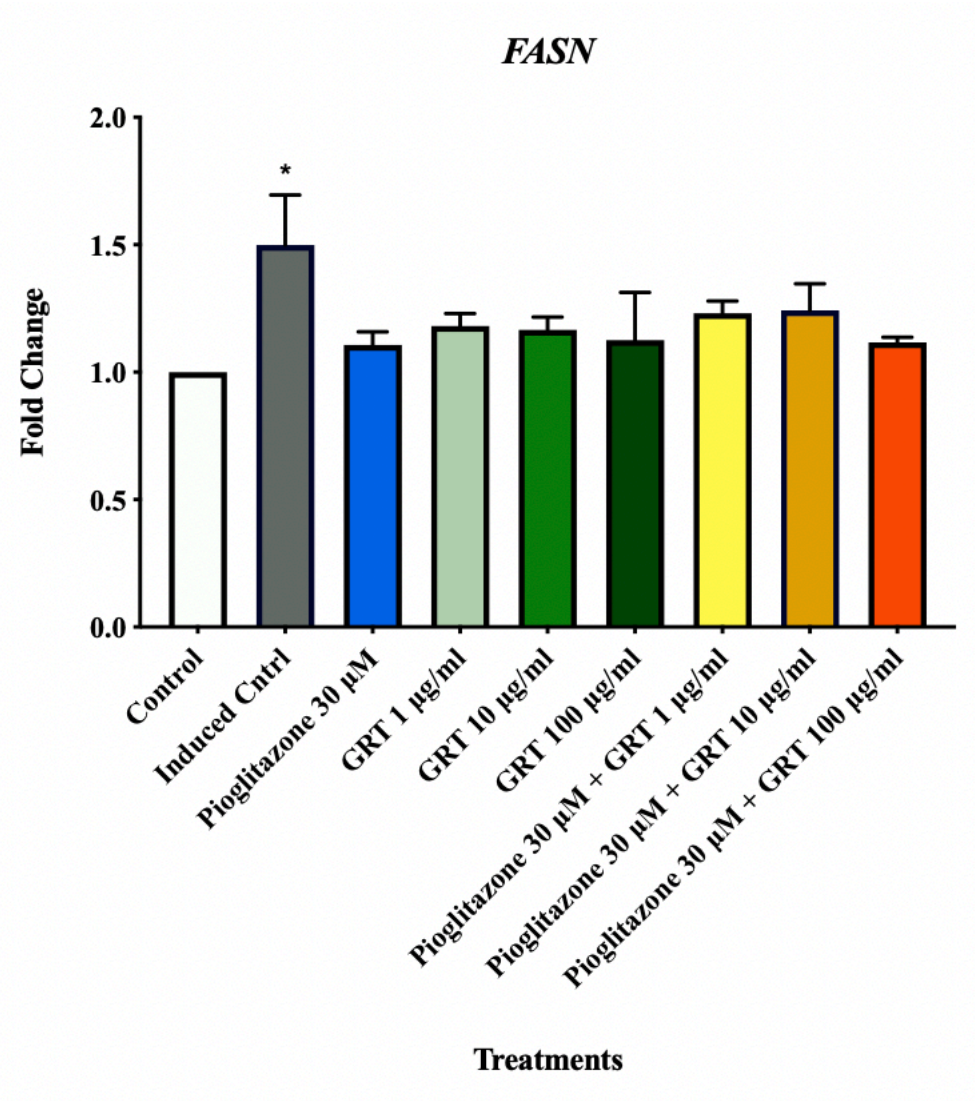

Figure 4.4 (c) *FASN* mRNA expression of C3A cell-lysates normalised to *β-actin*, showing the effects of 24 h steatosis induction [1 mM oleic acid] along with the anti-steatotic effects of various treatments with pioglitazone and/or Afriplex GRT (GRT). Data represented as mean ± SEM (n = 3), where *P < 0.05, when compared to the normal control.

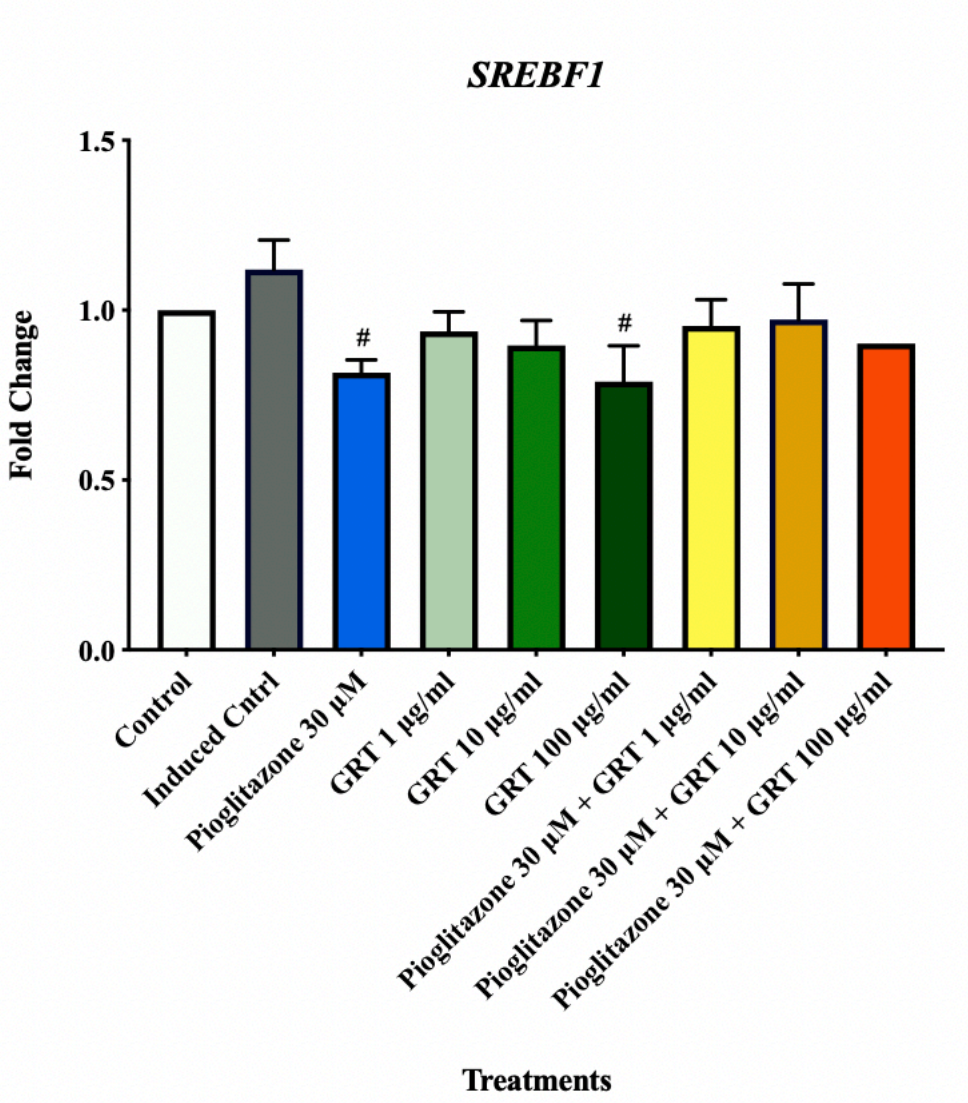

Figure 4.4 (d) *SREBF1* mRNA expression of C3A cell-lysates normalised to *β-actin*, showing the effects of 24 h steatosis induction [1 mM oleic acid] along with the anti-steatotic effects of various treatments with pioglitazone and/or Afriplex GRT (GRT). Data represented as mean ± SEM (n = 3), where $^{\#}P < 0.05$ when compared to the induced control.

Figure 4.5 data shows mRNA expression of genes involved in glucose metabolism and insulin signalling, fold change was calculated using the equation: fold change = $\left(\frac{\text{treatment - normal control}}{\text{normal control}}\right)$ and the treatments were compared to the control which was set at 1. *GLUT2* in Figure 4.5 (**a**) showed a slight upregulation in expression due to oleic acid treatment in the induced control when compared to the normal control, but the difference was not significantly different. Treatment with the low dose combination treatment (pioglitazone 30 µM + Afriplex GRT 1 µg/mL) showed a significant down-regulation when compared to the normal control ($p < 0.01$), and more so when compared to the induced control ($p < 0.0001$). Treatment with the high dose combination treatment (pioglitazone 30 µM + Afriplex GRT 100 µg/mL) significantly downregulated the mRNA expression of *GLUT2* when compared with the induced control ($p < 0.05$). Further, *G6PC* in Figure 4.5 (**b**) was slightly down-regulated in the induced control when compared with the normal control, and across the various treatments when compared to the normal control except for the mid-dose combination treatment (pioglitazone 30 µM + Afriplex GRT 10 µg/mL), which was slightly upregulated when compared to the normal control. *IRS-1* in Figure 4.5 (**c**) also showed a slight upregulation in the induced control when compared to the normal control however this was not significant. Treatment with Afriplex GRT interestingly showed a significant down-regulation when compared to the induced control ($p < 0.05$), the trend was slightly dose-dependent although the significance was similar across the concentrations of Afriplex GRT. *PCK1* in Figure 4.5 (**d**) showed no significant differences when comparing the induced control to normal control. Treatment with the low and mid-dose combination treatment (pioglitazone 30 µM + Afriplex GRT 1 µg/mL) ($p < 0.01$) and (pioglitazone 30 µM + Afriplex GRT 10 µg/mL) ($p < 0.05$), showed a significant upregulation when compared to both normal and induced controls, with the low dose combination treatment (pioglitazone 30 µM + Afriplex GRT 1 µg/mL) more significant.

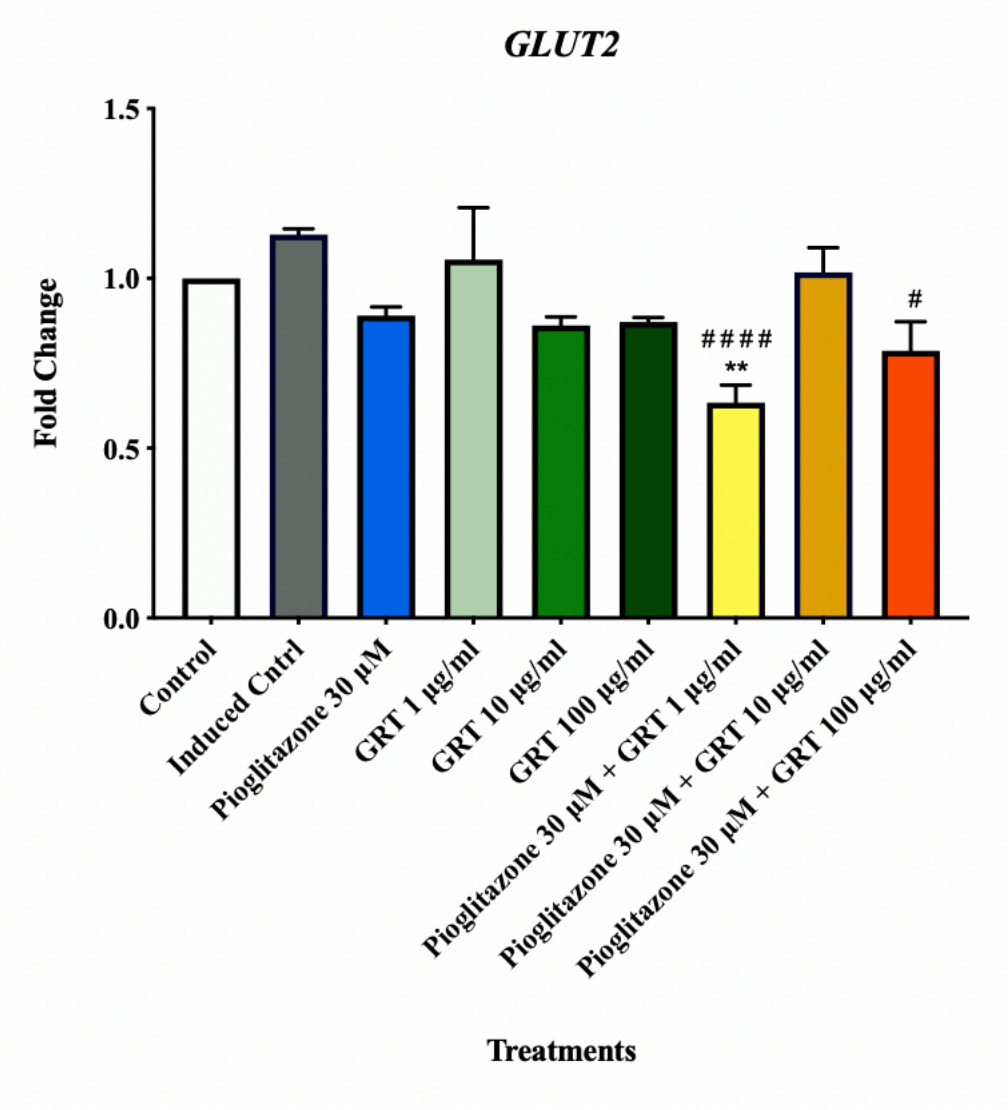

Figure 4.5 (a) *GLUT2* mRNA expression of C3A cell-lysates normalised to *β-actin*, showing the effects of 24 h steatosis induction [1 mM oleic acid] and the anti-steatotic effects of various treatments with pioglitazone and/or Afriplex GRT (GRT). Data represented as mean ± SEM (n = 3), where **P < 0.01, when compared to the normal control and $^{\#}$P < 0.05, $^{\#\#\#\#}$P < 0.0001 when compared to the induced control.

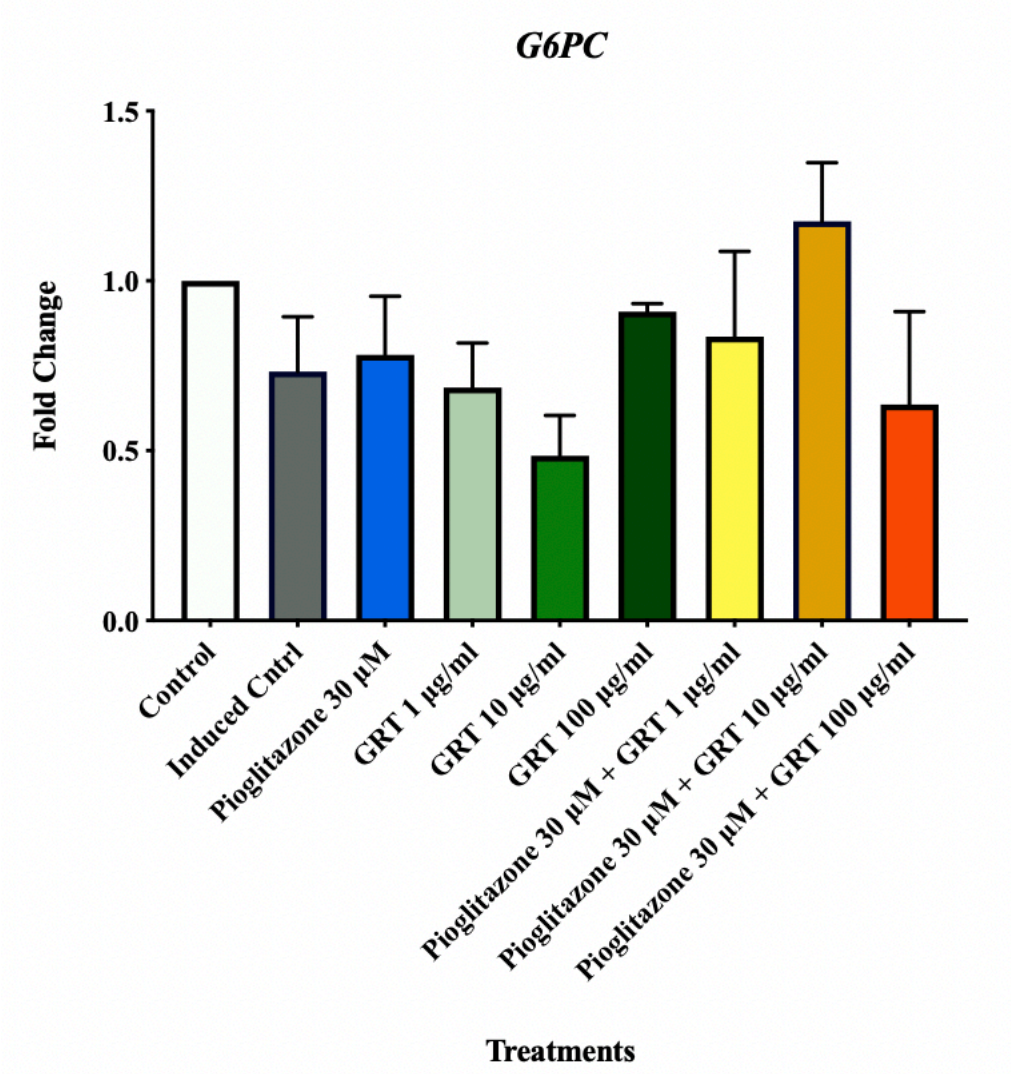

Figure 4.5 (b) *G6PC* mRNA expression of C3A cell-lysates normalised to *β-actin*, showing the effects of 24 h steatosis induction [1 mM oleic acid] and the anti-steatotic effects of various treatments with pioglitazone and/or Afriplex GRT (GRT). Data represented as mean ± SEM (n = 3).

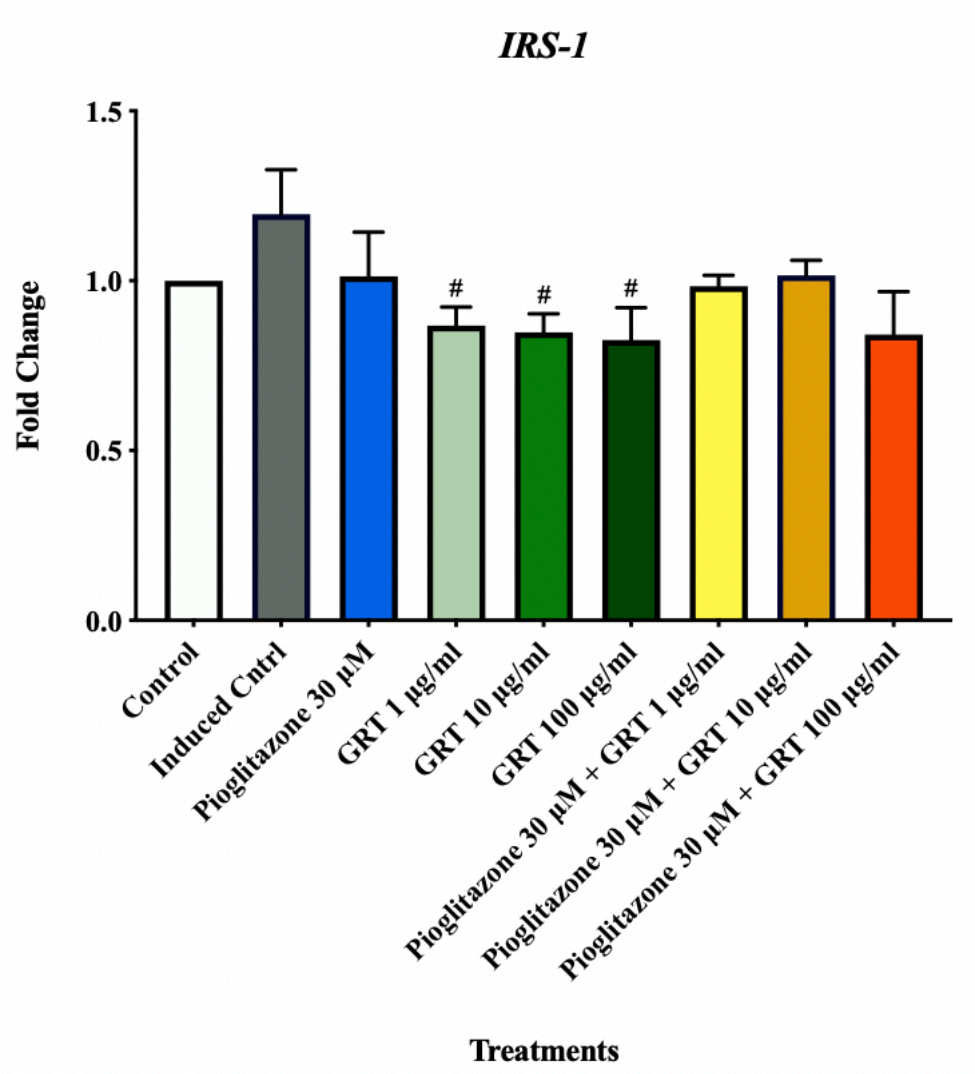

Figure 4.5 (c) *IRS-1* mRNA expression of C3A cell-lysates normalised to *β-actin*, showing the effects of 24 h steatosis induction [1 mM oleic acid] and the anti-steatotic effects of various treatments with pioglitazone and/or Afriplex GRT (GRT). Data represented as mean ± SEM (n = 3), where $^{\#}P < 0.05$ when compared to the induced control.

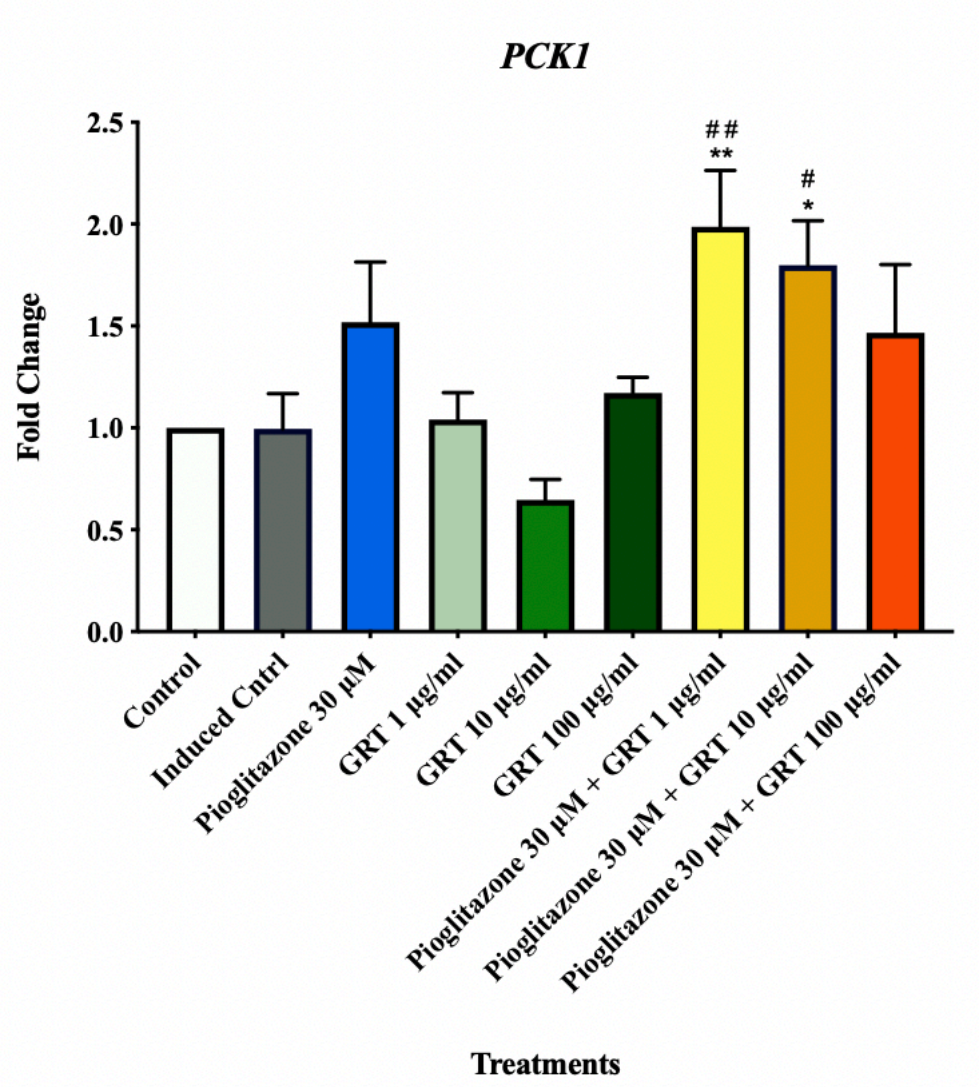

Figure 4.5 (d) *PCK1* mRNA expression of C3A cell-lysates normalised to *β-actin*, showing the effects of 24 h steatosis induction [1 mM oleic acid] and the anti-steatotic effects of various treatments with pioglitazone and/or Afriplex GRT (GRT). Data represented as mean ± SEM (n = 3), where *P < 0.05, **P < 0.01, when compared to the normal control and $^{\#}$P < 0.05, $^{\#\#}$P < 0.01 when compared to the induced control.

No effect was observed with the mRNA expression data (Figure 4.6), of genes involved in lipid and glucose metabolism as well as oxidative stress, fold change was calculated using the equation: fold change = $\left(\frac{\text{treatment - normal control}}{\text{normal control}}\right)$ and the treatments were compared to the control which was set at 1. *PPAR-*α mRNA Figure 4.6 (**a**) was not affected by both the oleic acid-induced stress and the various treatments. However, *PPAR-*γ (Figure 4.6 (**b**)) was slightly upregulated in the induced control when compared to the normal control. Treatment with pioglitazone 30 µM reduced *PPAR-*γ when compared to both normal ($p < 0.05$) and induced controls ($p < 0.01$). Treatment with Afriplex GRT 10 µg/mL ($p < 0.01$) and Afriplex GRT 100 µg/mL ($p < 0.05$) also showed a significant down-regulation when compared to the induced control, with Afriplex GRT 10 µg/ml being more significant. Interestingly the greater effect was observed following the high dose combination treatment (pioglitazone 30 µM + Afriplex GRT 100 µg/mL) when compared to both normal ($p < 0.001$) and induced controls ($p < 0.0001$). Treatment with Afriplex GRT 10 µg/mL and Afriplex GRT 100 µg/mL induced a significant reduction of *SOD2* Figure 4.6 (**c**) when compared to the induced control ($p < 0.01$). Afriplex GRT 10 µg/mL, showed a significant upregulation of *GPX2* Figure 4.6 (**d**) when compared to the normal control ($p < 0.05$).

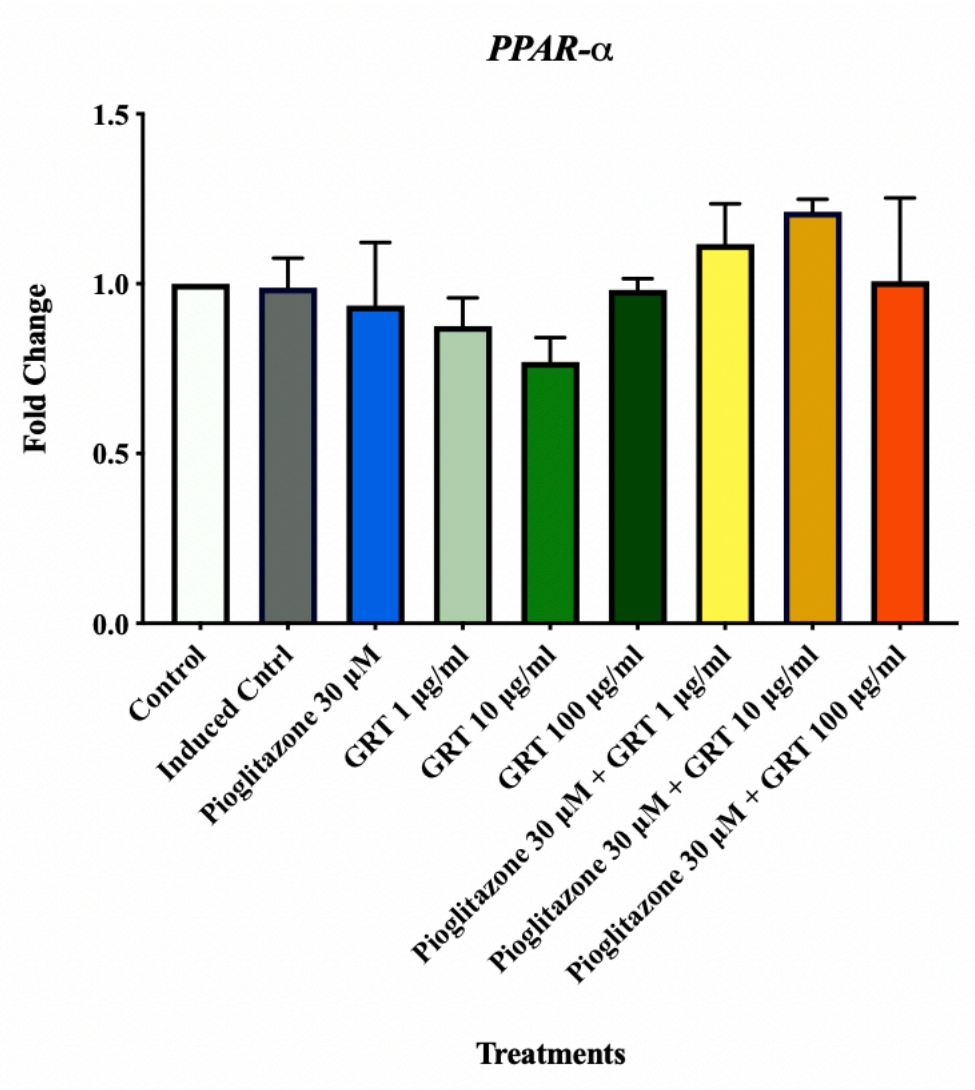

Figure 4.6 (a) *PPAR*-α mRNA expression of C3A cell-lysates normalised to *β-actin*, showing the effects of 24 h steatosis induction [1 mM oleic acid] and the anti-steatotic effects of various treatments with pioglitazone and/or Afriplex GRT (GRT). Data represented as mean ± SEM (n = 3).

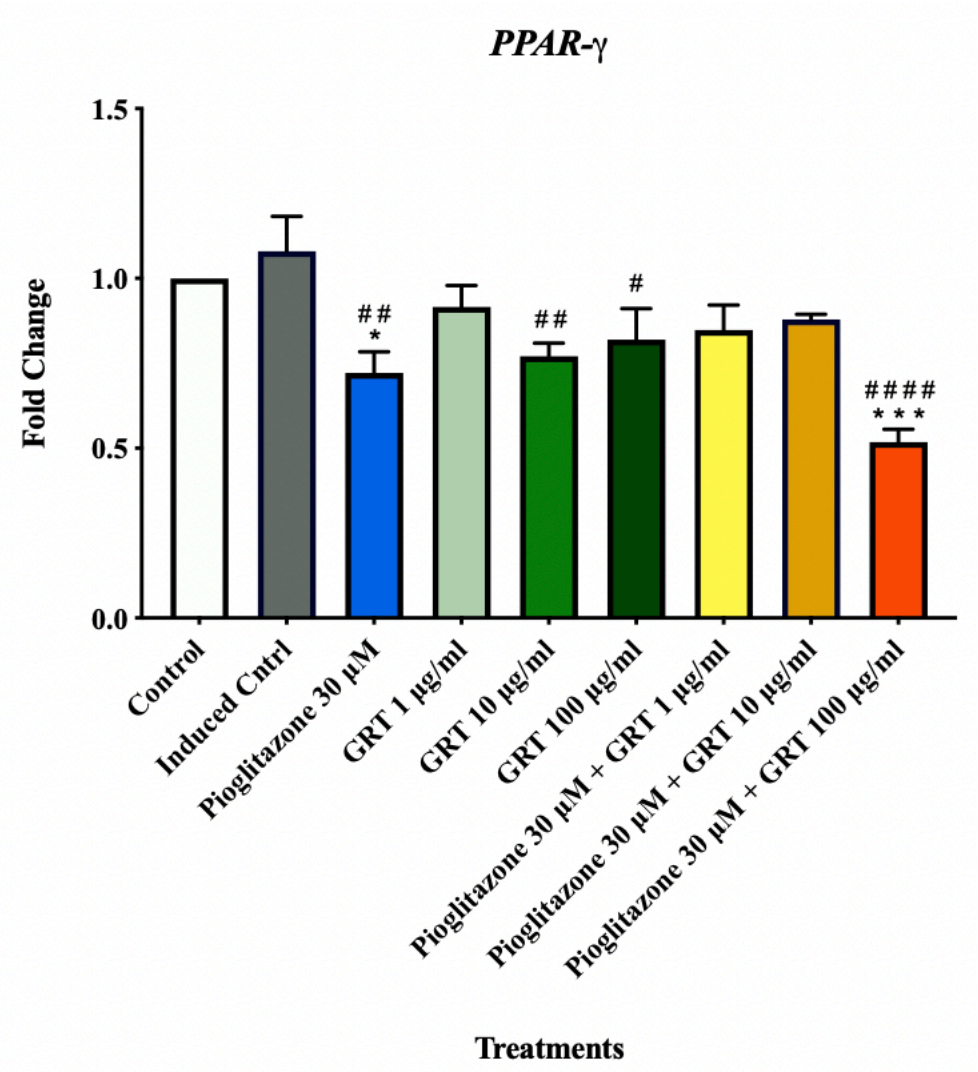

Figure 4.6 (b) *PPAR-γ* mRNA expression of C3A cell-lysates normalised to *β-actin*, showing the effects of 24 h steatosis induction [1 mM oleic acid] and the anti-steatotic effects of various treatments with pioglitazone and/or Afriplex GRT (GRT). Data represented as mean ± SEM (n = 3), where *P < 0.05, ***P < 0.001 when compared to the normal control and $^{\#}$P < 0.05, $^{\#\#}$P < 0.01, $^{\#\#\#\#}$P < 0.0001 when compared to the induced control.

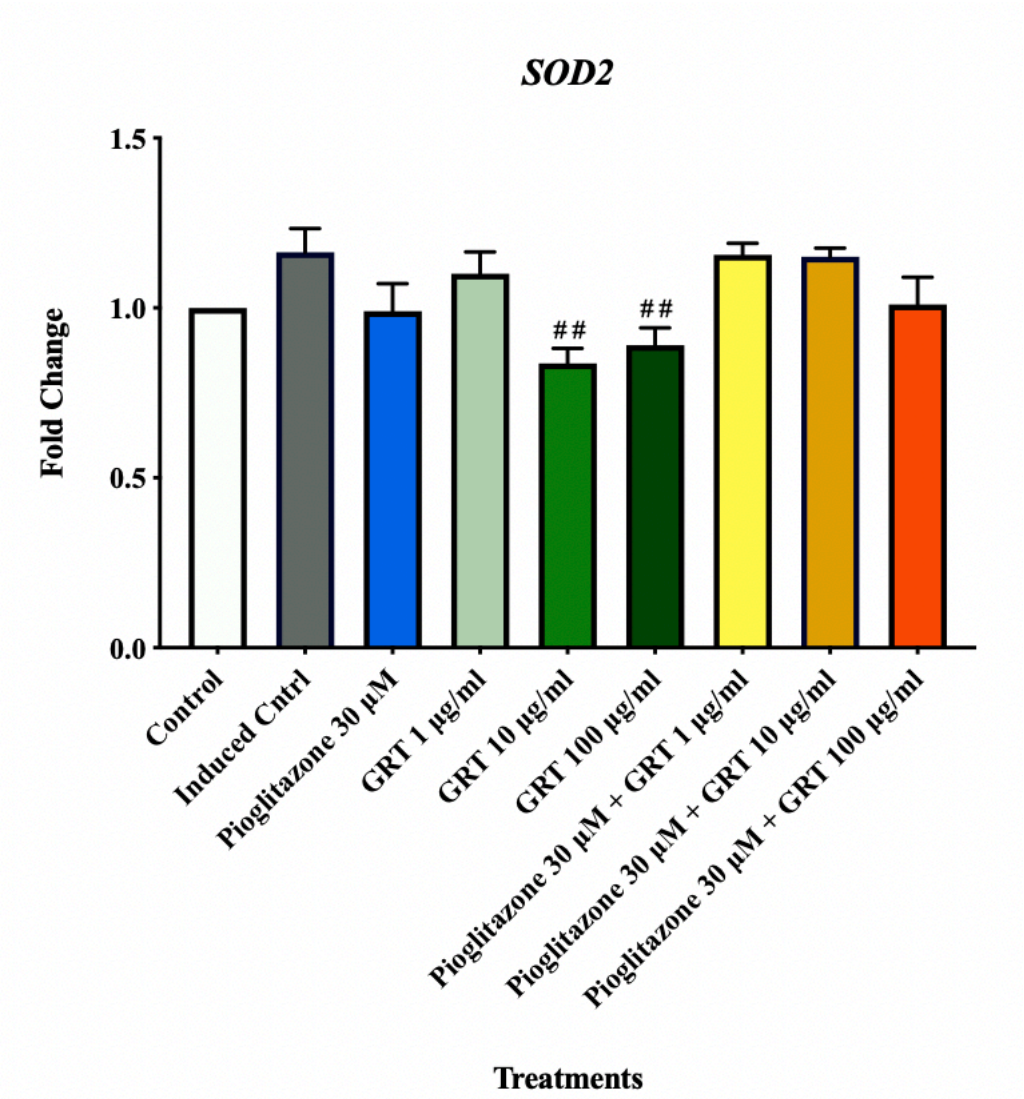

Figure 4.6 (c) *SOD2* mRNA expression of C3A cell-lysates normalised to *β-actin*, showing the effects of 24 h steatosis induction [1 mM oleic acid] and the anti-steatotic effects of various treatments with pioglitazone and/or Afriplex GRT (GRT). Data represented as mean ± SEM (n = 3), where $^{##}P < 0.01$ when compared to the induced control.

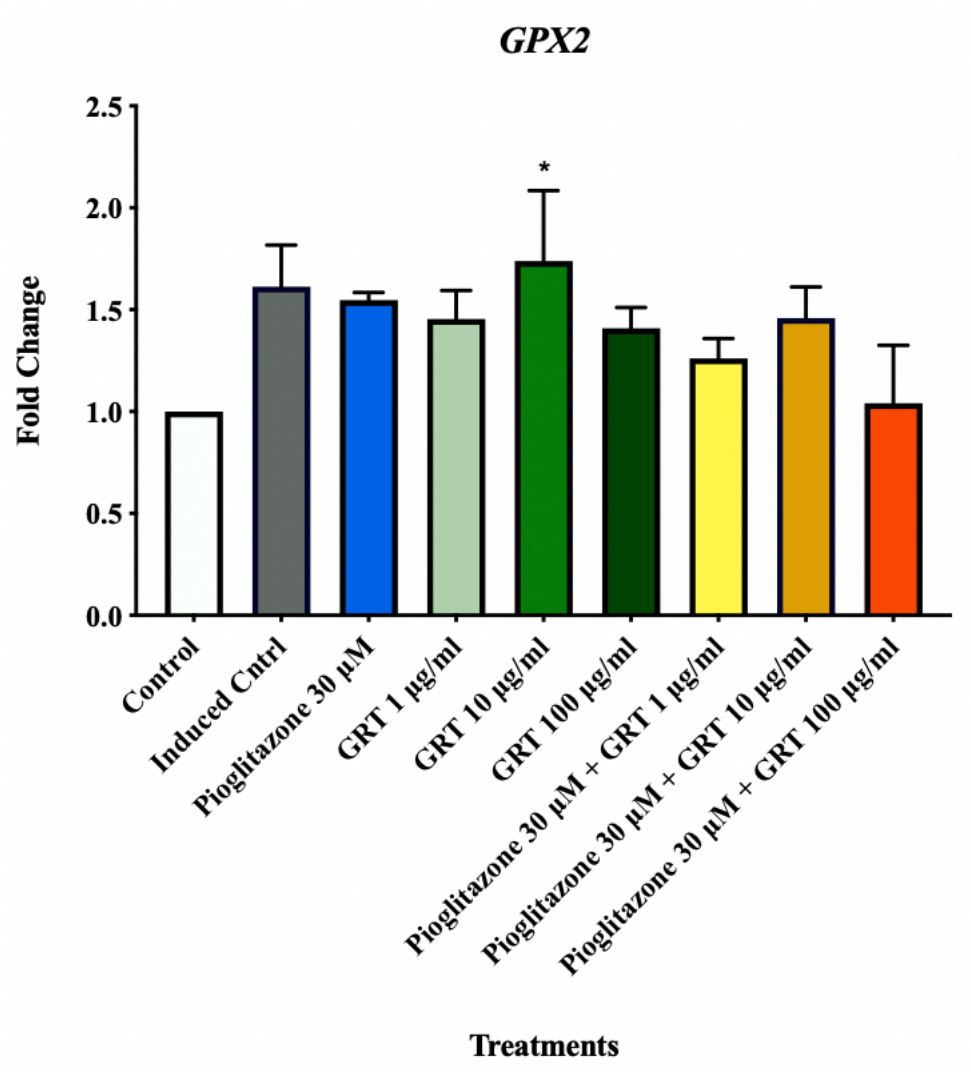

Figure 4.6 (d) *GPX2* mRNA expression of C3A cell-lysates normalised to *β-actin*, showing the effects of 24 h steatosis induction [1 mM oleic acid] and the anti-steatotic effects of various treatments with pioglitazone and/or Afriplex GRT (GRT). Data represented as mean ± SEM (n = 3), where *P < 0.05 when compared to the normal control.

4.3 *In vitro* protein expression (Western blotting)

Figure 4.7 shows the protein expression of C3A for the proteins involved in lipid and glucose metabolism, fold change was calculated using the equation: fold change = $\left(\frac{\text{treatment - normal control}}{\text{normal control}}\right)$ and the treatments were compared to the control which was set at 1. pAKT/AKT ratio in Figure 4.7 (**a**) showed no significant differences when comparing the induced control to normal control. Treatment with pioglitazone 30 µM showed a significant upregulation when compared to the induced control ($p < 0.05$). Treatment with Afriplex GRT 10 µg/mL significantly down-regulated pAKT/AKT ratio when compared to the normal control ($p < 0.05$), while interestingly, treatment with Afriplex GRT 10 µg/mL showed an even greater significant down-regulation when compared to the normal control and induced control ($p < 0.0001$). This was also seen with the low dose combination treatment (pioglitazone 30 µM + Afriplex GRT 1 µg/mL), were pAKT/AKT ratio was significantly down-regulated when compared to the normal ($p < 0.0001$) and the induced controls ($p < 0.01$), respectively. The same was observed with the mid-dose combination treatment (pioglitazone 30 µM + Afriplex GRT 10 µg/mL) as pAKT/AKT ratio was significantly down-regulated when compared to the normal ($p < 0.0001$) and the induced controls ($p < 0.001$), respectively. pAMPK-α/AMPK-α ratio in Figure 4.7 (**b**) showed no significant difference with the induced control when compared to the normal control. However, treatment with Afriplex GRT 10 µg/mL significantly upregulated pAMPK-α/AMPK-α ratio when compared to both normal ($p < 0.01$) and induced controls ($p < 0.05$). No other significant differences observed across the various treatments. MLYCD in Figure 4.7 (**c**) expression was not affected by all treatments.

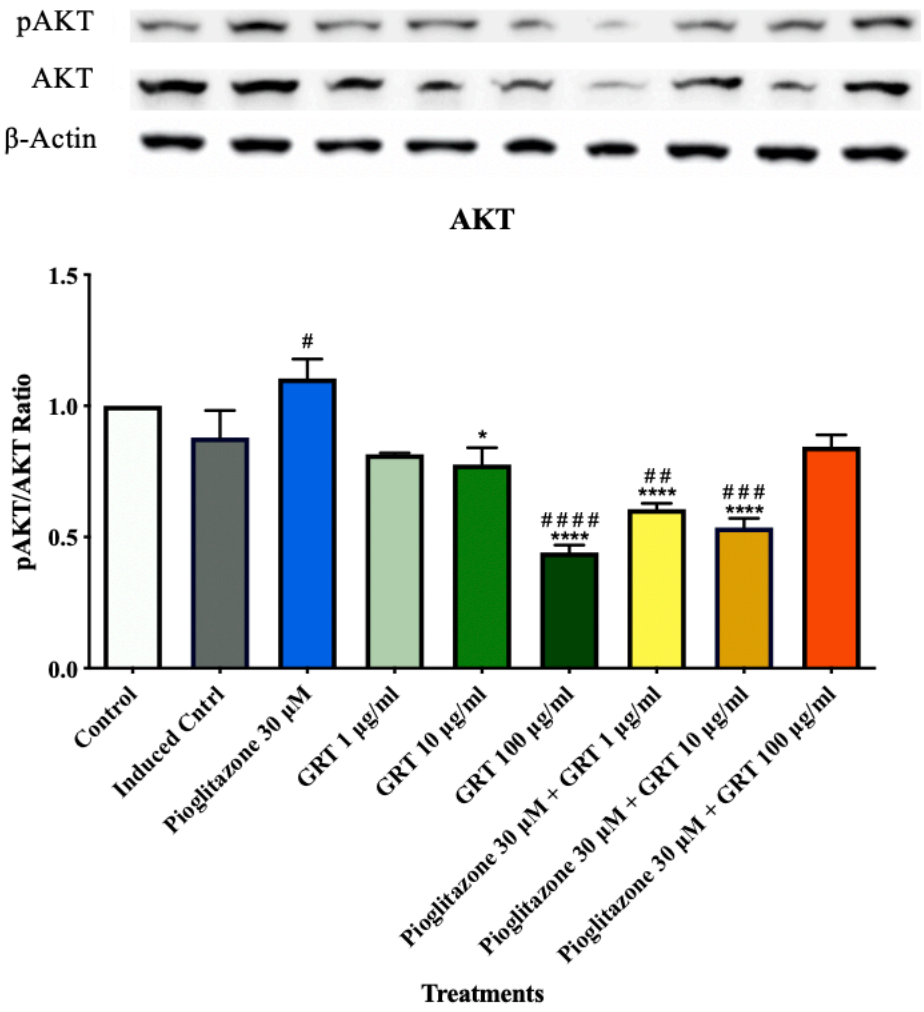

Figure 4.7 (a) pAKT/AKT ratio protein expression of C3A cell-lysates normalised to β-actin, showing the effects of 24 h steatosis induction [1 mM oleic acid] along with the and the anti-steatotic effects of various treatments with pioglitazone and/or Afriplex GRT (GRT). Images are a representation of one experiment, captured using a ChemiDoc MP (Bio-Rad, Hercules, USA). Histogram illustrates densitometric quantification data from the images captured following the Western blot analysis. The band intensity of the blots was quantified using an ImageLab™ software v6.0.1 (Bio-Rad.com). Data represented as mean ± SEM (n = 4), where *P < 0.05, ****P < 0.0001 when compared to the normal control and $^{\#}P < 0.05$, $^{\#\#}P < 0.01$, $^{\#\#\#}P < 0.001$, $^{\#\#\#\#}P < 0.0001$ when compared to the induced control. Lane 1: Control, lane 2: induced control, lane 3: Pio 30 µM, lane 4: GRT 1 µg/mL, lane 5: GRT 10 µg/mL, lane 6: GRT 100 µg/mL, lane 7: Pio + GRT 1 µg/mL, lane 8: Pio + GRT 10 µg/mL, lane 9: Pio + GRT 100 µg/mL.

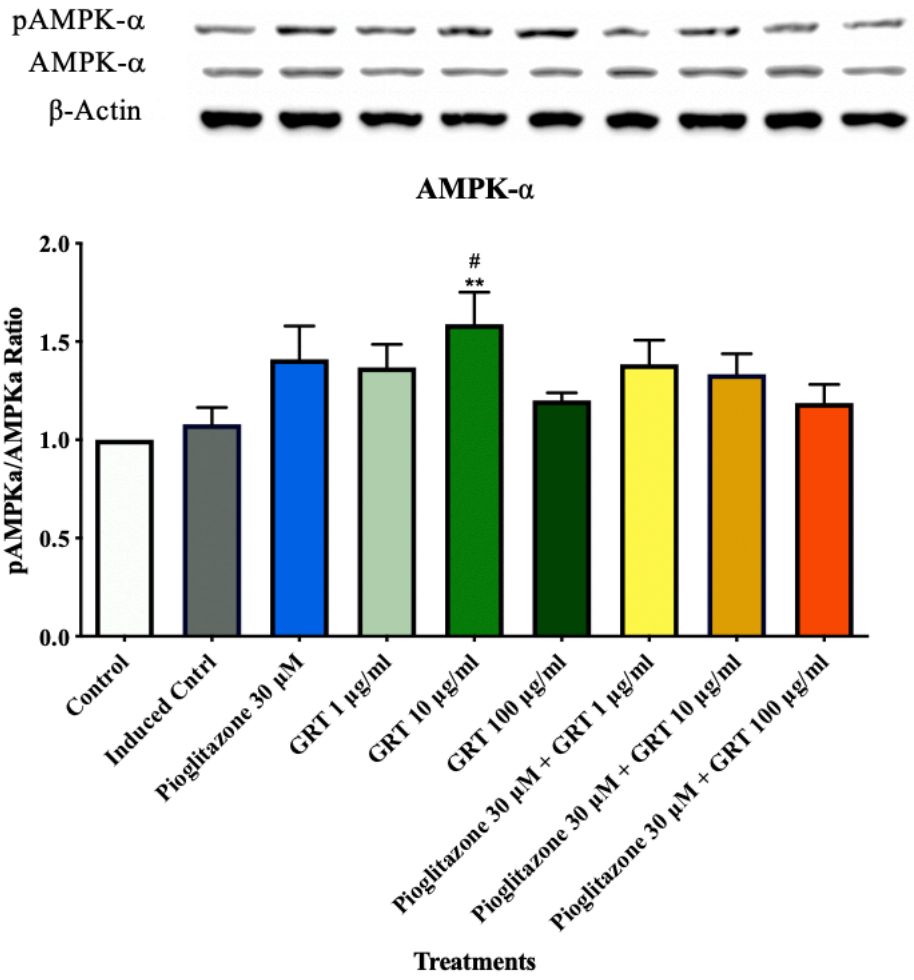

Figure 4.7 (b) pAMPK-α/AMPK-α ratio protein expression of C3A cell-lysates normalised to β-actin, showing the effects of 24 h steatosis induction [1 mM oleic acid] and the anti-steatotic effects of various treatments with pioglitazone and/or Afriplex GRT (GRT). Images are a representation of one experiment, captured using a ChemiDoc MP (Bio-Rad, Hercules, USA). Histogram illustrates densitometric quantification data from the images captured following the Western blot analysis. The band intensity of the blots was quantified using an ImageLab™ software v6.0.1 (Bio-Rad.com). Data represented as mean ± SEM (n = 4), where **$P < 0.01$ when compared to the normal control and $^{\#}P < 0.05$ when compared to the induced control. Lane 1: Control, lane 2: induced control, lane 3: Pio 30 µM, lane 4: GRT 1 µg/ml, lane 5: GRT 10 µg/mL, lane 6: GRT 100 µg/mL, lane 7: Pio + GRT 1 µg/mL, lane 8: Pio + GRT 10 µg/mL, lane 9: Pio + GRT 100 µg/mL.

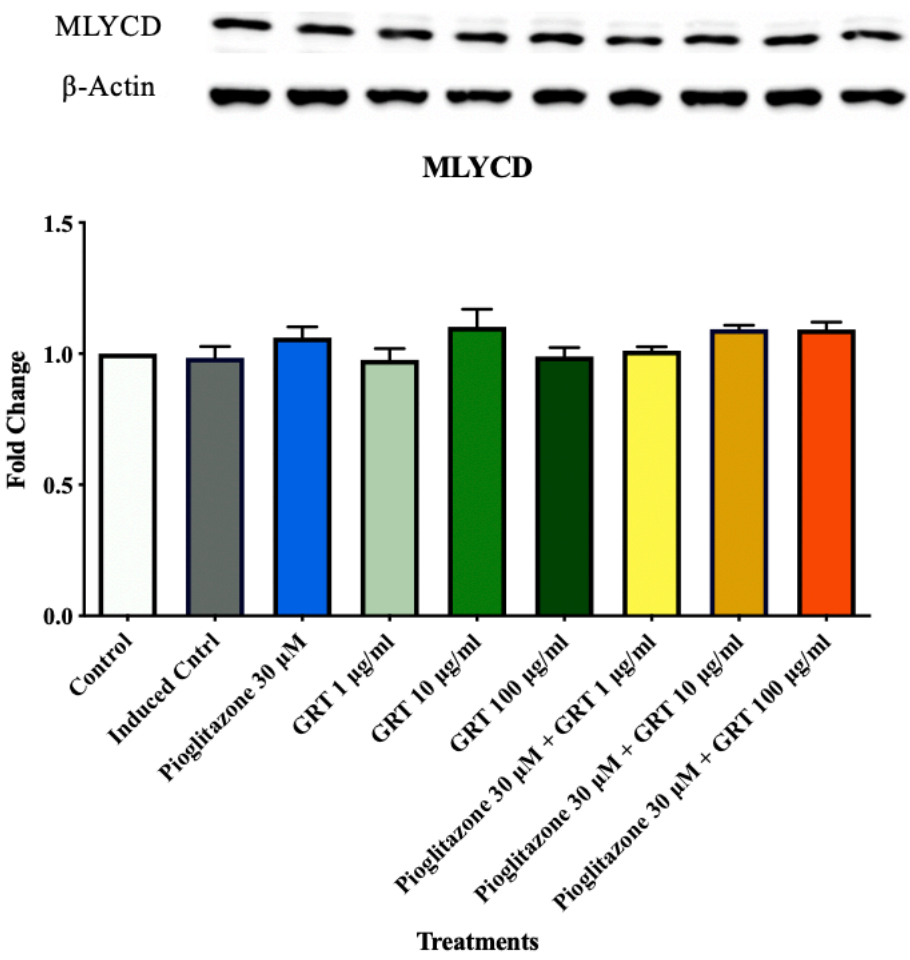

Figure 4.7 (c) MLYCD protein expression of C3A cell-lysates normalised to β-actin, showing the effects of 24 h steatosis induction [1 mM oleic acid] and the anti-steatotic effects of various treatments with pioglitazone and/or Afriplex GRT (GRT). Images are a representation of one experiment, captured using a ChemiDoc MP (Bio-Rad, Hercules, USA). Histogram illustrates densitometric quantification data from the images captured following the Western blot analysis. The band intensity of the blots was quantified using an ImageLab™ software v6.0.1 (Bio-Rad.com). Data represented as mean ± SEM (n = 4). Lane 1: Control, lane 2: induced control, lane 3: Pio 30 µM, lane 4: GRT 1 µg/mL, lane 5: GRT 10 µg/mL, lane 6: GRT 100 µg/mL, lane 7: Pio + GRT 1 µg/mL, lane 8: Pio + GRT 10 µg/mL, lane 9: Pio + GRT 100 µg/mL.

Protein expression data (Figure 4.8) from C3A lysates of proteins involved in apoptosis, oxidative stress and inflammatory response, fold change was calculated using the equation: fold change = $\left(\frac{\text{treatment - normal control}}{\text{normal control}}\right)$ and the treatments were compared to the control which was set at 1. Oleic acid-induced stress (induced control) significantly down-regulated the expression of Caspase-3 in Figure 4.8 (**a**) when compared with the normal control ($p < 0.0001$). The various treatments also induced a significant down regulation of capsase-3 when compared to the control, however no significant differences were observed when compared to the induced control. GSTZ-1 in Figure 4.8 (**b**) showed a significant upregulation with the induced control when compared to the normal control ($p < 0.0001$). Interestingly, the various treatments showed a significant down regulation when compared to both normal and induced controls, except for the high dose combination treatment (pioglitazone 30 µM + Afriplex GRT 100 µg/mL), which was only significantly down regulated when compared to the induced control and not the normal control. TNF-α in Figure 4.8 (**c**) expression showed a slight down regulation with the induced control when compared to the normal control although the data was not significantly different. Treatment with Afriplex GRT 1 µg/mL ($p < 0.05$) and Afriplex GRT 10 µg/mL ($p < 0.01$) showed a significant down regulation of TNF-α expression when compared to the normal control. This was also seen with the low and mid dose combination treatments (pioglitazone 30 µM + Afriplex GRT 1 µg/mL) and (pioglitazone 30 µM + Afriplex GRT 10 µg/mL), as the data sets were both significantly down regulated when compared to the normal control ($p < 0.001$).

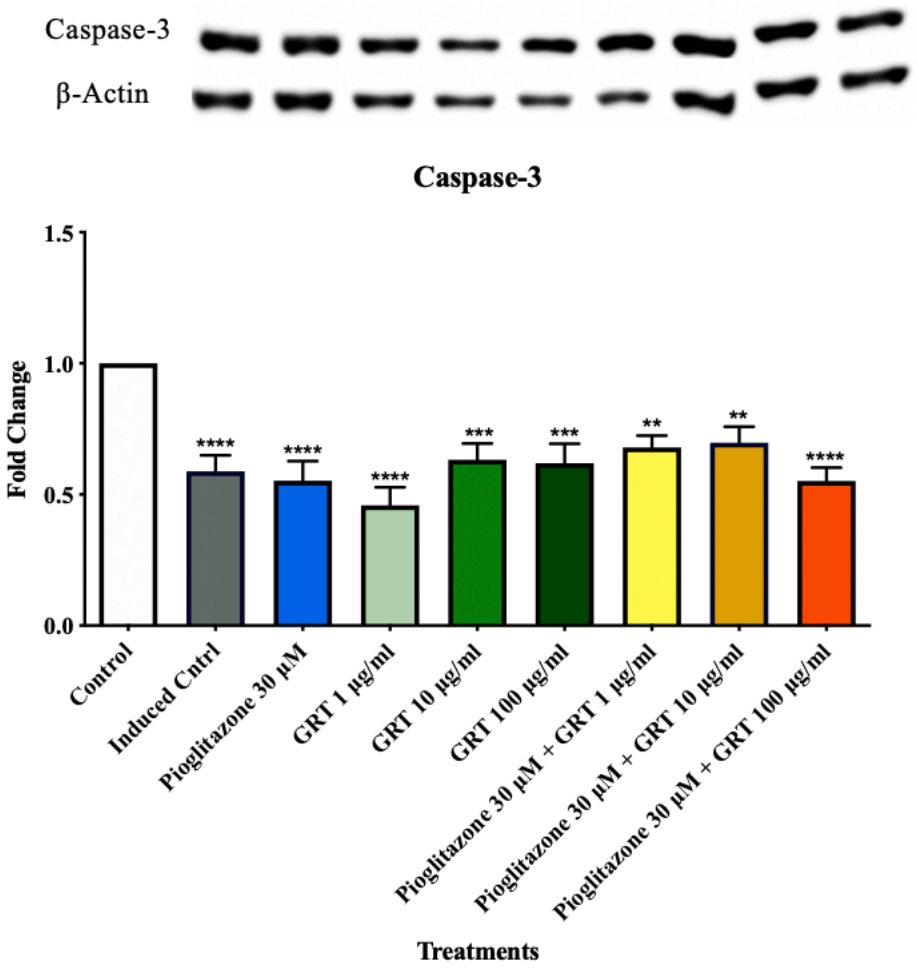

Figure 4.8 (a) Caspase-3 protein expression of C3A cell-lysates normalised to β-actin, showing the effects of 24 h steatosis induction [1 mM oleic acid] and the anti-steatotic effects of various treatments with pioglitazone and/or Afriplex GRT (GRT). Images are a representation of one experiment, captured using a ChemiDoc MP (Bio-Rad, Hercules, USA). Histogram illustrates densitometric quantification data from the images captured following the Western blot analysis. The band intensity of the blots was quantified using an ImageLab™ software v6.0.1 (Bio-Rad.com). Data represented as mean ± SEM (n = 4), where **P < 0.01, ***P < 0.001, ****P < 0.0001 when compared to the normal control. Lane 1: Control, lane 2: induced control, lane 3: Pio 30 µM, lane 4: GRT 1 µg/mL, lane 5: GRT 10 µg/mL, lane 6: GRT 100 µg/mL, lane 7: Pio + GRT 1 µg/mL, lane 8: Pio + GRT 10 µg/mL, lane 9: Pio + GRT 100 µg/mL.

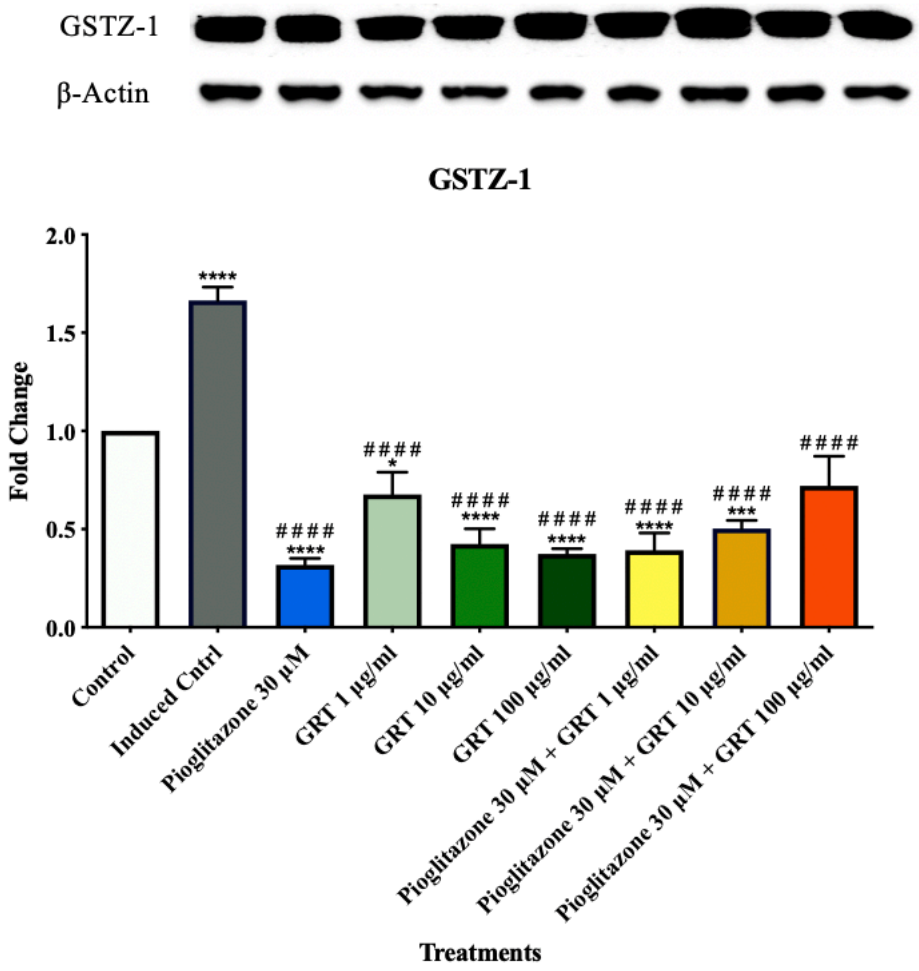

Figure 4.8 (b) GSTZ-1 protein expression of C3A cell-lysates normalised to β-actin, showing the effects of 24 h steatosis induction [1 mM oleic acid] and the anti-steatotic effects of various treatments with pioglitazone and/or Afriplex GRT (GRT). Images are a representation of one experiment, captured using a ChemiDoc MP (Bio-Rad, Hercules, USA). Histogram illustrates densitometric quantification data from the images captured following the Western blot analysis. The band intensity of the blots was quantified using an ImageLab™ software v6.0.1 (Bio-Rad.com). Data represented as mean ± SEM (n = 4), where *P < 0.05, ***P < 0.001, ****P < 0.0001 when compared to the normal control and $^{\#\#\#\#}$P < 0.0001 when compared to the induced control. Lane 1: Control, lane 2: induced control, lane 3: Pio 30 µM, lane 4: GRT 1 µg/mL, lane 5: GRT 10 µg/mL, lane 6: GRT 100 µg/mL, lane 7: Pio + GRT 1 µg/mL, lane 8: Pio + GRT 10 µg/mL, lane 9: Pio + GRT 100 µg/mL.

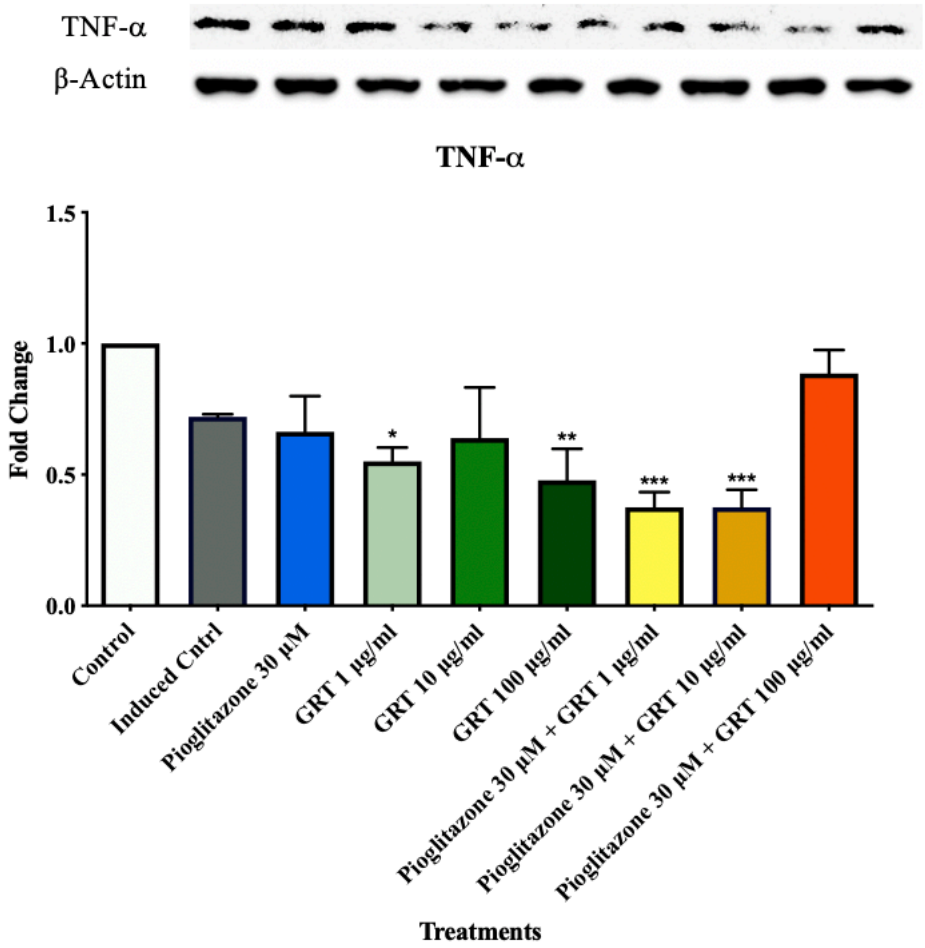

Figure 4.8 (c) TNF-α protein expression of C3A cell-lysates normalised to β-actin, showing the effects of 24 h steatosis induction [1 mM oleic acid] and the anti-steatotic effects of various treatments with pioglitazone and/or Afriplex GRT (GRT). Images are a representation of one experiment, captured using a ChemiDoc MP (Bio-Rad, Hercules, USA). Histogram illustrates densitometric quantification data from the images captured following the Western blot analysis. The band intensity of the blots was quantified using an ImageLab™ software v6.0.1 (Bio-Rad.com). Data represented as mean ± SEM (n = 4), where *P < 0.05, **P < 0.01, ***P < 0.001 when compared to the normal control. Lane 1: Control, lane 2: induced control, lane 3: Pio 30 µM, lane 4: GRT 1 µg/mL, lane 5: GRT 10 µg/mL, lane 6: GRT 100 µg/mL, lane 7: Pio + GRT 1 µg/mL, lane 8: Pio + GRT 10 µg/mL, lane 9: Pio + GRT 100 µg/mL.

Figure 4.9 shows the protein expression from C3A lysates of proteins involved in insulin signalling as well as lipid and glucose metabolism, fold change was calculated using the equation: fold change = $\left(\frac{\text{treatment - normal control}}{\text{normal control}}\right)$ and the treatments were compared to the control which was set at 1. IRS-1 in Figure 4.9 (**a**) was significantly upregulated by oleic acid treatment (induced control) when compared with the normal control ($p < 0.05$). Interestingly, the various treatments significantly downregulated protein expression of IRS-1 when compared to the induced control, except for Afriplex GRT 1 µg/mL, which did not significantly regulate IRS-1 expression when compared to both controls. Pi3K in Figure 4.9 (**b**) expression was also showed to be significantly upregulated for the induced control when compared to the normal control ($p < 0.001$) while the various treatments were able to significantly downregulate Pi3K protein expression when compared to the induced control. PPAR-γ in Figure 4.9 (**c**) expression showed a slight downregulation by the induced control when compared to the normal control although the difference was not significantly different. Treatment with Afriplex GRT 1 µg/mL showed a significant upregulation when compared to the induced control ($p < 0.01$). Treatment with the mid-dose combination treatment (pioglitazone 30 µM + Afriplex GRT 10 µg/mL) showed a significant down-regulation when compared to the normal control ($p < 0.05$).

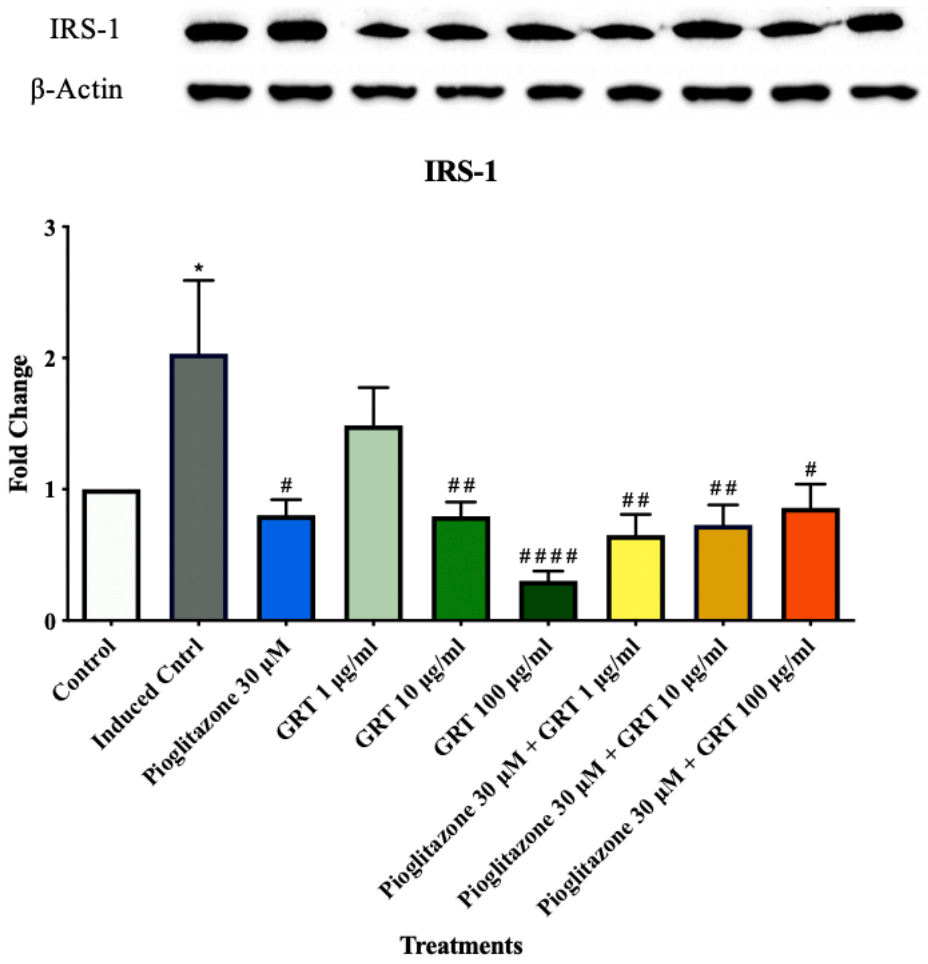

Figure 4.9 (a) IRS-1 protein expression of C3A cell-lysates normalised to β-actin, showing the effects of 24 h steatosis induction [1 mM oleic acid] and the anti-steatotic effects of various treatments with pioglitazone and/or Afriplex GRT (GRT). Images are a representation of one experiment, captured using a ChemiDoc MP (Bio-Rad, Hercules, USA). Histogram illustrates densitometric quantification data from the images captured following the Western blot analysis. The band intensity of the blots was quantified using an ImageLab™ software v6.0.1 (Bio-Rad.com). Data represented as mean ± SEM (n = 4), where *P < 0.05, when compared to the normal control and $^{\#}P < 0.05$, $^{\#\#}P < 0.01$, $^{\#\#\#\#}P < 0.0001$ when compared to the induced control. Lane 1: Control, lane 2: induced control, lane 3: Pio 30 µM, lane 4: GRT 1 µg/mL, lane 5: GRT 10 µg/mL, lane 6: GRT 100 µg/mL, lane 7: Pio + GRT 1 µg/mL, lane 8: Pio + GRT 10 µg/mL, lane 9: Pio + GRT 100 µg/mL.

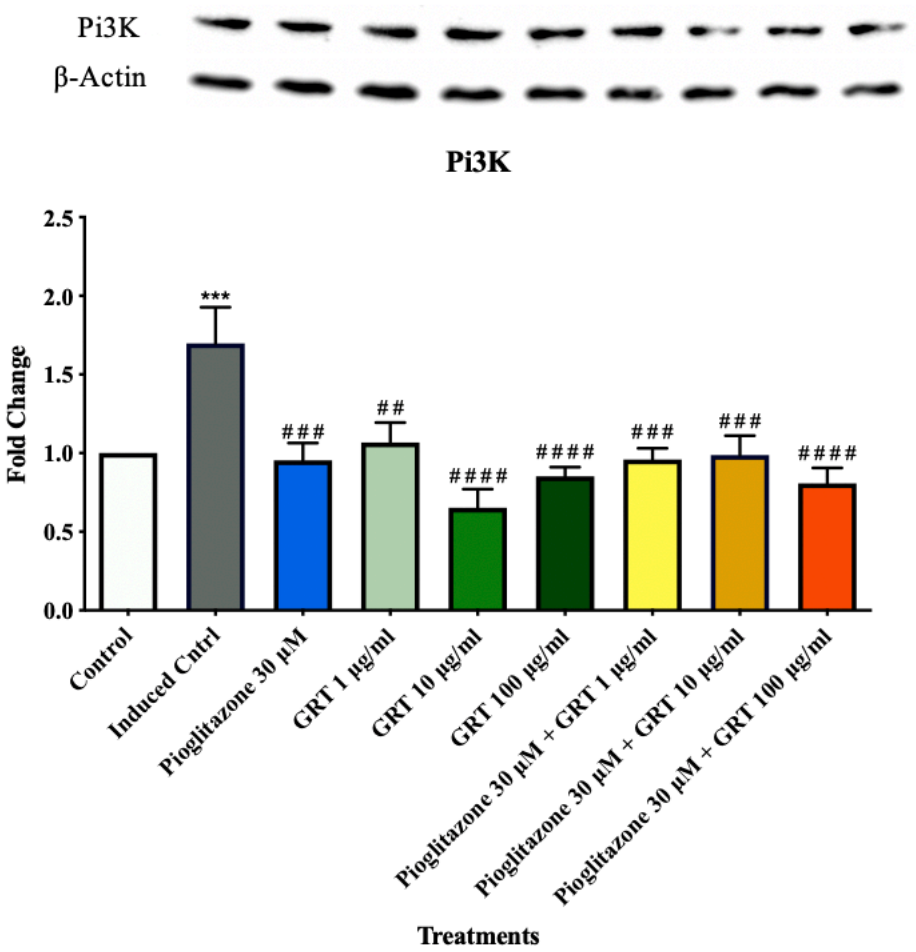

Figure 4.9 (b) Pi3K protein expression of C3A cell-lysates normalised to β-actin, showing the effects of 24 h steatosis induction [1 mM oleic acid] and the anti-steatotic effects various treatments with pioglitazone and/or Afriplex GRT (GRT). Images are a representation of one experiment, captured using a ChemiDoc MP (Bio-Rad, Hercules, USA). Histogram illustrates densitometric quantification data from the images captured following the Western blot analysis. The band intensity of the blots was quantified using an ImageLab™ software v6.0.1 (Bio-Rad.com). Data represented as mean ± SEM (n = 4), where ***$P < 0.001$ when compared to the normal control and $^{\#\#}P < 0.01$, $^{\#\#\#}P < 0.001$, $^{\#\#\#\#}P < 0.0001$ when compared to the induced control. Lane 1: Control, lane 2: induced control, lane 3: Pio 30 µM, lane 4: GRT 1 µg/mL, lane 5: GRT 10 µg/mL, lane 6: GRT 100 µg/mL, lane 7: Pio + GRT 1 µg/mL, lane 8: Pio + GRT 10 µg/mL, lane 9: Pio + GRT 100 µg/mL.

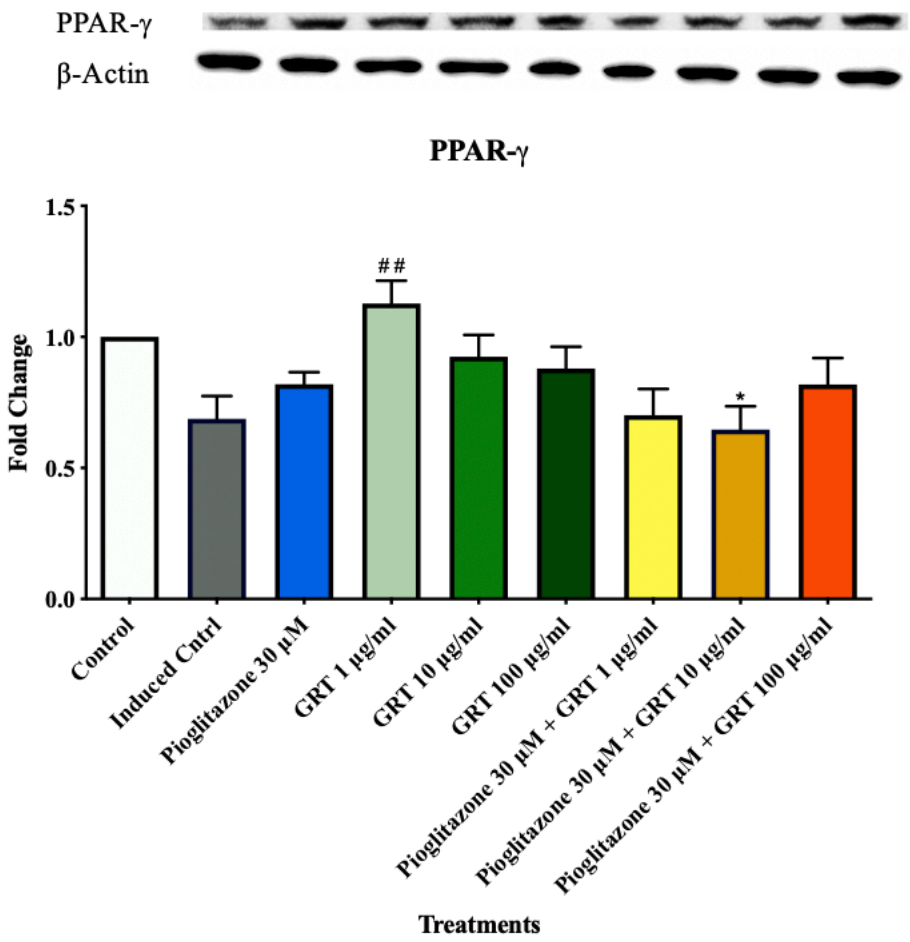

Figure 4.9 (c) PPAR-γ protein expression of C3A cell-lysates normalised to β-actin, showing the effects of 24 h steatosis induction [1 mM oleic acid] and the anti-steatotic effects of various treatments with pioglitazone and/or Afriplex GRT (GRT). Images are a representation of one experiment, captured using a ChemiDoc MP (Bio-Rad, Hercules, USA). Histogram illustrates densitometric quantification data from the images captured following the Western blot analysis. The band intensity of the blots was quantified using an ImageLab™ software v6.0.1 (Bio-Rad.com). Data represented as mean ± SEM (n = 4), where *P < 0.05, when compared to the normal control and $^{\#\#}$P < 0.01 when compared to the induced control. Lane 1: Control, lane 2: induced control, lane 3: Pio 30 µM, lane 4: GRT 1 µg/mL, lane 5: GRT 10 µg/mL, lane 6: GRT 100 µg/mL, lane 7: Pio + GRT 1 µg/mL, lane 8: Pio + GRT 10 µg/mL, lane 9: Pio + GRT 100 µg/mL.

4.4 *In vivo* metabolic parameters

4.4.1 *Body weight gain and liver weights*

Figure 4.10 shows the percentage weight gain over time measured weekly for 10 weeks between the groups of mice used in the study, Figure 4.10 (**a**). The data shows significant changes in the various treatment groups at week 1 of treatment when compared to the lean control group, with the exception of the mice treated with Pioglitazone 15 mg/kg. This is expected as, from week 2 to week 10, significant increases in body weight by percentage was observed with the obese control as well as across the various treatment groups when compared to the lean control group. This is due to the genetic mutation of the leptin-receptor (*Leprdb*) of these obese mice that results in loss of satiety leading to increased food intake, obesity and spontaneous development of diabetes overtime as shown by the data in Figure 4.10 (**a**). No significant changes were exhibited when comparing the various treatment groups to the obese control. At termination mice livers were weighed according to their groups and the data was plotted on a histogram represented by Figure 4.10 (**b**). Data shows a significant increase in liver weight for the obese control group when compared to the lean control group ($p < 0.05$). Interestingly, treatment with Pioglitazone 15 mg/kg ($p < 0.001$), Afriplex GRT 74 mg/kg ($p < 0.01$) and Afriplex GRT 740 mg/kg ($p < 0.01$) showed an even greater increase in liver weight compared to the obese control and when compared to the lean control. No significant changes were observed when comparing the obese control to any of the various treatment groups.

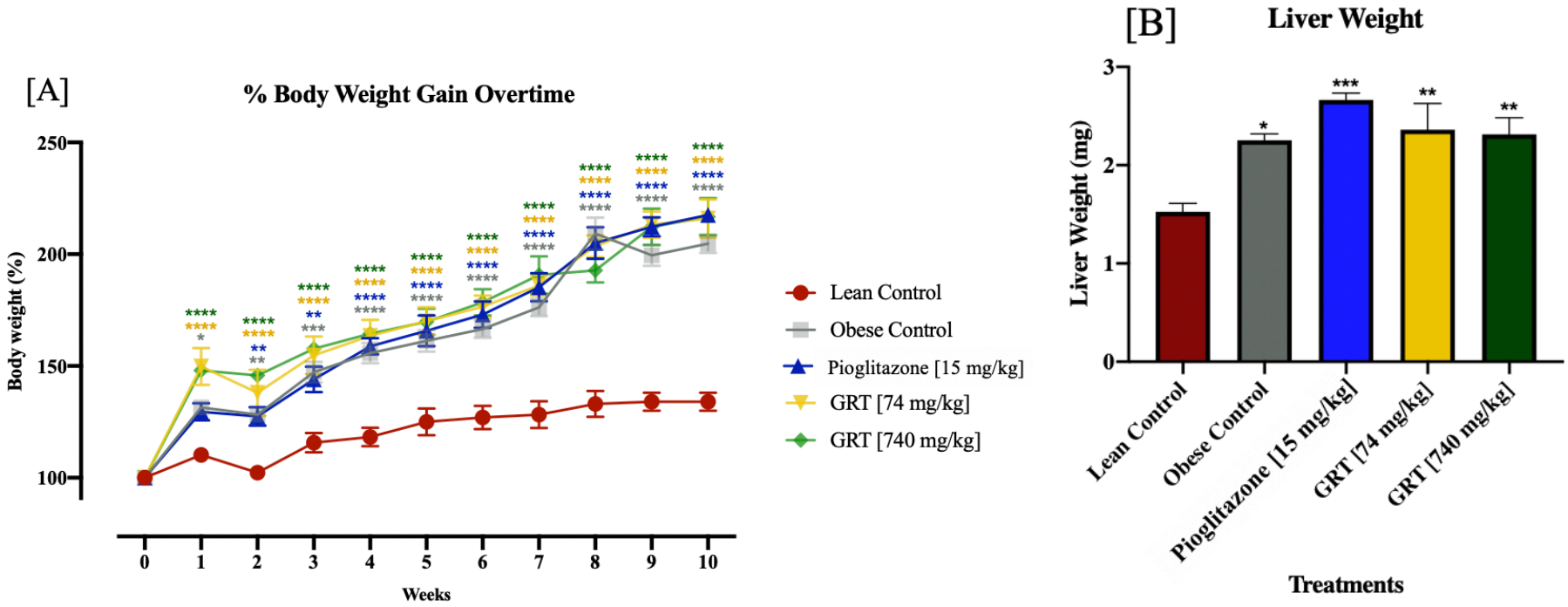

Figure 4.10 (a) Effect of pioglitazone and GRT on total body weight % measured overtime and **(b)** liver weights measured at termination for *lean (db/+)*, untreated and treated obese *(db/db)* mice, which received daily oral doses of pioglitazone 15 mg/kg and Afriplex GRT (GRT) at 74 or 740 mg/kg/body weight (BW) for 10 weeks. Data expressed as mean ± SEM of eight mice per group, where *P < 0.05, **P < 0.01, ***P < 0.001 and ****P < 0.0001, when compared to the lean control.

4.4.2 *Oral glucose tolerance test (OGTT)*

Figure 4.11 shows an assessment of an oral glucose tolerance test conducted on the various experimental groups. A line graph was formulated from the data over time in Figure 4.11 (**a**) and an area under the curve analysis was formulated and illustrated in Figure 4.11 (**b**). Obese control mice presented with a significant increase in blood glucose ($p < 0.0001$) when compared to the lean control. Mice treated with pioglitazone 15 mg/kg showed a significant increase in glucose levels ($p < 0.01$) when compared to the lean control but less so than the obese control ($p = 0.5191$). This was also observed with the treatment with Afriplex GRT 74 mg/kg ($p < 0.01$) and Afriplex GRT 740 mg/kg ($p < 0.05$), as a significant increase in glucose levels was observed when compared to the lean control in a dose-dependent manner. No significant differences were observed when comparing data of the treated mice to the obese control.

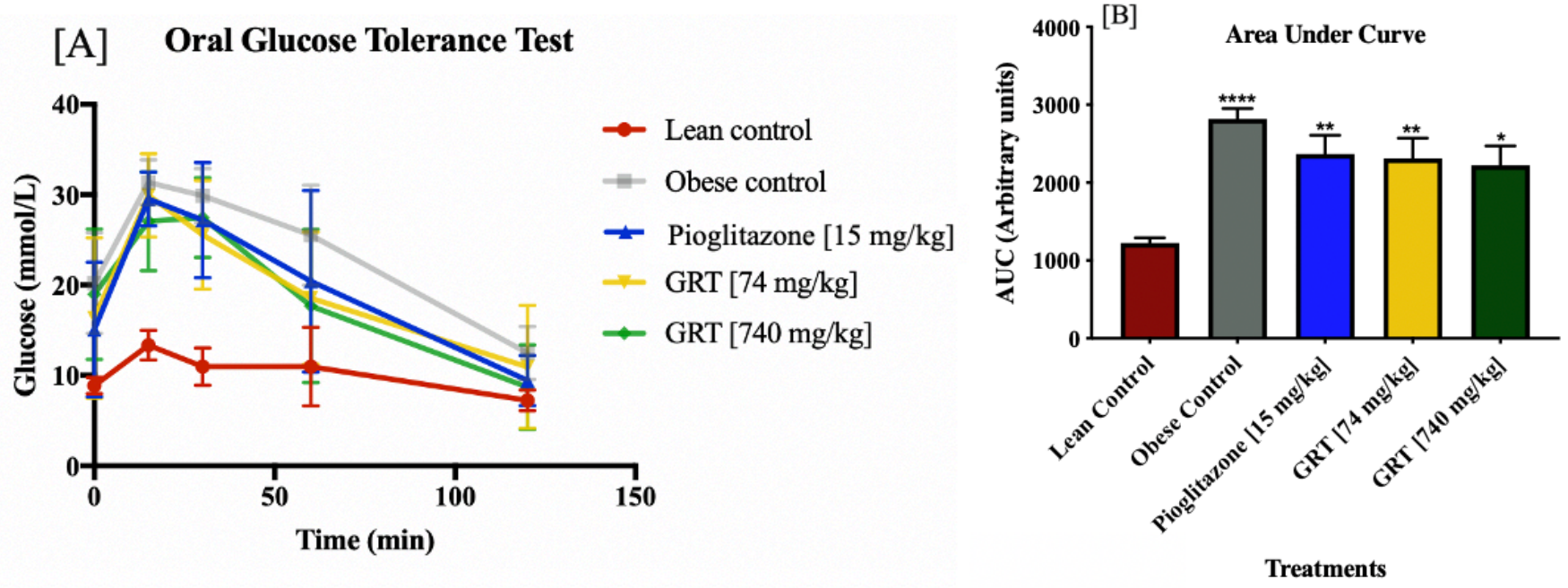

Figure 4.11 (a) Effect of pioglitazone and GRT on oral glucose tolerance for lean *(db/+)*, untreated and treated obese *(db/db)* mice, which received daily oral doses of pioglitazone 15 mg/kg and Afriplex GRT (GRT) at 74 or 740 mg/kg body weight (BW) for 10 weeks. Data expressed as mean ± SEM of eight mice per group. (**b**) Represents area under the curve data, where *P < 0.05, **P < 0.01 and ****P < 0.0001, when compared to the lean control.

4.4.3 *Histological analysis (H&E Staining)*

Histological assessment of H&E stained liver sections Figure 4.12 of lean (*db/*$^{+}$) and obese (*db/db*) mice across the different treatment groups. Normal hepatocytes should exhibit typical polygonal shape with a pink granular cytoplasm. In contrast, larger (hypertrophic) rounded hepatocytes with clear reticular cytoplasm, substantial lipid inclusions (ballooning), is considered evidence of steatosis. Thus, this criteria was used to determine significant morphological changes in the various treatment groups of the H&E stained liver sections. Histology of the lean non-diabetic mouse liver demonstrated normal morphology and including the presence of some lipid droplets. The obese control (*db/db*) showed a substantially different morphology when compared to the lean control (*db/*$^{+}$) with increased lipid accumulation (steatosis) observed with the swelling of the hepatocytes. The intracellular lipid droplets included larger coalescence lipid droplets, classified as mixed medio-microvesicular steatosis. Treatment with pioglitazone 15 mg/kg substantially improved the lipid accumulation pattern to a microvesicular steatotic pattern (smaller lipid droplets) when compared to the obese control (*db/db*). Treatment with Afriplex GRT 74 mg/kg and 740 mg/kg further reduced lipid accumulation, however, the difference was still not comparable to the lean control.

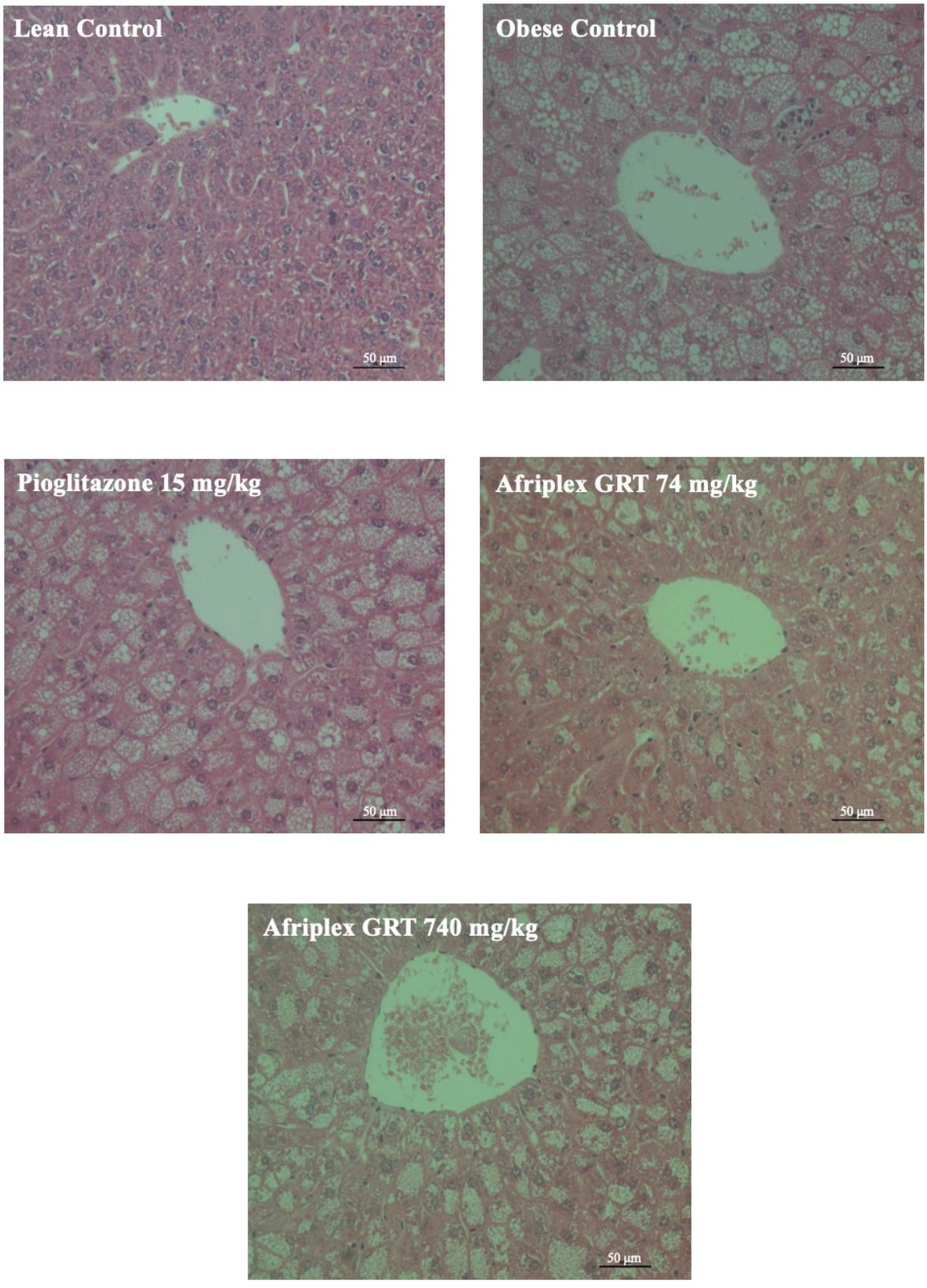

Figure 4.12 Liver histopathology of lean *(db/+)*, untreated and treated obese *(db/db)* mice, which received daily oral doses of pioglitazone 15 mg/kg and Afriplex GRT (GRT) at 74 or 740 mg/kg/body weight (BW) for 10 weeks. Liver sections stained with haematoxylin and eosin (H&E). Liver sections were captured at 200x magnification using a Nikon Eclipse Ti/S Light Microscope (scale represents: 50 µm).

4.5 *In vivo* mRNA expression (qRT-PCR)

Figure 4.13 illustrates graphs generated from mRNA expression data of genes involved in lipid metabolism, fold change was calculated using the equation: fold change = $\left(\frac{\text{treatment - normal control}}{\text{normal control}}\right)$ and the treatments were compared to the control which was set at 1. In Figure 4.13 (**a**) *Chrebp* was shown to be significantly down-regulated in obese mice along with the various treatment groups, when compared to the lean control group ($p < 0.0001$). Pioglitazone 15 mg/kg ($p < 0.001$) and Afriplex GRT 740 mg/kg ($p < 0.05$) treatment significantly down-regulated *Chrebp* expression when compared to the obese control group. *FASN* in Figure 4.13 (**b**) was significantly down-regulated in the obese mice group along with the various treatment groups when compared to the lean control ($p < 0.0001$). Pioglitazone 15 mg/kg ($p < 0.001$) and Afriplex GRT 740 mg/kg ($p < 0.05$) treatment down-regulated *Fasn* expression when compared to the obese control. *Srebf1* in Figure 4.13 (**c**) was significantly down-regulated in the obese mice when compared to the lean control group ($p < 0.0001$) and the pioglitazone 15 mg/kg ($p < 0.0001$) and Afriplex GRT 740 mg/kg ($p < 0.001$) treatment led to a significant downregulation of *Srebf1* when compared to the obese control.

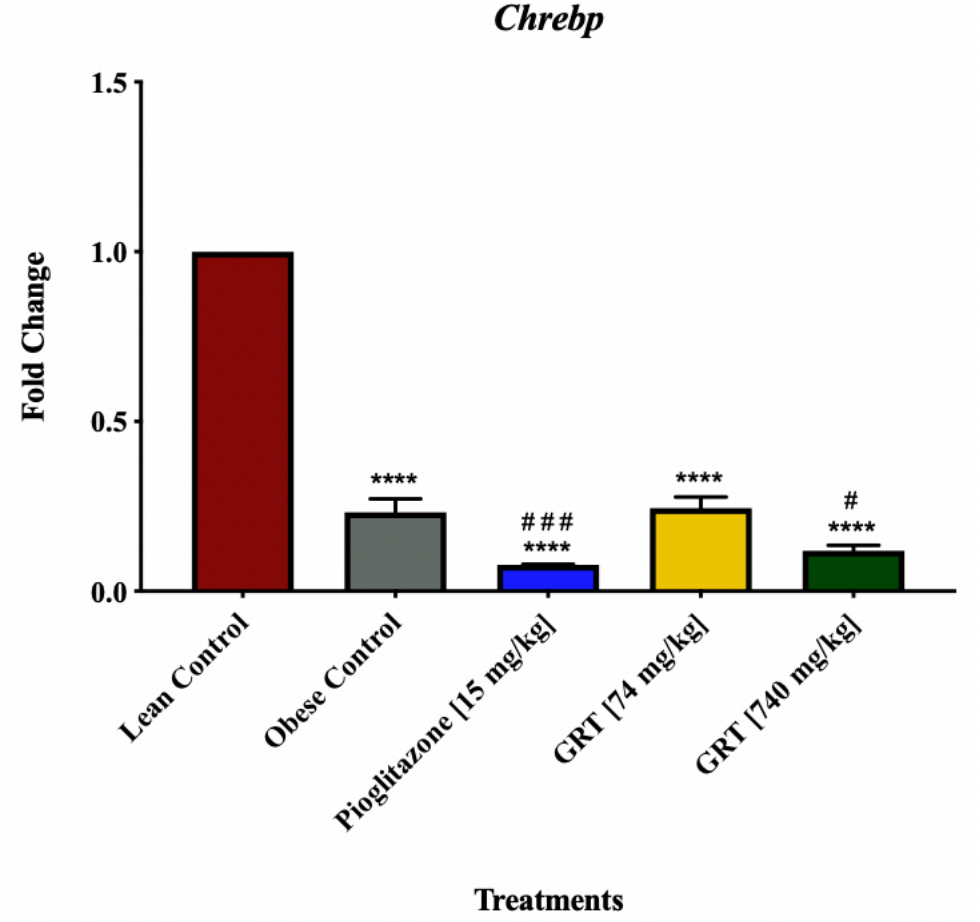

Figure 4.13 (a) *Chrebp* mRNA expression of *in vivo* NAFLD model liver tissue lysates normalised to *Hprt*, showing the expression in the lean and obese controls and the effects of mono treatments with pioglitazone or Afriplex GRT (GRT). Data represented as mean ± SEM (n = 3), where ****P < 0.0001, when compared to the lean control and $^{\#}P < 0.05$ and $^{\#\#\#}P < 0.001$ when compared to the obese control.

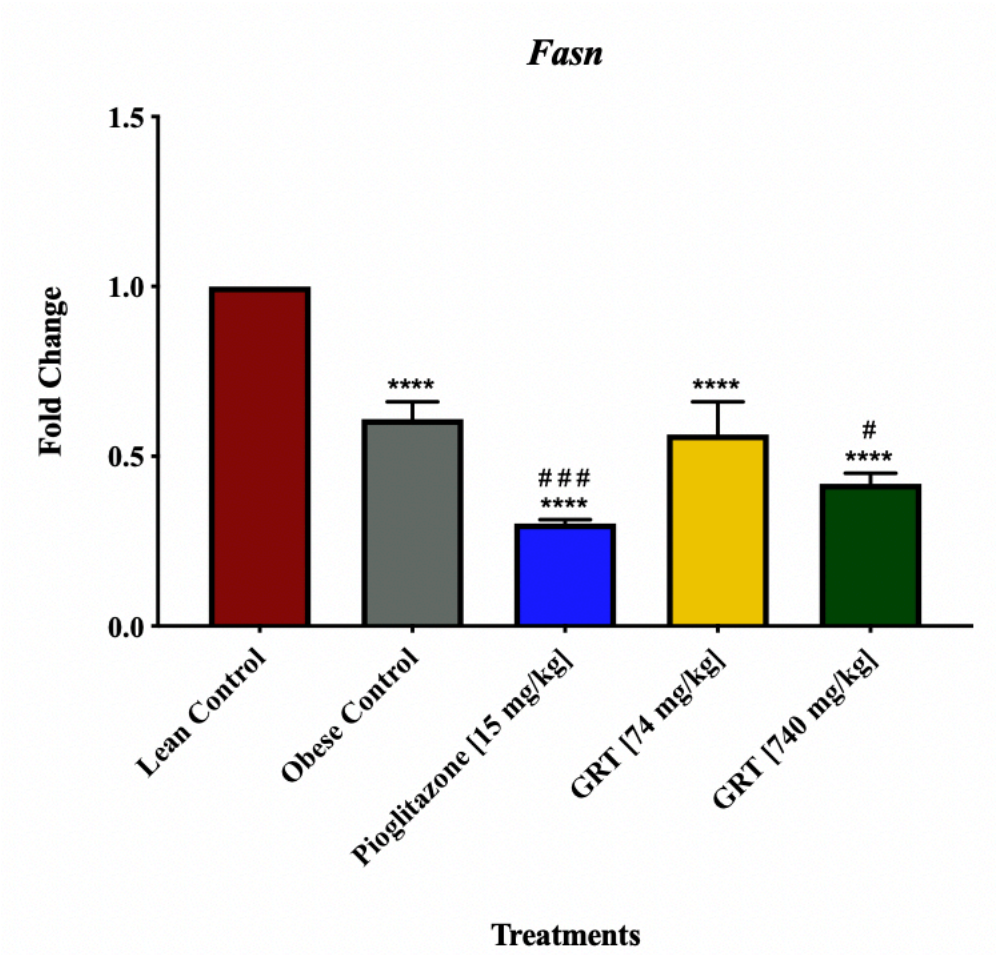

Figure 4.13 (b) *Fasn* mRNA expression of *in vivo* NAFLD model liver tissue lysates normalised to *Hprt*, showing the expression in the lean and obese controls and the effects of mono treatments with pioglitazone or Afriplex GRT (GRT). Data represented as mean ± SEM (n = 3), where ****P < 0.0001 when compared to the lean control; $^{\#}$P < 0.05 and $^{\#\#\#}$P < 0.001 when compared to the obese control.

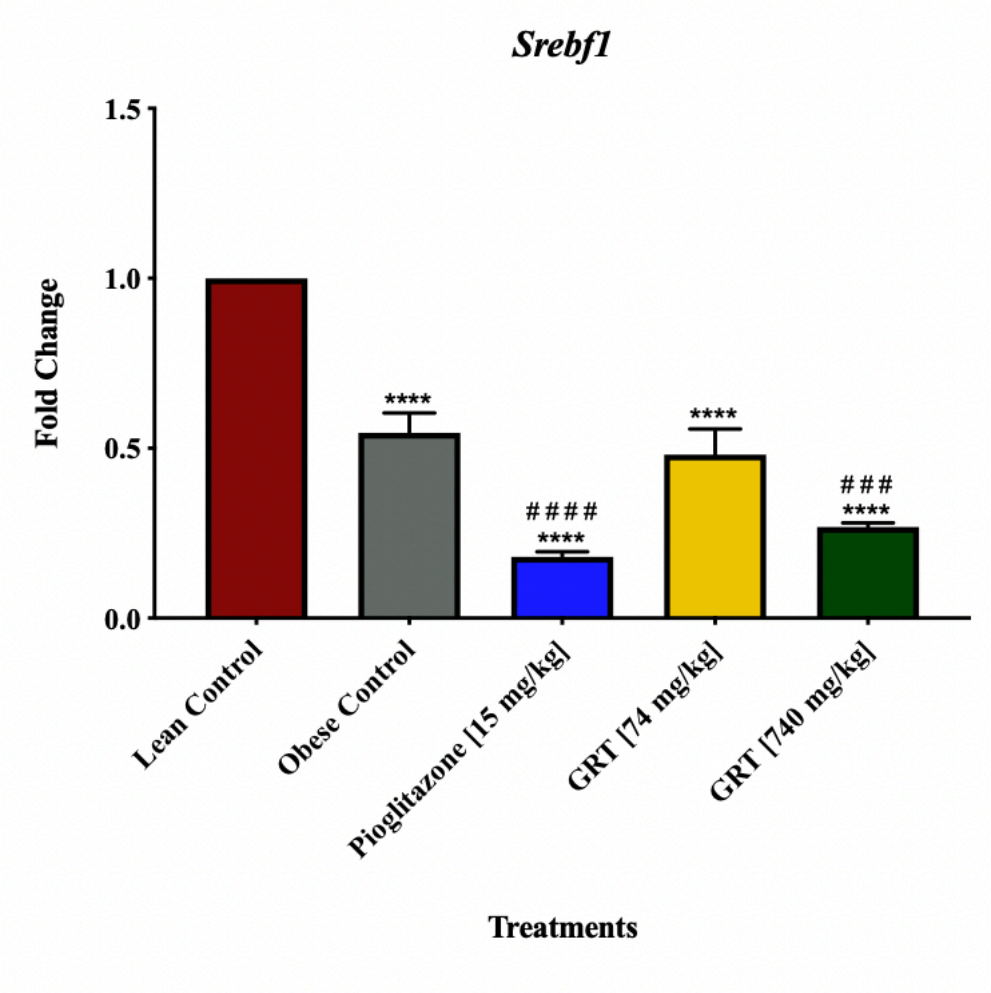

Figure 4.13 (c) *Srebf1* mRNA expression of *in vivo* NAFLD model liver tissue lysates normalised to *Hprt*, showing the expression in the lean and obese controls and the effects of mono treatments with pioglitazone or Afriplex GRT (GRT). Data represented as mean ± SEM (n = 3), where ****P < 0.0001 when compared to the lean control; $^{###}$P < 0.001 and $^{####}$P < 0.0001 when compared to the obese control.

Figure 4.14, demonstrates the mRNA expression data of genes involved in glucose metabolism and insulin signalling, fold change was calculated using the equation: fold change = $\left(\frac{\text{treatment - normal control}}{\text{normal control}}\right)$ and the treatments were compared to the control which was set at 1. *Glut2* in Figure 4.14 (**a**) showed a slight downregulation in the obese control and low dose Afriplex GRT [74 mg/kg] groups, however, the difference was not significant, when compared to the lean control group. Mice treated with pioglitazone 15 mg/kg ($p < 0.0001$) and Afriplex GRT 740 mg/kg ($p < 0.001$) showed a significant downregulation of *GLUT2* when compared to the lean control, in addition a significant down-regulation was observed when compared to the obese control ($p < 0.01$) and ($p < 0.05$), respectively. *Irs-1* in Figure 4.14 (**b**) showed a significant down regulation in the obese control, and across the various treatment groups when compared to the lean control ($p < 0.0001$). No significant change was observed when comparing the various treatments to the obese control. *Ppar-γ* in Figure 4.14 (**c**) showed a slight upregulation by both low and high dose of Afriplex GRT treatments when compared to the lean control, however this was not significant. No change was observed in the obese control, when compared to the lean control and the pioglitazone 15 mg/kg treatment group showed a slight down regulation, however no significance was observed.

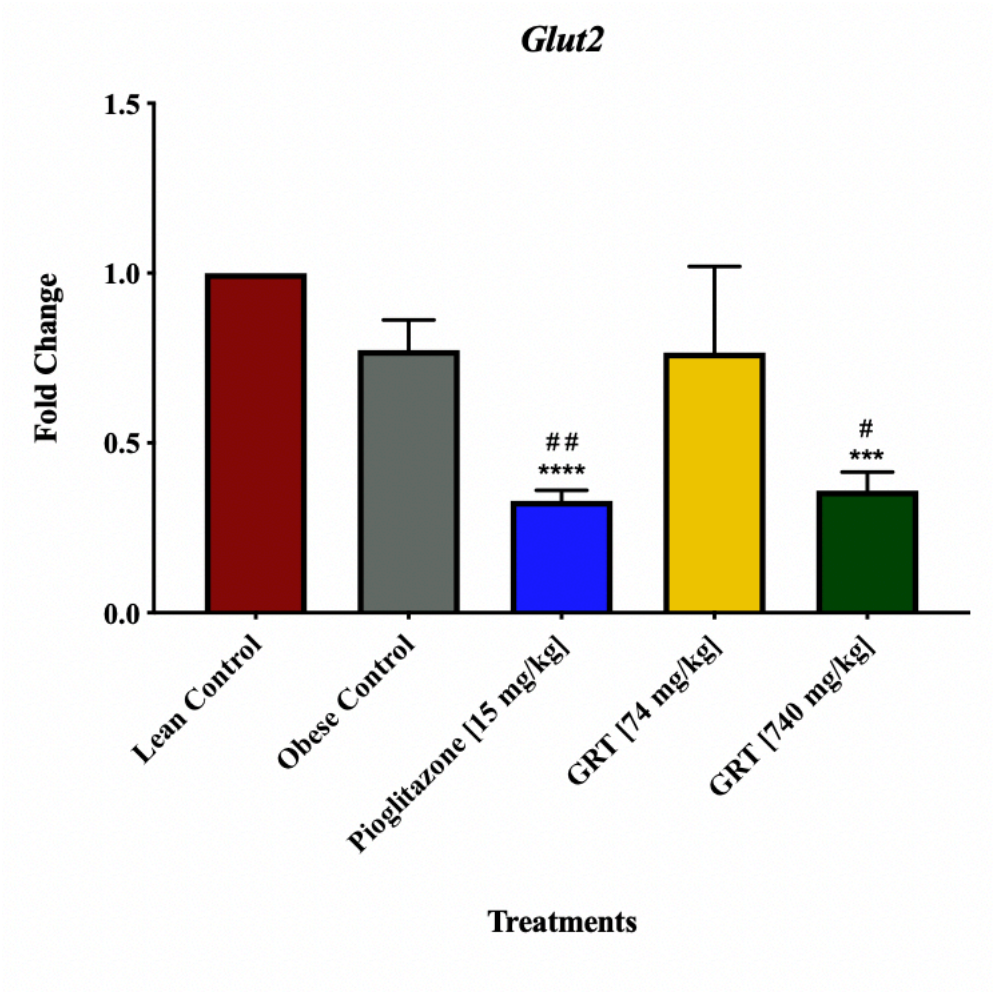

Figure 4.14 (a) *Glut2* mRNA expression of *in vivo* NAFLD model liver tissue lysates normalised to *Hprt*, showing the expression in the lean and obese controls and the effects of mono treatments with pioglitazone or Afriplex GRT (GRT). Data represented as mean ± SEM (n = 3), where ***P < 0.001, ****P < 0.0001 when compared to the lean control; $^{\#}$P < 0.05 and $^{\#\#}$P < 0.01 when compared to the obese control.

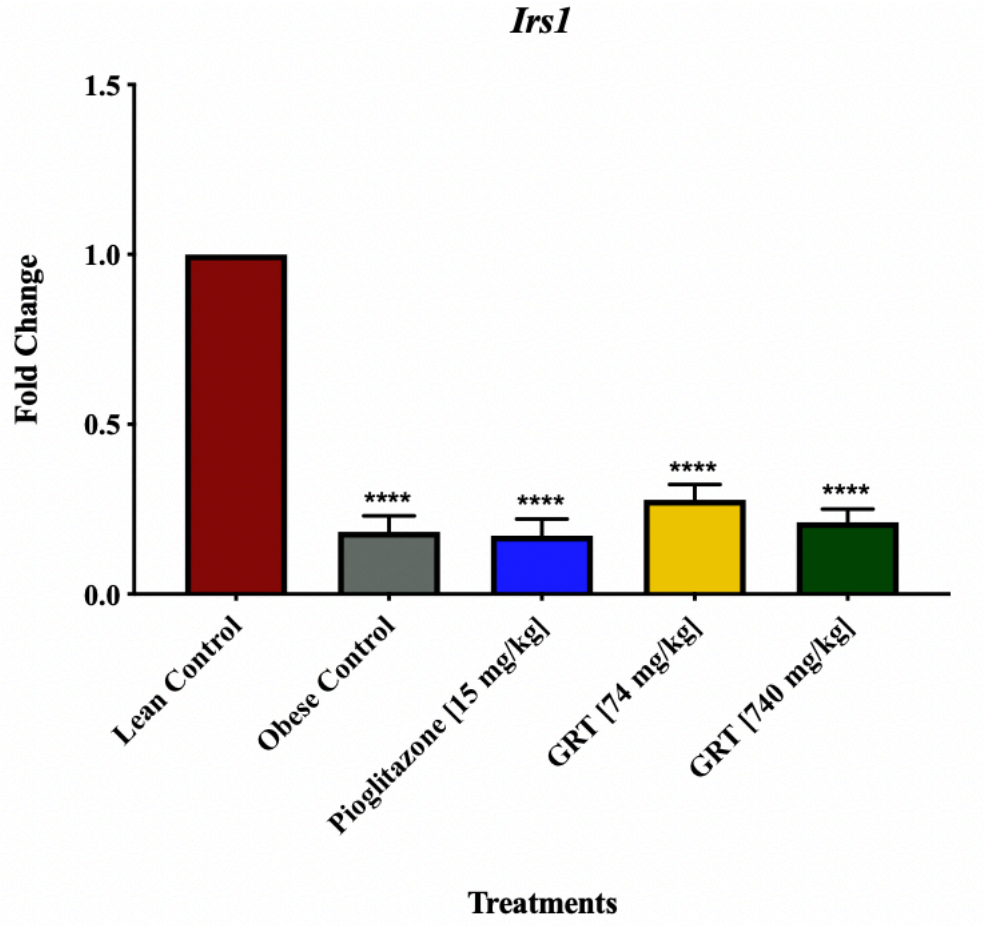

Figure 4.14 (b) *Irs-1* mRNA expression of *in vivo* NAFLD model liver tissue lysates normalised to *Hprt*, showing the expression in the lean and obese controls and the effects of mono treatments with pioglitazone or Afriplex GRT (GRT). Data represented as mean ± SEM (n = 3), where ****P < 0.0001 when compared to the lean control.

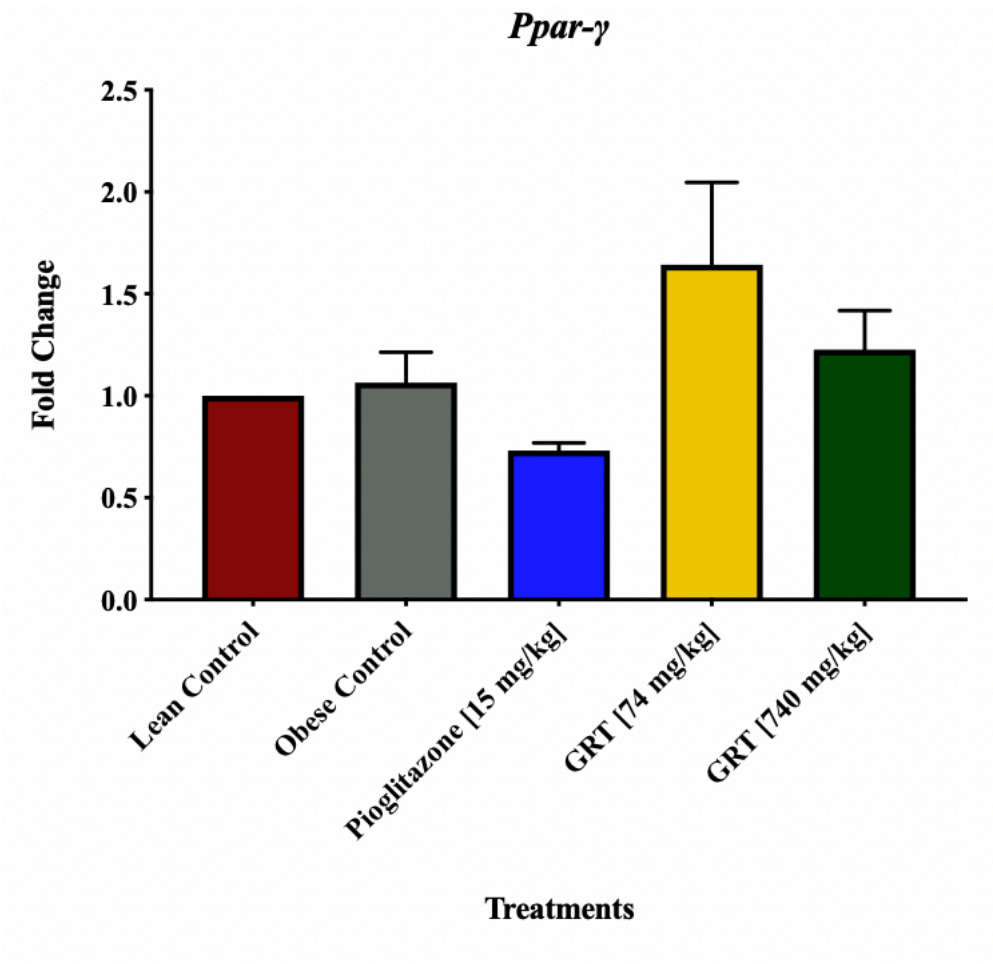

Figure 4.14 (c) *Ppar-γ* mRNA expression of *in vivo* NAFLD model liver tissue lysates normalised to *Hprt*, showing the expression in the lean and obese controls and the effects of mono treatments with pioglitazone or Afriplex GRT (GRT). Data represented as mean ± SEM (n = 3).

The mRNA expression data (Figure 4.15) of genes involved in apoptosis *(Casp 3)*, lipid and glucose metabolism *(PPAR-α)* as well as an oxidative stress response (*SOD2*), fold change was calculated using the equation: $\text{fold change} = \left(\frac{\text{treatment - normal control}}{\text{normal control}}\right)$ and the treatments were compared to the control which was set at 1. *Casp3,* Figure 4.15 (**a**) showed significant downregulation in the obese mice group along with the various treatment groups, when compared to the lean control group ($p < 0.0001$). Pioglitazone 15 mg/kg ($p < 0.001$) and Afriplex GRT 740 mg/kg ($p < 0.01$) treatment groups induced a significant down-regulation when compared to the obese control group. *PPAR-α* in Figure 4.15 (**b**) showed a significant down-regulation with the obese control, and across the various treatment groups when compared to the lean control ($p < 0.0001$). Mice treated with pioglitazone 15 mg/kg ($p < 0.0001$) and Afriplex GRT 740 mg/kg ($p < 0.001$) showed a significant downregulation of *SOD2* when compared to the lean control, furthermore a significant down-regulation was observed when compared to the obese control ($p < 0.01$) and ($p < 0.05$), respectively (Figure 4.15 (**c**)).

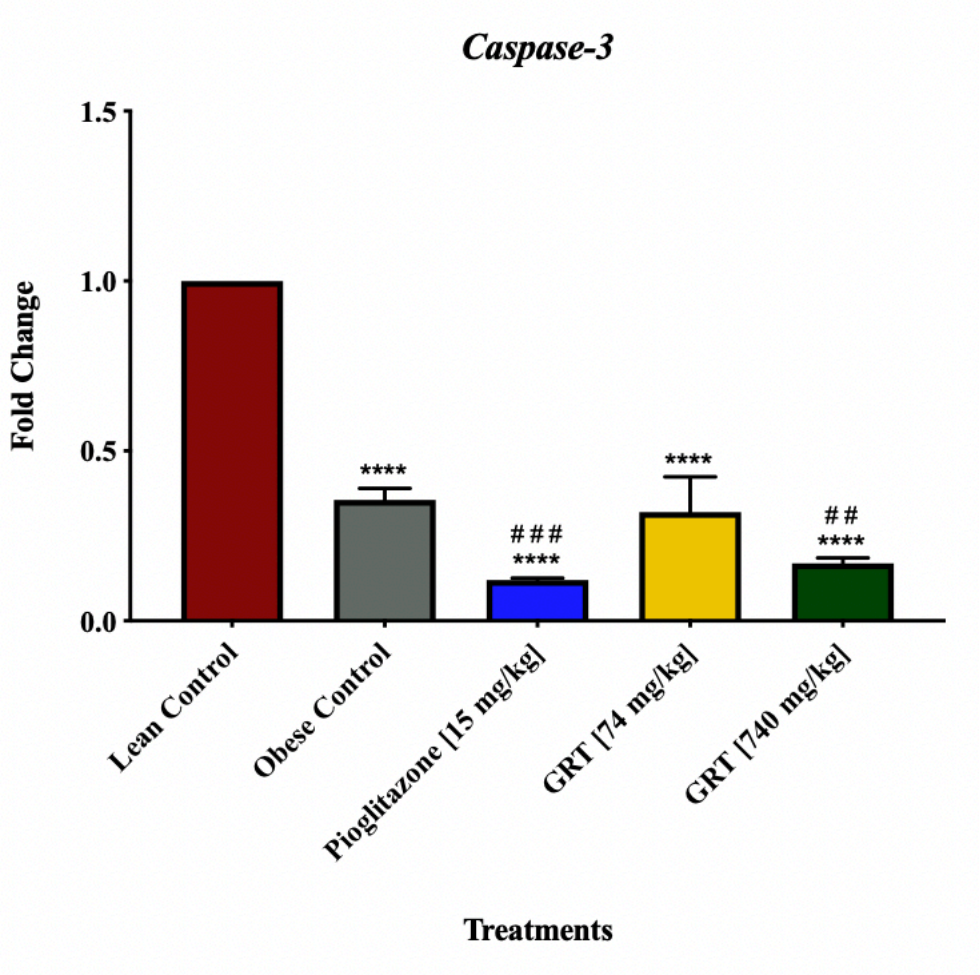

Figure 4.15 (a) *Caspase-3* mRNA expression of *in vivo* NAFLD model liver tissue lysates normalised to *Hprt*, showing the expression in the lean and obese controls and the effects of mono treatments with pioglitazone or Afriplex GRT (GRT). Data represents Mean ± SEM (n = 3), where ****P < 0.0001 when compared to the lean control; $^{\#\#}$P < 0.01 and $^{\#\#\#}$P < 0.001 when compared to the obese control.

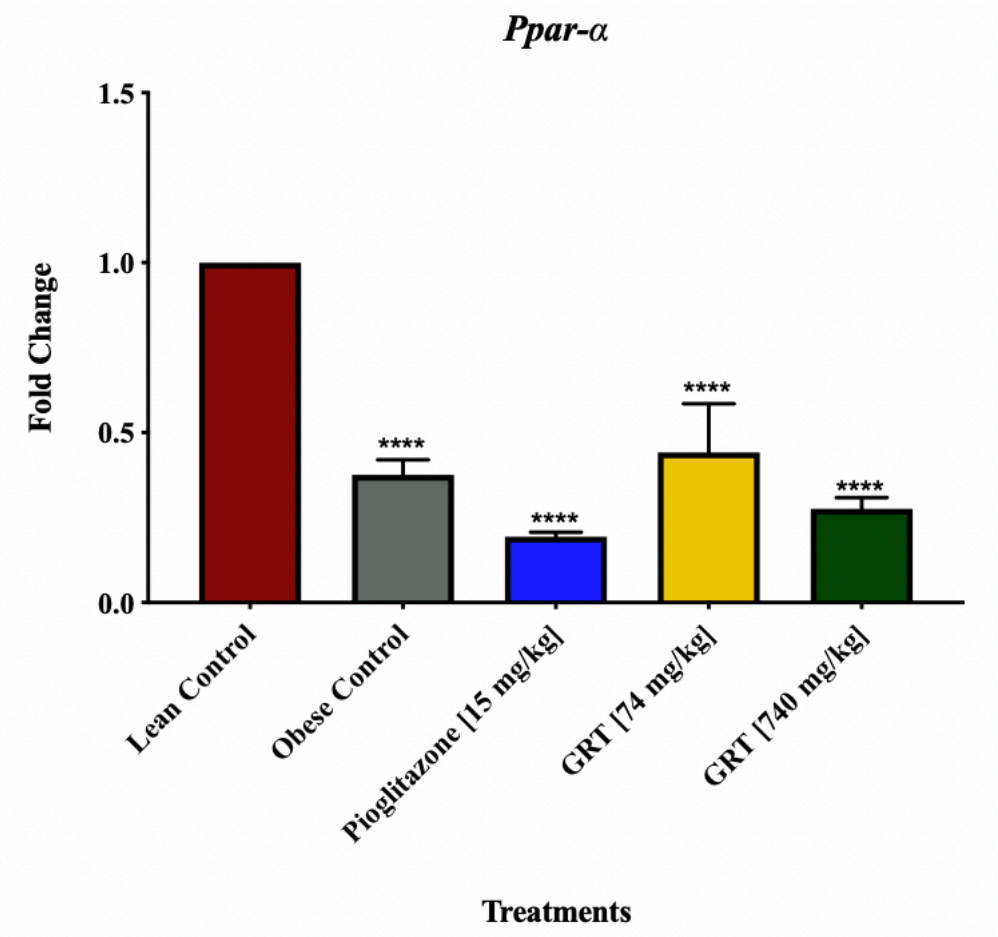

Figure 4.15 (b) *Ppar-α* mRNA expression of *in vivo* NAFLD model liver tissue lysates normalised to *Hprt*, showing the expression in the lean and obese controls and the effects of mono treatments with pioglitazone or Afriplex GRT (GRT). Data represents Mean ± SEM (n = 3), where ****P < 0.0001 when compared to the lean control.

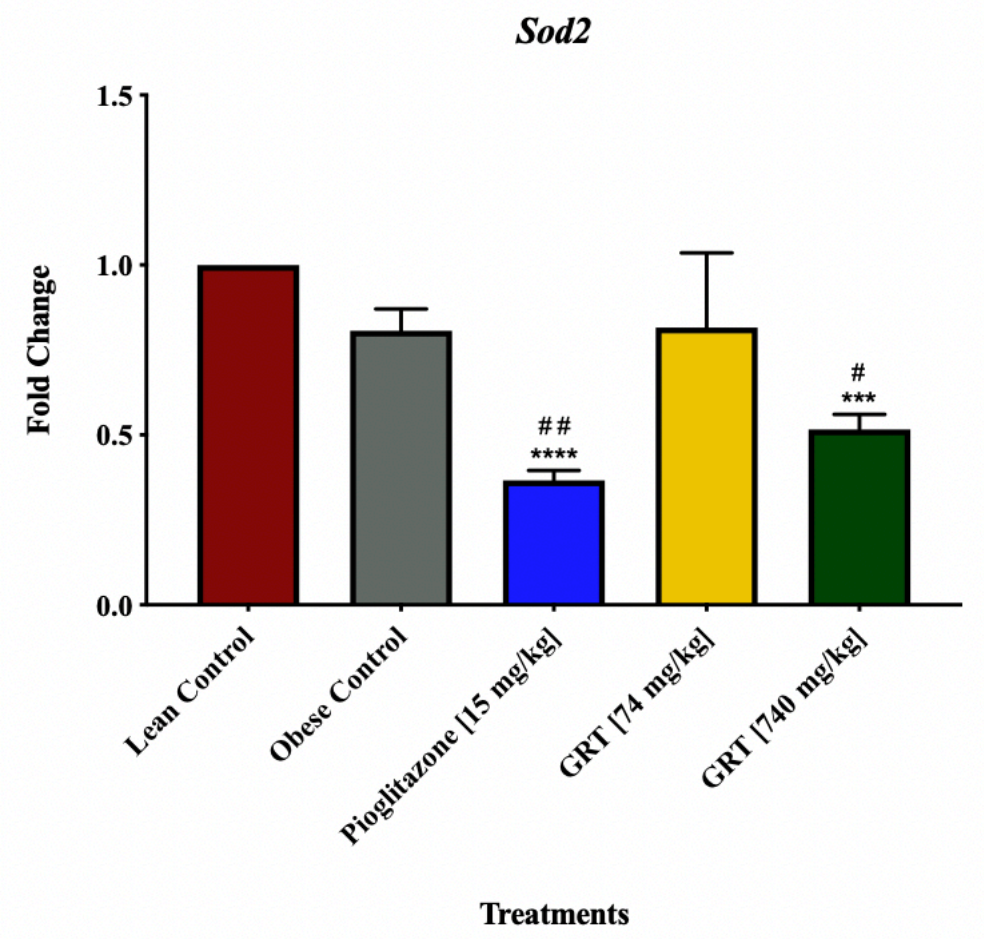

Figure 4.15 (c) *Sod2* mRNA expression of *in vivo* NAFLD model liver tissue lysates normalised to *Hprt*, showing the expression in the lean and obese controls and the effects of mono treatments with pioglitazone or Afriplex GRT (GRT). Data represents Mean ± SEM (n = 3), where ***P < 0.001, ****P < 0.0001 when compared to the lean control; $^{\#}$P < 0.05 and $^{\#\#}$P < 0.01 when compared to the obese control.

4.6 *In vivo* protein expression (Western blotting)

In Figute 4.16, the expression of proteins involved in lipid and glucose metabolism from mouse liver lysates is iilustrated. The fold change was calculated using the equation: fold change = $\left(\frac{\text{treatment - normal control}}{\text{normal control}}\right)$ and the treatments were compared to the control which was set at 1. Obese control mice presented with a significant increase in pAKT/AKT ratio, Figure 4.16 (**a**), when compared to the lean control ($p < 0.001$). Pioglitazone 15 mg/kg ($p < 0.0001$) treatment and Afriplex GRT 74 mg/kg (GRT 1) ($p < 0.01$) showed a significant down regulation when compared to the obese control. pAMPK-α/AMPK-α ratio in Figure 4.16 (**b**) showed a slight upregulation in the obese control when compared to the lean control, although no significance was observed, and subsequent treatment groups showed no significant differences when compared to both lean and obese controls. MLYCD in Figure 4.16 (**c**) treatment with pioglitazone 15 mg/kg showed a significant upregulation when compared to both lean ($p < 0.001$) and obese controls ($p < 0.01$). Treatment with Afriplex GRT 740 mg/kg (GRT 2) showed a significant upregulation when compared to the lean control ($p < 0.05$).

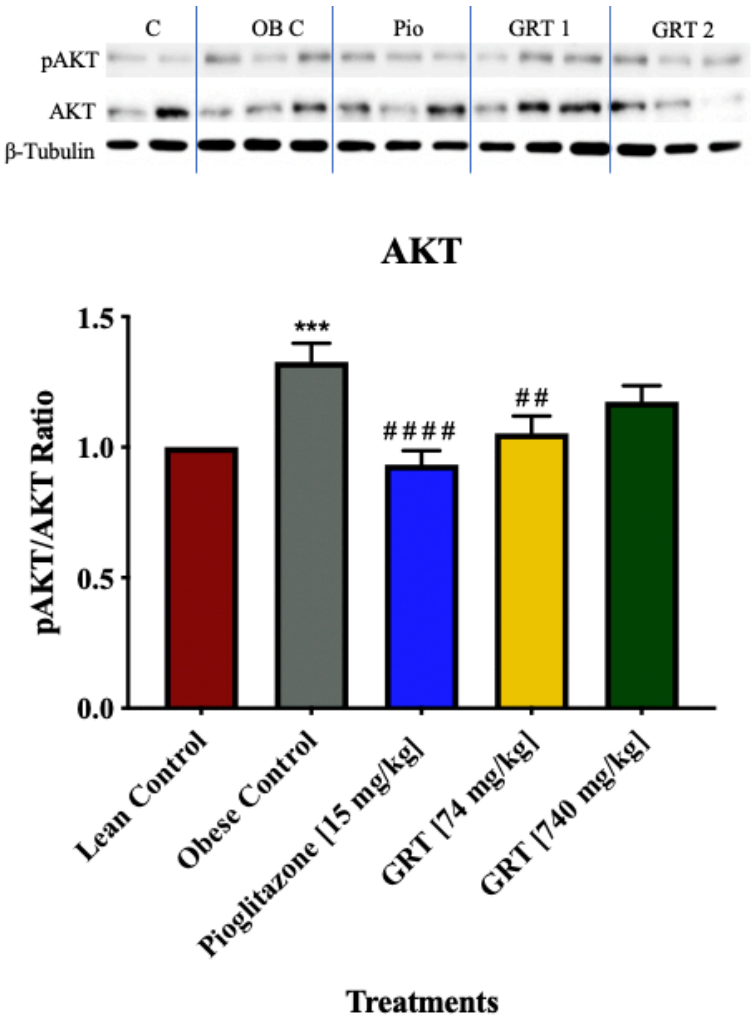

Figure 4.16 (a) pAKT/AKT ratio protein expression of *in vivo* NAFLD model liver tissue lysates, normalised to β-tubulin, showing the expression in the lean and obese controls and the effects of mono treatments with pioglitazone or Afriplex GRT (GRT). Images are a representation of one experiment, captured using a ChemiDoc MP (Bio-Rad, Hercules, USA). Histogram illustrates densitometric quantification data from the images captured following the Western blot analysis. The band intensity of the blots was quantified using an ImageLab™ software v6.0.1 (Bio-Rad.com). Data represented as mean ± SEM (n = 4), where ***P < 0.001 when compared to the lean control; $^{\#\#}$P < 0.01 and $^{\#\#\#\#}$P < 0.0001 when compared to the obese control. Lane 1 – 2 (Lean control), lane 3 – 5 (Obese control), lane 6 – 8 (Pio 15 mg/kg), lane 9 – 11 (GRT 74 mg/kg), lane 12 – 14 (GRT 740 mg/kg).

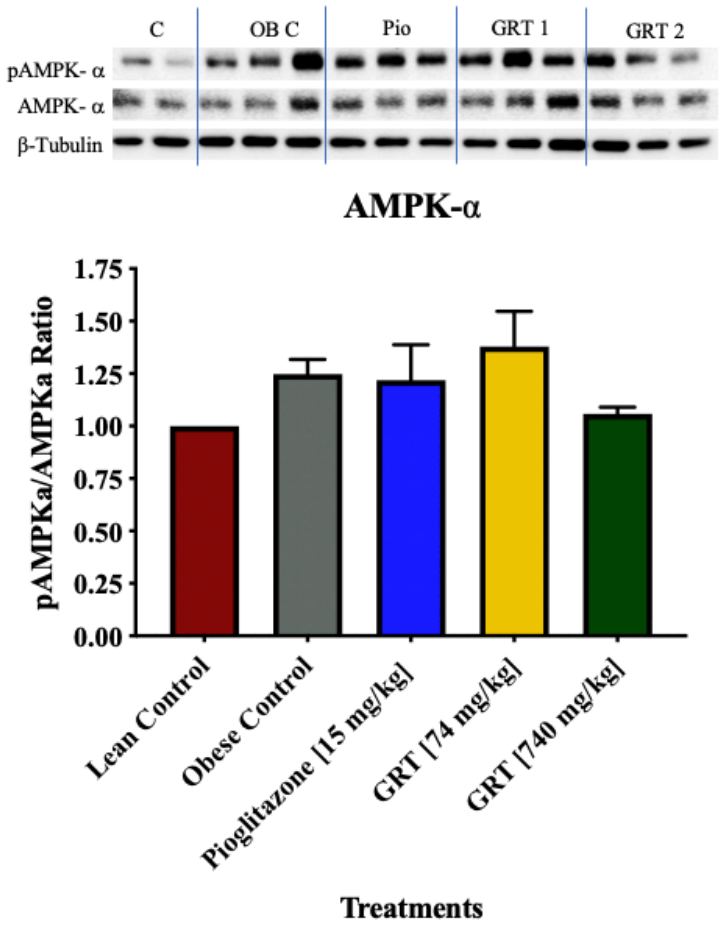

Figure 4.16 (b) pAMPK-α/AMPK-α ratio protein expression of *in vivo* NAFLD model liver tissue lysates, normalised to β-tubulin, showing the expression in the lean and obese controls and the effects of mono treatments with pioglitazone or Afriplex GRT (GRT). Images are a representation of one experiment, captured using a ChemiDoc MP (Bio-Rad, Hercules, USA). Histogram illustrates densitometric quantification data from the images captured following the Western blot analysis. The band intensity of the blots was quantified using an ImageLab™ software v6.0.1 (Bio-Rad.com). Data represented as mean ± SEM (n = 4). Lane 1 – 2 (Lean control), lane 3 – 5 (Obese control), lane 6 – 8 (Pio 15 mg/kg), lane 9 – 11 (GRT 74 mg/kg), lane 12 – 14 (GRT 740 mg/kg).

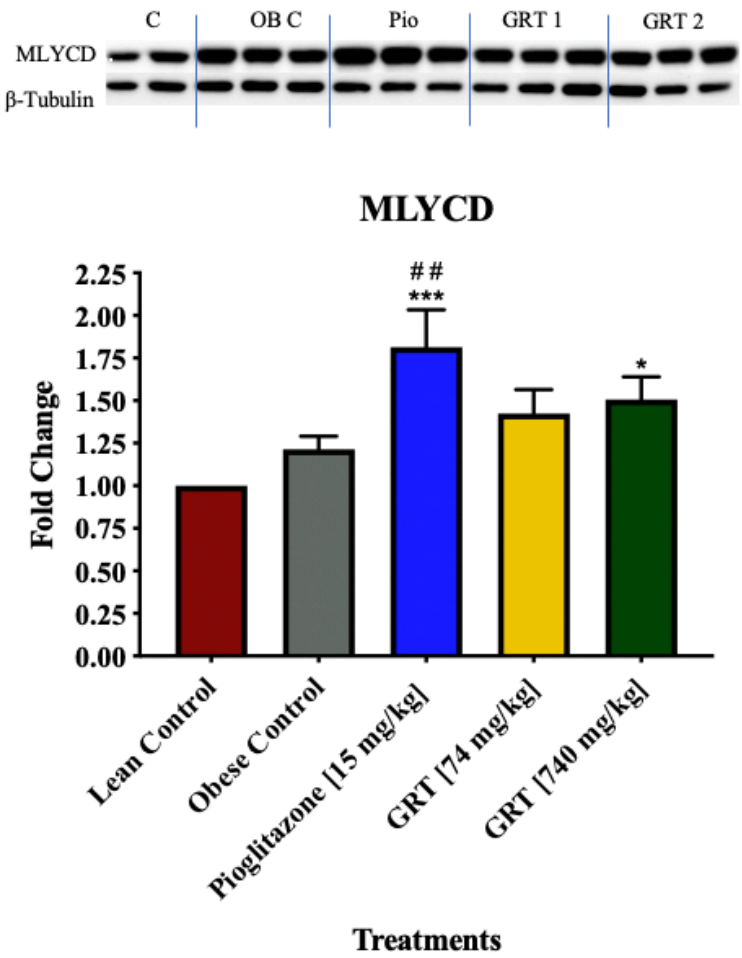

Figure 4.16 (c) MLYCD protein expression of *in vivo* NAFLD model liver tissue lysates, normalised to β-tubulin, showing the expression in the lean and obese controls and the effects of mono treatments with pioglitazone or Afriplex GRT (GRT). Images are a representation of one experiment, captured using a ChemiDoc MP (Bio-Rad, Hercules, USA). Histogram illustrates densitometric quantification data from the images captured following the Western blot analysis. The band intensity of the blots was quantified using an ImageLab™ software v6.0.1 (Bio-Rad.com). Data represented as mean ± SEM (n = 4), where *P < 0.05, ***P < 0.001 when compared to the lean control; $^{\#\#}$P < 0.01 when compared to the obese control. Lane 1 – 2 (Lean control), lane 3 – 5 (Obese control), lane 6 – 8 (Pio 15 mg/kg), lane 9 – 11 (GRT 74 mg/kg), lane 12 – 14 (GRT 740 mg/kg).

Expression of proteins from mouse liver lysates involved in apoptosis, oxidative stress, lipid and glucose metabolism as well as the inflammatory response is shown in Figure 4.17. The fold change was calculated using the equation: $\text{fold change} = (\frac{\text{treatment - normal control}}{\text{normal control}})$ and the treatments were compared to the control which was set at 1. Caspase-3 in Figure 4.17 (**a**) showed a significant down regulation when comparing the obese control to the lean control ($p < 0.0001$). Subsequent treatment groups with the various treatments also showed a significant down regulation when compared to the lean control, with GRT 2 significantly upregulating Caspase-3 when compared to the obese control ($p < 0.05$). GSTZ-1 in Figure 4.17 (**b**) expression showed a slight upregulation in the obese control when compared to the lean control, however, this was not significant and subsequent treatment groups with the various treatment regiments showed no significant differences when compared to both lean and obese controls. PPAR-α expression in Figure 4.17 (**c**) showed a slight upregulation in the obese control when compared to the lean control although the difference was not significant. Treatment with pioglitazone 15 mg/kg showed a significant upregulation when compared to the lean control ($p < 0.05$) while treatment with both doses of Afriplex GRT showed no significant differences when compared to both lean and obese controls. TNF-α expression in Figure 4.17 (**d**) showed no difference between the obese and the lean controls. Treatment with GRT 2 showed a significant down regulation when compared to both the lean ($p < 0.001$) and obese controls ($p < 0.001$).

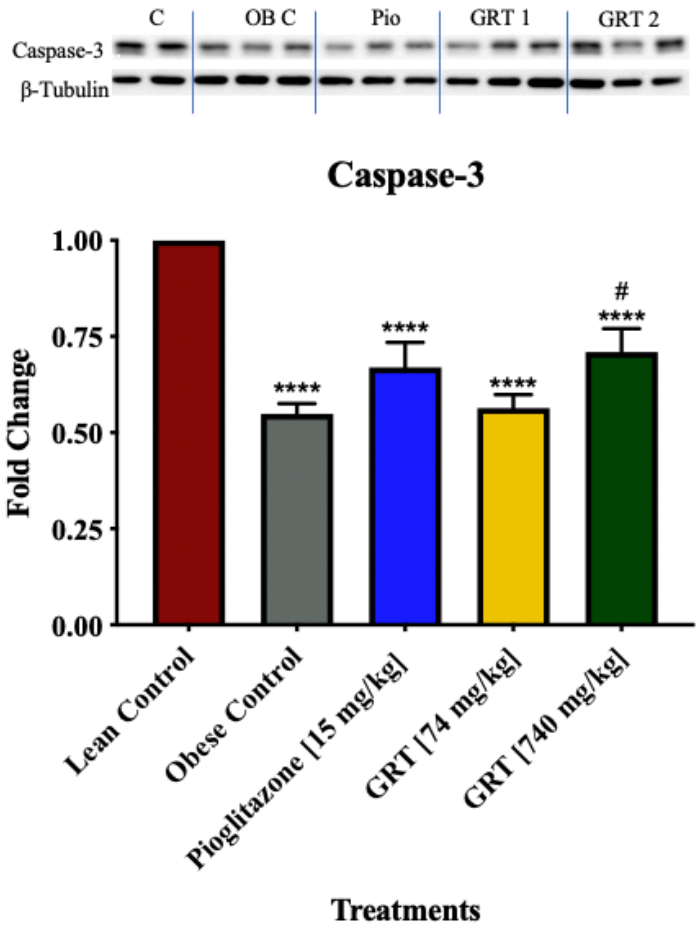

Figure 4.17 (a) Caspase-3 protein expression of *in vivo* NAFLD model liver tissue lysates, normalised to β-tubulin, showing the expression in the lean and obese controls and the effects of mono treatments with pioglitazone or Afriplex GRT (GRT). Images are a representation of one experiment, captured using a ChemiDoc MP (Bio-Rad, Hercules, USA). Histogram illustrates densitometric quantification data from the images captured following the Western blot analysis. The band intensity of the blots was quantified using an ImageLab™ software v6.0.1 (Bio-Rad.com). Data represented as mean ± SEM (n = 4), where ****$P < 0.0001$ when compared to the lean control and $^{\#}P < 0.05$ when compared to the obese control. Lane 1 – 2 (Lean control), lane 3 – 5 (Obese control), lane 6 – 8 (Pio 15 mg/kg), lane 9 – 11 (GRT 74 mg/kg), lane 12 – 14 (GRT 740 mg/kg).

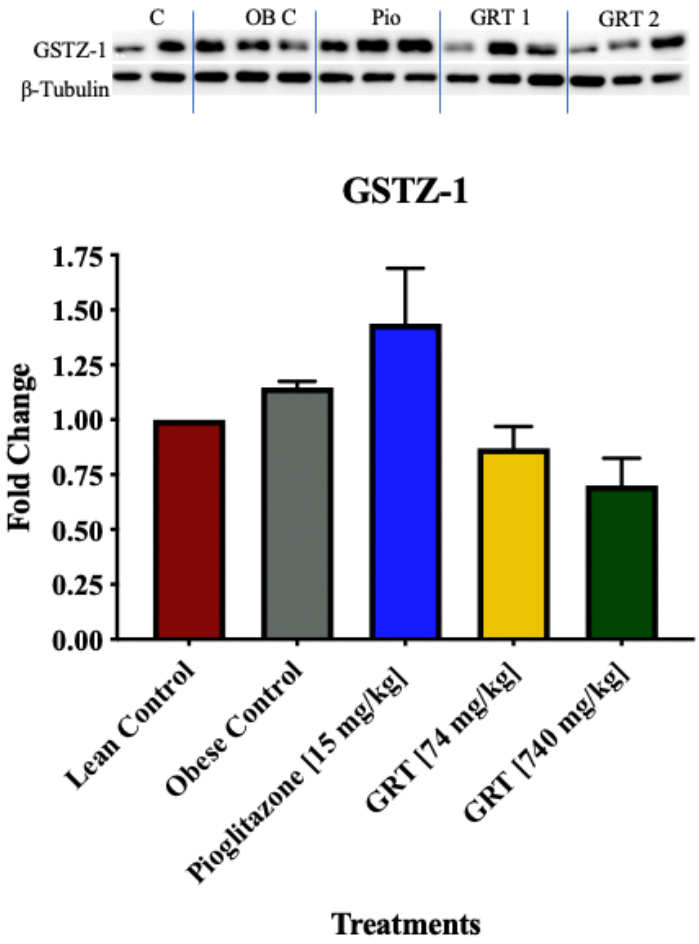

Figure 4.17 (b) GSTZ-1 protein expression of *in vivo* NAFLD model liver tissue lysates, normalised to β-tubulin, showing the expression in the lean and obese controls and the effects of mono treatments with pioglitazone or Afriplex GRT (GRT). Images are a representation of one experiment, captured using a ChemiDoc MP (Bio-Rad, Hercules, USA). Histogram illustrates densitometric quantification data from the images captured following the Western blot analysis. The band intensity of the blots was quantified using an ImageLab™ software v6.0.1 (Bio-Rad.com). Data represented as mean ± SEM (n = 4). Lane 1 – 2 (Lean control), lane 3 – 5 (Obese control), lane 6 – 8 (Pio 15 mg/kg), lane 9 – 11 (GRT 74 mg/kg), lane 12 – 14 (GRT 740 mg/kg).

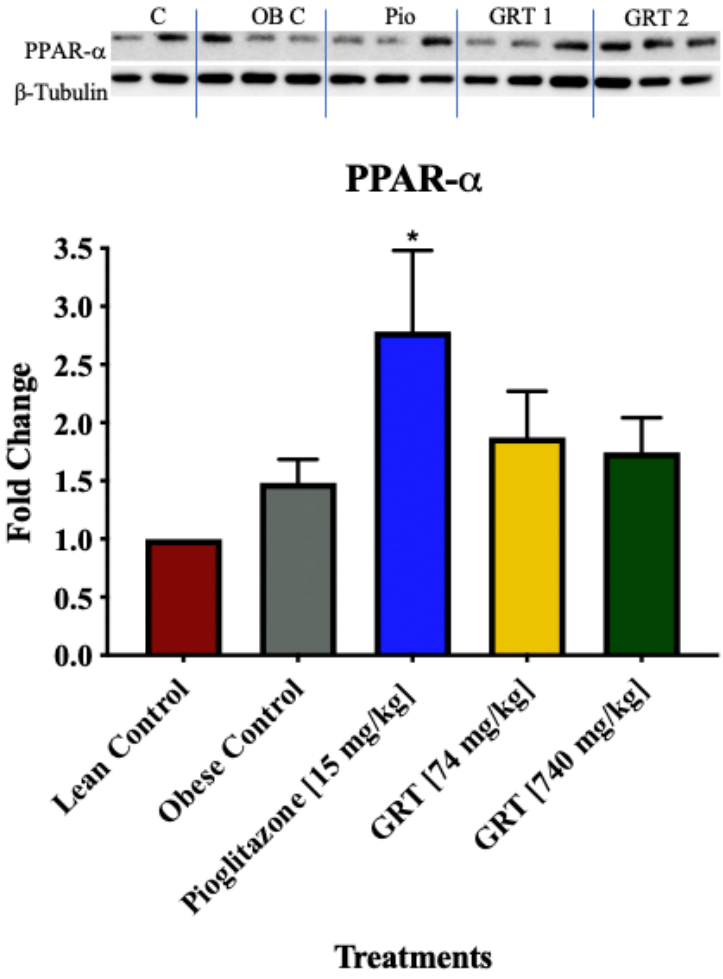

Figure 4.17 (c) PPAR-α protein expression of *in vivo* NAFLD model liver tissue lysates, normalised to β-tubulin, showing the expression in the lean and obese controls and the effects of mono treatments with pioglitazone or Afriplex GRT (GRT). Images are a representation of one experiment, captured using a ChemiDoc MP (Bio-Rad, Hercules, USA). Histogram illustrates densitometric quantification data from the images captured following the Western blot analysis. The band intensity of the blots was quantified using an ImageLab™ software v6.0.1 (Bio-Rad.com). Data represented as mean ± SEM (n = 4), where *P < 0.05 when compared to the lean control. Lane 1 – 2 (Lean control), lane 3 – 5 (Obese control), lane 6 – 8 (Pio 15 mg/kg), lane 9 – 11 (GRT 74 mg/kg), lane 12 – 14 (GRT 740 mg/kg).

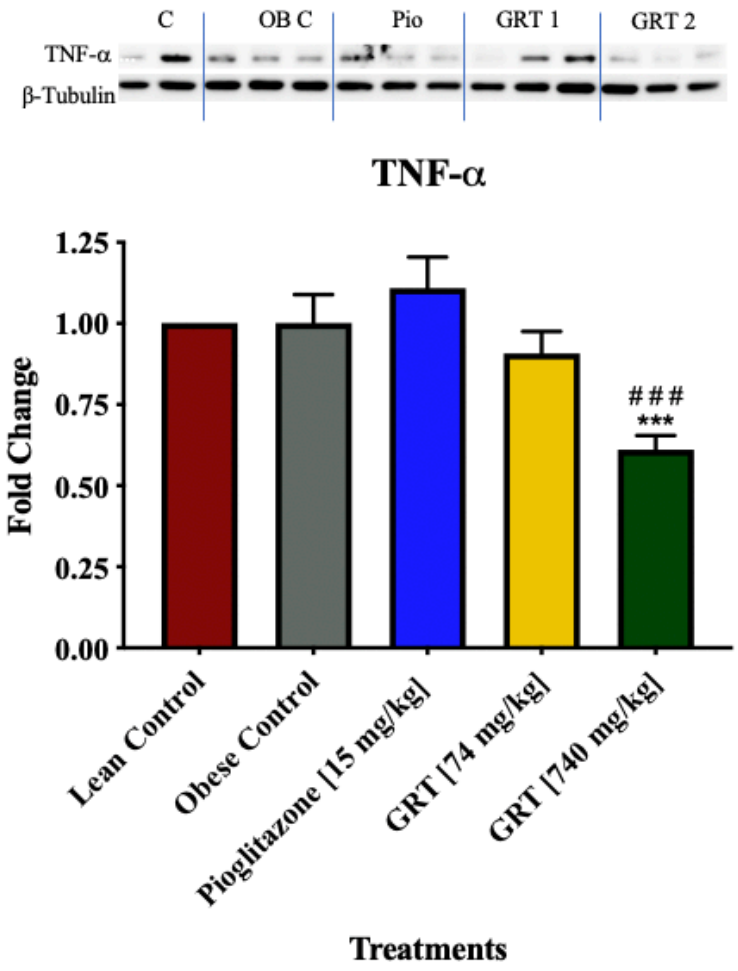

Figure 4.17 (d) TNF-α protein expression of *in vivo* NAFLD model liver tissue lysates, normalised to β-tubulin, showing the expression in the lean and obese controls and the effects of mono treatments with pioglitazone or Afriplex GRT (GRT). Images are a representation of one experiment, captured using a ChemiDoc MP (Bio-Rad, Hercules, USA). Histogram illustrates densitometric quantification data from the images captured following the Western blot analysis. The band intensity of the blots was quantified using an ImageLab™ software v6.0.1 (Bio-Rad.com). Data represented as mean ± SEM (n = 4), where ***$P < 0.001$ when compared to the lean control and $^{###}P < 0.001$, when compared to the obese control. Lane 1 – 2 (Lean control), lane 3 – 5 (Obese control), lane 6 – 8 (Pio 15 mg/kg), lane 9 – 11 (GRT 74 mg/kg), lane 12 – 14 (GRT 740 mg/kg).

4.7 Key findings

In C3A cells oleic acid induced significant amounts of intracellular lipid accumulation, as confirmed by the ORO assay. An MTT assay showed that the oleic acid treated cells retained over 70% mitochondrial activity, thus suggesting that the effect of treatment was not cytotoxic. Several genes involved in lipid and carbohydrate metabolism including *ChREBP*, *FASN* and *SREBF1* were significantly down-regulated by pioglitazone and Afriplex GRT treatment. *SOD2* and GSTZ-1, genes and proteins involved in hepatic oxidative stress were also down-regulated by Afriplex GRT and pioglitazone, suggestive of reduced hepatic oxidative stress *in vitro*. Protein expression of TNF-α and Caspase-3 was down-regulated by Afriplex GRT and pioglitazone, showing reduced inflammation and apoptosis. Afriplex GRT at the highest concentration prevented mitochondrial depolarisation induced by oleic acid. No apparent beneficial effects on oleic acid-induced steatosis by co-treatment of pioglitazone and Afriplex GRT was observed.

As expected the *db/db* mice were hyperglycaemic and obese at ten weeks. At necropsy the obese mice showed increased liver weights when compared to the lean control. The OGTT showed an improved glucose tolerance by treatment with Afriplex GRT in a dose-dependent manner. The H&E stained liver sections confirmed the NAFLD model by observed steatotic changes in the tissue architecture when comparing to the lean control. Pioglitazone treatment showed to reduce the size and abundance of lipid droplets. Afriplex GRT at the low dose reduced hepatocyte ballooning. The mRNA expression of *Chrebp*, *Fasn* and *Srebf1* was down-regulated by treatment with pioglitazone and Afriplex GRT. The mRNA and protein expression of *Sod2* and GSTZ-1, was down-regulated by Afriplex GRT and pioglitazone, indicating signs of reduced hepatic oxidative stress, similar to the *in vitro* model. The protein expression of TNF-α and Caspase-3 was also down-regulated by Afriplex GRT and pioglitazone, suggesting a reduction in inflammation and apoptosis in the mouse liver samples.

5. Discussion

5.1 Establishment of NAFLD Models

Hepatic steatosis, better described as increased hepatic lipid accumulation, results from an increased infiltration and accumulation of FFAs into the hepatocytes [1]. This increased flux of lipids into the liver is also known as fatty liver disease, and in the absence of alcohol the disease is termed as non-alcoholic fatty liver disease [8]. In order to mimic this ailment *in vitro*, C3A liver cells were exposed to oleic acid as described in subsection 3.2.1. Data obtained from the Oil red O (ORO) assay confirmed the presence of NAFLD in the induced control, which presented with a significant increase in intracellular lipid accumulation when compared to the normal control.

An MTT assay was performed parallel to the ORO to analyse the mitochondrial dehydrogenase activity within the model, measuring the overall cell metabolic activity and providing an approximation of the cell viability (Figure 4.1). The percentage viability of the cells was slightly decreased when compared to the uninduced normal control, this reduction in MTT activity by FFAs has previously been seen in MCF-7 cells by Pacheco *et al.* [155]. Barring the significant decrease in mitochondrial dehydrogenase activity, the cells still expressed over 70% mitochondrial activity, suggesting that the induction period with oleic acid was not toxic to the C3A liver cells, previously seen in a study by Jeong *et al.* [156].

In vivo, the study made use of tissue samples obtained from C57BL/6 lean (*db/*$^{+}$) and obese (*db/db*) male mice, a known animal model of NAFLD [6]. The obese mice showed significantly increased body weight over time and increased liver weights compared to their lean counterparts, suggesting an increase of FFAs into mice hepatic cells (Figure 4.10 (a) & (b)). Histological analysis confirmed a substantially different morphology when comparing the obese to the lean liver sections with increased lipid levels observed with the swelling of the hepatocytes as well as an increase in lipid droplet size and steatotic pattern classification (Figure 4.12). These are known characteristics of steatosis and the steatosis severity was confirmed through histological scoring, a method described by Trak-Smayra *et al.* [152]. Indeed, intracellular microvesicular, mediovesicular and microvacuolar lipid accumulation was observed in the obese mice, therefore, confirming the *in vivo* NAFLD model.

5.2 Effect of treatment on lipid and glucose utilisation by assessment of metabolic activity in models of NAFLD

Patients with dyslipidaemia and diabetes, express increased level of FFAs and glucose in their circulation, and are at increased risk for the development of NAFLD [36]. Insulin and glucose signalling play roles in *de novo* lipogenesis through sterol regulatory element-binding transcription factor 1 (SREBF1) and carbohydrate-response element-binding protein (ChREBP) pathways, respectively [157]. SREBF1 and ChREBP are major transcriptional regulators that induce key lipogenic enzymes such as FASN to promote lipogenesis in the liver. The role of ChREBP in regulating the transcription of genes related to glucose and lipid metabolism has been shown in the development of hepatic steatosis, via dyslipidaemia and glucose intolerance [158]. Both *in vitro* and *in vivo* mRNA expression of transcriptional regulators *SREBF1* and *ChREBP*, were down-regulated by treatment with pioglitazone and Afriplex GRT when compared to the oleic acid-induced/obese control (Figure 4.4 (b) & (d)) and Figure 4.13 (a) & (c)). The ORO data showed reduced lipid accumulation in the *in vitro* model by treatment with pioglitazone and Afriplex GRT (Figure 4.2). The use of treatment in combination showed an even greater reduction, suggesting that there may have been an additive effect by both regiments. The downstream mRNA expression of *FASN* was also down-regulated by treatment, suggesting that the mechanism by which Afriplex GRT reduces hepatic lipid content could be explained by the suppression of the above mentioned transcriptional regulators that induce lipogenic enzymes [159] (Figure 4.4 (c) and Figure 4.13 (b)).

The significant body weight gain over time in the *in vivo* model suggests increased lipogenesis and when comparing the data to the liver weights measured at terminations, the data confirms the translocation of excess fat into the hepatocytes (Figure 4.10 (a) & (b)). Histological analysis supports this as the H&E stained liver sections of the obese mice showed classical signs of hepatic steatosis [152]. In contrast, liver sections from obese mice treated with Afriplex GRT showed decreased steatosis when compared to the obese untreated control liver sections, the improved architecture of the liver suggest that Afriplex GRT may ameliorate hepatic steatosis, similarly reported by Beltrán-Debón R *et al.* [131] (Figure 4.12). Mice treated with pioglitazone, showed increased liver weight when compared to the liver weight of the obese control mice. However, with the histological analysis, an improvement was observed in liver architecture when compared to the obese control, suggesting that the drug reverses steatosis in the liver. The use of pioglitazone has been previously reported to enhance weight gain in patients with T2DM [160], thus supporting the increased liver weight observed in this study. The

overexpression of PPAR-α leads to the regulation of energy homeostasis by the expression of genes involved in fatty acid beta-oxidation [161]. In this study, it was found that *in vivo* mRNA expression of *PPAR-α* was significantly down-regulated by treatment with pioglitazone and Afriplex GRT, in comparison to the lean control (Figure 4.15 (b)). The mRNA expression of *PPAR-α* was not assessed *in vitro,* which is a limitation to the findings in the study. In addition to the mRNA expression, PPAR-α was found to be overexpressed in the mice treated with pioglitazone, at the protein level (Figure 4.17 (c)), suggesting that treatment with the drug induced the binding of multiple ribosomes, thereby increasing expression of the PPAR-α protein and subsequently inducing a lipolytic pathway *in vivo* [162].

The overexpression of active protein kinase B (pAKT) in the liver increases lipid synthesis which in turn results in NAFLD and hypertriglyceridemia [163]. Protein expression data from the *in vitro* model showed that treatment with Afriplex GRT reduced the AKT activity by pAKT/AKT ratio in a dose-dependent manner, when compared to both controls (Figure 4.7 (a)). This suppression of active AKT was similarly observed in the *in vivo* model by treatment with pioglitazone and Afriplex GRT (Figure 4.16 (a)). These results suggest that suppression of active AKT may have facilitated the reduction of lipid content by treatment with Afriplex GRT in both models of NAFLD, which is in agreement with the findings by Mazibuko-Mbeje *et al.* [164]. Malonyl-CoA decarboxylase (MLYCD) is an enzyme that is responsible for the reaction that converts malonyl-CoA to acetyl-CoA, which contributes to the breakdown of fatty acids. A study by An *et al.*, showed rats fed a high-fat diet had hepatic insulin resistance and hepatic lipid accumulation, ultimately ameliorated by the hepatic overexpression of MLYCD [165]. Therefore, a similar trend with the *in vivo* model was observed by the overexpression of MLYCD at the protein level with pioglitazone and Afriplex GRT treatment (Figure 4.16 (c)). This observation suggests that the treatment with pioglitazone and Afriplex GRT works via the overexpression of MLYCD, *in vivo*, subsequently ameliorating hepatic lipid accumulation. To the best of our knowledge this is the first study to report on the overexpression of MLYCD, *in vivo* by treatment with Afriplex GRT.

Alternatively, active 5' adenosine monophosphate-activated protein kinase (AMPK-α) improves glucose uptake, lowering blood glucose levels by increasing the utilisation of stored fat in the body, ultimately decreasing blood triglyceride levels [78]. *In vivo*, OGTT data showed that obese mice were less tolerant to glucose than their lean counterparts, confirming poor utilisation of glucose with the diseased model (Figure 4.11 (a) & (b)). Subsequent treatment

with pioglitazone and Afriplex GRT slightly enhanced glucose utilisation, however, no significances were observed when compared to their lean counterparts. At the protein level the expression of active AMPK-α showed no significant differences in the *in vivo* model, however the treatment with the low dose Afriplex GRT slightly upregulated active AMPK-α, in comparison to the lean control (Figure 4.16 (b)). The *in vitro* model showed that treatment with Afriplex GRT at a concentration of 10 µg/ml had a significant increase in pAMPK-α/AMPK-α ratio (Figure 4.7 (b)). Collectively the data observed from both models illustrate how active AMPK-α works in lipid reduction and how improved glucose utilisation is facilitated by treatment with Afriplex GRT, reported by Mazibuko-Mbeje *et al.* [164].

Glucose utilisation is a key factor in the development of NAFLD to NASH, where NASH is related to insulin resistance with a higher output of fatty acids and glucose to the liver [166]. *De novo* lipogenesis subsequently converts glucose into triglycerides contributing to hepatic steatosis. Silva *et al*., showed that the overexpression of glucose transporter (GLUT2) in mice fed a high fat diet contributed to the development of NASH by facilitated glucose uptake to hepatocytes [167]. The mRNA expression of *Glut2* was down-regulated in the *in vivo* treated with pioglitazone and Afriplex GRT (Figure 4.14 (a)). Additionally, co-treatment with pioglitazone and Afriplex GRT, *in vitro,* significantly down regulated *GLUT2* expression (Figure 4.5 (a)), which is suggestive of an additive effect by both treatments in combination, thus aiding in ameliorating hepatic lipid accumulation by suppressing facilitated glucose input into the hepatocytes. Glucose-6-phosphatase (G6PC) is an integral membrane protein of the endoplasmic reticulum, key in regulating the homeostasis of blood glucose concentrations by catalysing the hydrolysis of D-glucose 6-phosphate to D-glucose and orthophosphate, essentially providing recycled glucose to the cytoplasm of neutrophils to maintain normal function [168]. In this study, the mRNA expression of *G6PC* was reduced by the effects of steatosis induction with oleic acid in the *in vitro* model (Figure 4.5 (b)). However, treatment with pioglitazone or Afriplex GRT showed no significant changes. Thus, suggesting that the mode of action at which the treatments ameliorated hepatic lipid accumulation had no role in glucose regulation through *G6PC*, reported by Mazibuko *et al.* [144].

5.3 Effect of treatment on insulin signalling pathways in models of NAFLD

Numerous molecular and physiological changes occur during insulin resistance, resulting in the accumulation of lipids within the liver [12]. Insulin-dependent activation of AKT via phosphoinositide 3 kinase (PI3K) in the liver stimulates the storage of glucose as glycogen and regulates the pathways which suppress gluconeogenesis [163]. Moreover, dysfunctional AKT is associated with insulin resistance as well as impaired glucose tolerance [169]. In this study, the protein expression of PI3K was significantly down-regulated by treatment with pioglitazone and Afriplex GRT in the *in vitro* model (Figure 4.9 (b)). Therefore, suggesting that the suppression of PI3K contributed to a reduction of glucose uptake and increased fatty acid oxidation, thus leading to the reduction in hepatic lipid accumulation and gluconeogenesis, similarly reported by Mazibuko *et al.* [144].

Conventionally, lipid accumulation in hepatocytes is a result of obesity, as well as insulin resistance through, which there is an increased release of FFAs from adipocytes [13]. The rise in insulin and glucose levels in the circulation triggers *de novo* fatty acid synthesis, contributing to the abnormal retention of FFAs in hepatocytes [71,72]. When insulin binds to the insulin receptor substrate (IRS) its tyrosine kinase is activated through phosphorylation. IRS-1 is abundantly expressed in hepatocytes and tyrosine-phosphorylated IRS-1 bind to and activate PI3K, subsequently activating a serine/threonine kinase AKT [170]. AKT-dependent phosphorylation of forkhead box-containing protein O subfamily-1 (FOXO1) suppresses the expression of G6PC resulting in the inhibition of hepatic glucose output [170,171]. Insulin also stimulates the pathway by the upregulation of FASN thereby increasing hepatic lipogenesis [170,172]. *In vitro*, the upregulation of IRS-1 in both mRNA and protein expression (Figure 4.5 (c) and Figure 4.9 (a)) was seen by induction with oleic acid, this stimulates the upregulation of FASN confirming the increase of hepatic lipid content with the induced control. Subsequent treatment with either pioglitazone or Afriplex GRT as well as the combination treatment thereof showed a down-regulation of IRS-1 with both the mRNA and protein expression. Therefore, suggesting that the suppressed expression of IRS-1 had caused a downstream inhibition of lipogenic enzymes, ultimately reducing hepatic steatosis in the *in vitro* model. The *in vivo* model had shown that the (*db/db*) mice had a low expression of *Irs-1* mRNA when compared to the lean control and no effect was seen from using various treatment (Figure 4.14 (b)). This result was expected because the *db/db* mouse model has previously been shown to be insulin resistant [173]. Due to the model variation, it therefore implied that the treatment

reduced the activity of lipogenic genes using different pathways for the *in vivo* model compared to the *in vitro* model.

In literature, pioglitazone has been classified as a PPAR-γ agonist which decreases the release of FFAs through storage of triglycerides in adipose tissues. Pioglitazones' action on PPAR-γ inhibits the production of proinflammatory cytokines primarily on white adipose tissue and reduces lipid accumulation by improving insulin sensitivity in the liver [174]. The mRNA expression of *PPAR-γ* in both the *in vitro* and *in vivo* models of NAFLD was down-regulated by treatment with pioglitazone, and Afriplex GRT (Figure 4.6 (b) and Figure 4.14 (c)). The combination treatment in the *in vitro* model showed an even greater down-regulation of *PPAR-γ* mRNA expression, therefore suggesting that there may have been an additive effect by both regiments. At the protein level, PPAR-γ expression showed to be significantly upregulated in the *in vitro* model (Figure 4.9 (c)). Therefore, the low expression at gene level and subsequent upregulation at the protein level suggests that Afriplex GRT may have induced the binding of multiple ribosomes, thereby increasing expression of the PPAR-γ protein [162].

5.4 Effect of treatment on oxidative stress markers involved in the pathophysiology of NAFLD

Hepatic oxidative stress is considered a "second hit" in the pathogenesis of NASH. In NAFLD, mitochondrial dysfunction, peroxisomal and microsomal fatty acid oxidation and lipid peroxidation are the major generators of excessive amounts of ROS [14]. Superoxide dismutase and glutathione peroxidase are antioxidant enzymes that protect against oxidative damage caused by free radical attack [127,175]. *In vitro* mRNA expression of *SOD2* was significantly down-regulated by treatment with Afriplex GRT when compared to the induced control (Figure 4.6 (c)), signifying a reduction in antioxidant enzyme expression and potentially a reduction in enzyme activity contributing to reduced hepatic oxidative stress. Diabetes causes the production of free radicals in large amounts, this, in turn, results in the increased expression of antioxidant enzymes [176]. In contrast, the mRNA expression of *Sod2* was significantly down-regulated by treatment with pioglitazone and Afriplex GRT, in the *db/db* model (Figure 4.15 (c)). These results suggest that both *in vitro* and *in vivo* models presented with a reduction in antioxidant enzyme activity after treatment, aiding in the prevention of cellular damage. Alternatively, the mRNA expression of glutathione peroxidase (*GPX2*) was upregulated by the induction with oleic acid *in vitro* (Figure 4.6 (d)). Subsequent treatment with pioglitazone and Afriplex GRT showed no significant reduction, therefore suggesting that the *in vitro* model

alleviated hepatic oxidative stress by following a pathway different to *GPX2*, as seen with the reduction in *SOD2* mRNA expression. At the protein level, GSTZ-1 was significantly upregulated by induction with oleic acid in the *in vitro* model (Figure 4.8 (b)), however, a significant down-regulation of GSTZ-1 was observed by treatment with pioglitazone, Afriplex GRT and the combination treatments. This suggests that indeed the induction of hepatic steatosis with oleic acid induced hepatic oxidative stress to the *in vitro* model, as reported by Garcia-Ruiz *et al.* [177]. Subsequent treatment reduced the expression of GSTZ-1, thus suppressing the abundance of the antioxidant enzyme and its function in alleviating ROS. In the *in vivo* model, a similar reduction in GSTZ-1 was seen, by treatment with Afriplex GRT at a protein level (Figure 4.17 (b)), therefore in both *in vitro* and *in vivo* models Afriplex GRT facilitated the reduction in oxidative stress caused by fat infiltration into the liver by reduced expression levels of GSTZ-1, similarly to the findings by Jiang *et al*. [178].

5.5 Mechanistical analysis of treatment against hepatic steatosis by assessment of inflammatory response markers

The cascade of events highlighted by the progression of the disease is linked to the NF-κB, TNF-α and IL-6, which are the major pro-inflammatory cytokines that regulate innate and adaptive immune responses [85,88]. This activates a cascade of downstream inflammatory signalling kinases, namely; inhibitor kappa B kinase and C-Jun-N-terminal kinase [89]. At the protein level, TNF-α expression was significantly down-regulated by the treatment with Afriplex GRT in both *in vitro* and *in vivo* models (Figure 4.8 (c) and Figure 4.17 (d)). This result was expected as Afriplex GRT has been previously reported to have anti-inflammatory properties [25], therefore, suggesting that Afriplex GRT protects against hepatic inflammation by its action on inflammatory cytokines [127,132].

5.6 The effect of treatment on pro-apoptotic markers involved in NAFLD pathogenesis

Malhi *et al*., conducted a study that highlighted how hepatic lipoapoptosis was exhibited throughout the pathogenesis of NAFLD in several models using monounsaturated and saturated fatty acids as a mode of induction [100]. The JC-1 dye selectively enters the mitochondria of cells and changes colour from green to red due to change in the mitochondrial membrane potential and as such, healthy cells fluoresce red and unhealthy cells fluoresce green [149]. The observed decrease in mitochondrial membrane potential indicated by the JC-1 assay as cell fluorescence changed from green to red when compared to the induced control suggests induction of apoptosis via the intrinsic pathway in cells treated with Afriplex GRT (Figure 4.3).

In the *in vivo* model, the mRNA expression of *Caspase-3* was down-regulated in the (*db/db*) obese mice (Figure 4.15 (a)), while subsequent treatment with pioglitazone and Afriplex GRT had no significant effect. A similar trend was observed by both the *in vitro* and *in vivo* models at a protein level and both models of hepatic steatosis had not experienced apoptosis (Figure 4.8 (a) and Figure 4.17 (a)), in fact, the expression of Caspase-3 was reduced compared to the normal controls, which is suggestive of an anti-apoptosis response, similarly reported by Flanagan *et al*. [179]. Contrasting this statement, the treatment with the high dose Afriplex GRT in the *in vivo* model resulted in an upregulation of caspase-3 when compared to the obese control, suggesting that Afriplex GRT at a high dose may have pro-oxidant and pro-apoptotic activity.

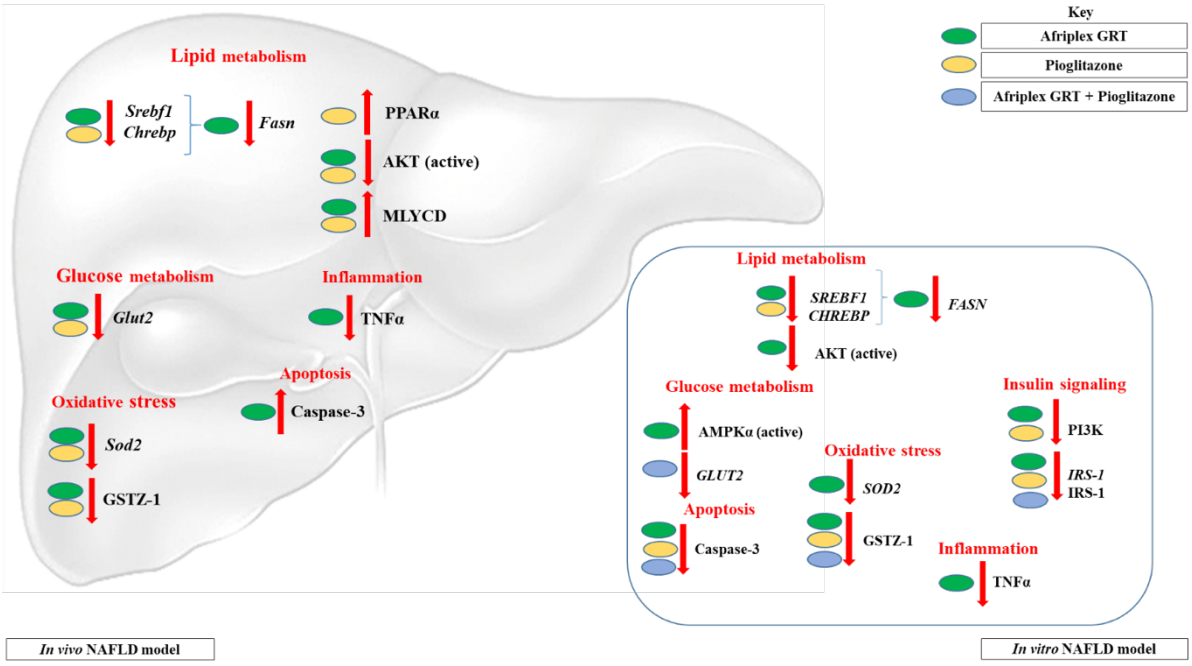

Figure 5.1: Mechanistic summary of experimentally induced NAFLD models in response to mono/co-treatment with Afriplex GRT and/or pioglitazone. **SREBF1** – Sterol regulatory element-binding factor-1, **ChREBP** – Carbohydrate-response element-binding protein, **FASN** – Fatty acid synthase, **PPAR-α** – Peroxisome proliferator-activated receptor α, **AKT** – Protein kinase B, **MLYCD** – Malonyl-CoA Decarboxylase, **TNF-α** – Tumour necrosis factor α, **GLUT2** – Glucose transporter 2, **SOD2** – Superoxide dismutase 2, **GSTZ-1** – Glutathione S-transferase Zeta 1, **PI3K** – Phosphoinositide 3-kinases, **IRS-1** – Insulin receptor substrate 1, **AMPK-α** – 5' Adenosine monophosphate-activated protein kinase-α.

6. Conclusion

The study hypothesised that Afriplex GRT could mitigate hepatic steatosis and aimed at investigating the hepatoprotective effects of Afriplex GRT and pioglitazone against hepatic oxidative stress, apoptosis and inflammation in an *in vitro* and *in vivo* model of NAFLD.

Oleic acid induced hepatic steatosis in C3A liver cells was dose-dependently reduced by Afriplex GRT, more so by its combination with pioglitazone. The mechanism by which Afriplex GRT reduced hepatic lipid content in both models was observed by the suppression of transcriptional regulators *SREBF1* and *ChREBP,* which in turn suppressed the expression of lipogenic enzymes. The overexpression of PPARα and MLYCD proteins may have led to the induced activity of a lipolytic pathway *in vivo,* supporting the histological reduction in lipid droplets observed from treatment with Afriplex GRT.

The insulin signalling cascade plays an important role in hepatic homeostasis mediated by IRS-1 and persistent insulin signalling in the liver is shown to promote lipogenesis by the conversion of excess glucose into hepatic fatty acids. Oleic acid induction overexpressed *IRS-1* and IRS-1 *in vitro*, causing a downstream upregulation of *FASN*. Afriplex GRT subsequently reversed the effects caused by oleic acid-induced hepatic steatosis by suppression of *IRS-1* and IRS-1 expression, thereby suppressing the expression of lipogenic enzymes in this model. The *db/db* mouse model showed signs of insulin resistance by a reduced *Irs-1* mRNA expression, leading to the reduced activity of lipogenic genes in a pathway other than the insulin signalling cascade. On the contrary a reduction in *Glut2* mRNA expression was seen by treatment with Afriplex GRT, indicating a possible suppression in hepatic facilitated glucose input.

The increased expression of antioxidant enzymes (*SOD2*, *GPX2* and GSTZ-1) prior treatment indicated an increased enzyme activity linked to hepatic oxidative stress. Although these enzymes may not serve as markers of oxidative stress per se, treatment with Afriplex GRT suppressed antioxidant enzymes *SOD2* and GSTZ-1*,* in both models. The differential expression of the antioxidant enzymes caused by Afriplex GRT in this study has, therefore, showed potential to possibly enhance the reduction in oxidative stress caused by hepatic fat infiltration.

At the protein level, the expression of TNF-α was significantly down-regulated by treatment with Afriplex GRT in both *in vitro* and *in vivo* models of NAFLD. Therefore, the suppression

in TNF-α expression suggests and that Afriplex GRT has potential in alleviating the progression of hepatic steatosis to steatohepatitis by its action on inflammatory cytokines.

The observed decrease in mitochondrial membrane potential indicated by the JC-1 assay as cell fluorescence changed from red to green by the induced control suggests an induction of apoptosis via the intrinsic pathway in cells treated with oleic acid. The mRNA expression of *Caspase-3, in vivo,* showed to be down regulated by treatment with pioglitazone and Afriplex GRT. At a protein level, models of hepatic steatosis showed a down regulation of the executioner caspase (Caspase-3) when compared to the normal control, thereby suggesting that capsase-3 is down-regulated in hepatic steatosis. However, treatment with the highest dose of Afriplex GRT *in vivo* resulted in an up-regulation of caspase-3 when compared to the obese control. Therefore, Afriplex GRT at a high dose may possess pro-apoptotic activities even in hepatic steatosis.

7. Concluding Remark and Future Perspectives

Altogether, this study confirmed the modulatory benefits of Afriplex GRT as a potential therapeutic agent for NAFLD by its action on both *in vitro* and *in vivo* models. Limitations were identified in certain aspects of the study, which unfortunately led to inconclusive findings. Gene and protein expressions of antioxidant enzymes related to hepatic oxidative stress were analysed, which do not necessarily account for the enzyme activity. Instead, oxidative stress markers could have assessed, using high throughput assays for more conclusive results, therefore this issue will be further investigated. A wider range of inflammatory markers could also be assessed, in order to fully elucidate the mechanism of action Afriplex GRT has on hepatic steatosis. Although subject to further analysis, the herbal extract shows promise in mitigating metabolic disorders related to poor diet and insulin resistance.

8. References

1. James O, Day C. Non-alcoholic steatohepatitis: another disease of affluence. *Lancet*. 1999;353(9165):1634-1636.

2. Tessari P, Coracina A, Cosma A, Tiengo A. Hepatic lipid metabolism and non-alcoholic fatty liver disease. *Nutr Metab Cardiovasc Dis*. 2009;19(4):291-302.

3. Ludwig J, Viggiano TR, Mcgill DB, Oh BJ. Nonalcoholic steatohepatitis: Mayo Clinic experiences with a hitherto unnamed disease. In: *Mayo Clinic Proceedings*. Vol 55. ; 1980:434-438.

4. Puri P, Sanyal AJ. Nonalcoholic fatty liver disease: definitions, risk factors, and workup. *Clin Liver Dis*. 2012;1(4):99.

5. Szczepaniak LS, Nurenberg P, Leonard D, et al. Magnetic resonance spectroscopy to measure hepatic triglyceride content: prevalence of hepatic steatosis in the general population. *Am J Physiol Metab*. 2005;288(2):E462-E468.

6. Anstee QM, Goldin RD. Mouse models in non-alcoholic fatty liver disease and steatohepatitis research. *Int J Exp Pathol*. 2006;87(1):1-16.

7. Alam S, Mustafa G, Alam M, Ahmad N. Insulin resistance in development and progression of nonalcoholic fatty liver disease. *World J Gastrointest Pathophysiol*. 2016;7(2):211.

8. Musso G, Gambino R, Cassader M. Recent insights into hepatic lipid metabolism in non-alcoholic fatty liver disease (NAFLD). *Prog Lipid Res*. 2009;48(1):1-26.

9. Perumpail BJ, Khan MA, Yoo ER, Cholankeril G, Kim D, Ahmed A. Clinical epidemiology and disease burden of nonalcoholic fatty liver disease. *World J Gastroenterol*. 2017;23(47):8263.

10. Chalasani N, Younossi Z, Lavine JE, et al. The diagnosis and management of nonalcoholic fatty liver disease: practice guidance from the American Association for the Study of Liver Diseases. *Hepatology*. 2018;67(1):328-357.

11. Petta S, Muratore C, Craxì A. Non-alcoholic fatty liver disease pathogenesis: The present and the future. *Dig Liver Dis*. 2009;41(9):615-625.

doi:https://doi.org/10.1016/j.dld.2009.01.004

12. Utzschneider KM, Kahn SE. The Role of Insulin Resistance in Nonalcoholic Fatty Liver Disease. *J Clin Endocrinol Metab*. 2006;91(12):4753-4761. doi:10.1210/jc.2006-0587

13. Czaja MJ, Ding W-X, Donohue TM, et al. Functions of autophagy in normal and diseased liver. *Autophagy*. 2013;9(8):1131-1158.

14. Tilg H, Moschen AR. Insulin resistance, inflammation, and non-alcoholic fatty liver disease. *Trends Endocrinol Metab*. 2008;19(10):371-379. doi:10.1016/j.tem.2008.08.005

15. Karlas T, Wiegand J, Berg T. Gastrointestinal complications of obesity: non-alcoholic fatty liver disease (NAFLD) and its sequelae. *Best Pract Res Clin Endocrinol Metab*. 2013;27(2):195-208.

16. Ribeiro PS, Cortez-Pinto H, Solá S, et al. Hepatocyte apoptosis, expression of death receptors, and activation of NF-κ B in the liver of nonalcoholic and alcoholic steatohepatitis patients. *Am J Gastroenterol*. 2004;99(9):1708-1717.

17. Belfort R, Harrison SA, Brown K, et al. A placebo-controlled trial of pioglitazone in subjects with nonalcoholic steatohepatitis. *N Engl J Med*. 2006;355(22):2297-2307.

18. Ahmed Labib Abdul-Kafy Adel Ibrahim Abdul-Aziz, Mohammed Gaber Keshka HHS. Effect of Metformin, Pioglitazone and Rosuvastatin on Induced Non-alcoholic Fatty Liver in Rats. *Egypt J Hosp Med*. 2019;76(4):4021-4028.

19. Xing Y, Ye S, Chen Y, Hu W, Chen Y. Hydrochloride pioglitazone protects diabetic rats against podocyte injury through preserving glomerular podocalyxin expression. *Arq Bras Endocrinol Metabol*. 2014;58(6):630-639.

20. Feige JN, Auwerx J. Transcriptional coregulators in the control of energy homeostasis. *Trends Cell Biol*. 2007;17(6):292-301.

21. Desouza C V, Shivaswamy V. Pioglitazone in the treatment of type 2 diabetes: safety and efficacy review. *Clin Med Insights Endocrinol Diabetes*. 2010;3:CMED-S5372.

22. Ajuwon OR, Oguntibeju OO, Marnewick JL. Amelioration of lipopolysaccharide-induced liver injury by aqueous rooibos (Aspalathus linearis) extract via inhibition of

pro-inflammatory cytokines and oxidative stress. *BMC Complement Altern Med*. 2014;14(1):392.

23. Joubert E, de Beer D. Rooibos (Aspalathus linearis) beyond the farm gate: From herbal tea to potential phytopharmaceutical. *South African J Bot*. 2011;77(4):869-886.

24. Joubert E, de Beer D, Malherbe CJ, et al. Occurrence and sensory perception of Z-2-(β-D-glucopyranosyloxy)-3-phenylpropenoic acid in rooibos (Aspalathus linearis). *Food Chem*. 2013;136(2):1078-1085.

25. Muller CJF, Malherbe CJ, Chellan N, Yagasaki K, Miura Y, Joubert E. Potential of rooibos, its major C-glucosyl flavonoids, and Z-2-(beta-D-glucopyranosyloxy)-3-phenylpropenoic acid in prevention of metabolic syndrome. *Crit Rev Food Sci Nutr*. 2018;58(2):227-246. doi:10.1080/10408398.2016.1157568

26. Petrovska BB. Historical review of medicinal plants' usage. *Pharmacogn Rev*. 2012;6(11):1.

27. Malviya N, Jain S, Malviya S. Antidiabetic potential of medicinal plants. *Acta Pol Pharm*. 2010;67(2):113-118.

28. Resnick HE, Jones K, Ruotolo G, et al. Insulin resistance, the metabolic syndrome, and risk of incident cardiovascular disease in nondiabetic American Indians: the Strong Heart Study. *Diabetes Care*. 2003;26(3):861-867.

29. Grundy SM, Brewer Jr HB, Cleeman JI, Smith Jr SC, Lenfant C. Definition of metabolic syndrome: report of the National Heart, Lung, and Blood Institute/American Heart Association conference on scientific issues related to definition. *Circulation*. 2004;109(3):433-438.

30. Kneeman JM, Misdraji J, Corey KE. Secondary causes of nonalcoholic fatty liver disease. *Therap Adv Gastroenterol*. 2012;5(3):199-207.

31. Duvnjak L, Duvnjak M. The metabolic syndrome - an ongoing story. *J Physiol Pharmacol*. 2009;60 Suppl 7:19-24.

32. Ghemrawi R, Battaglia-Hsu SF, Arnold C. Endoplasmic Reticulum Stress in Metabolic Disorders. *Cells*. 2018;7(6). doi:10.3390/cells7060063

33. Meex RCR, Watt MJ. Hepatokines: linking nonalcoholic fatty liver disease and insulin resistance. *Nat Rev Endocrinol*. 2017;13(9):509-520. doi:10.1038/nrendo.2017.56

34. Lafontan M, Langin D. Lipolysis and lipid mobilization in human adipose tissue. *Prog Lipid Res*. 2009;48(5):275-297. doi:https://doi.org/10.1016/j.plipres.2009.05.001

35. Gaggini M, Morelli M, Buzzigoli E, DeFronzo RA, Bugianesi E, Gastaldelli A. Non-alcoholic fatty liver disease (NAFLD) and its connection with insulin resistance, dyslipidemia, atherosclerosis and coronary heart disease. *Nutrients*. 2013;5(5):1544-1560.

36. Katsiki N, Mikhailidis DP, Mantzoros CS. Non-alcoholic fatty liver disease and dyslipidemia: An update. *Metabolism*. 2016;65(8):1109-1123. doi:https://doi.org/10.1016/j.metabol.2016.05.003

37. Enkhmaa B, Surampudi P, Anuurad E, Berglund L. Lifestyle Changes: Effect of Diet, Exercise, Functional Food, and Obesity Treatment on Lipids and Lipoproteins. In: Feingold KR, Anawalt B, Boyce A, et al., eds. *Endotext*. MDText.com, Inc.; 2000.

38. Nikolic D, Castellino G, Banach M, et al. PPAR Agonists, Atherogenic Dyslipidemia and Cardiovascular Risk. *Curr Pharm Des*. 2017;23(6):894-902. doi:10.2174/1381612822666161006151134

39. Katsiki N, Athyros VG, Karagiannis A, Mikhailidis DP. High-density Lipoprotein, Vascular Risk, Cancer and Infection: A Case of Quantity and Quality? *Curr Med Chem*. 2014;21(25):2917-2926. https://www.ingentaconnect.com/content/ben/cmc/2014/00000021/00000025/art00008

40. Chatrath H, Vuppalanchi R, Chalasani N. Dyslipidemia in patients with nonalcoholic fatty liver disease. *Semin Liver Dis*. 2012;32(1):22-29. doi:10.1055/s-0032-1306423

41. Ioannou GN. The role of cholesterol in the pathogenesis of NASH. *Trends Endocrinol Metab*. 2016;27(2):84-95.

42. Musso G, Gambino R, Cassader M. Cholesterol metabolism and the pathogenesis of non-alcoholic steatohepatitis. *Prog Lipid Res*. 2013;52(1):175-191.

43. Russell DW. Cholesterol biosynthesis and metabolism. *Cardiovasc drugs Ther*. 1992;6(2):103-110.

44. Yki-Järvinen H. Liver fat in the pathogenesis of insulin resistance and type 2 diabetes. *Dig Dis*. 2010;28(1):203-209.

45. Fabbrini E, Magkos F, Mohammed BS, et al. Intrahepatic fat, not visceral fat, is linked with metabolic complications of obesity. *Proc Natl Acad Sci*. 2009;106(36):15430-15435.

46. Williamson RM, Price JF, Glancy S, et al. Prevalence of and risk factors for hepatic steatosis and nonalcoholic fatty liver disease in people with type 2 diabetes: the Edinburgh Type 2 Diabetes Study. *Diabetes Care*. 2011;34(5):1139-1144.

47. Vernon G, Baranova A, Younossi ZM. Systematic review: the epidemiology and natural history of non-alcoholic fatty liver disease and non-alcoholic steatohepatitis in adults. *Aliment Pharmacol Ther*. 2011;34(3):274-285.

48. Dronamraju KR. *Infectious Disease and Host-Pathogen Evolution*. Cambridge University Press; 2004.

49. Bacon BR, Farahvash MJ, Janney CG, Neuschwander-Tetri BA. Nonalcoholic steatohepatitis: an expanded clinical entity. *Gastroenterology*. 1994;107(4):1103-1109.

50. Finkelstein EA, Ruhm CJ, Kosa KM. Economic causes and consequences of obesity. *Annu Rev Public Heal*. 2005;26:239-257.

51. Donnelly KL, Smith CI, Schwarzenberg SJ, Jessurun J, Boldt MD, Parks EJ. Sources of fatty acids stored in liver and secreted via lipoproteins in patients with nonalcoholic fatty liver disease. *J Clin Invest*. 2005;115(5):1343-1351.

52. Smith GI, Shankaran M, Yoshino M, et al. Insulin resistance drives hepatic de novo lipogenesis in nonalcoholic fatty liver disease. *J Clin Invest*. 2020;130(3).

53. Fabbrini E, Sullivan S, Klein S. Obesity and nonalcoholic fatty liver disease: biochemical, metabolic, and clinical implications. *Hepatology*. 2010;51(2):679-689.

54. Sunny NE, Bril F, Cusi K. Mitochondrial adaptation in nonalcoholic fatty liver disease: novel mechanisms and treatment strategies. *Trends Endocrinol Metab*. 2017;28(4):250-260.

55. Chowdhury A, Younossi ZM. Global epidemiology and risk factors for nonalcoholic

fatty liver disease. In: *Alcoholic and Non-Alcoholic Fatty Liver Disease*. Springer; 2016:21-40.

56. Araújo AR, Rosso N, Bedogni G, Tiribelli C, Bellentani S. Global epidemiology of non-alcoholic fatty liver disease/non-alcoholic steatohepatitis: what we need in the future. *Liver Int*. 2018;38:47-51.

57. Sutti S, Jindal A, Locatelli I, et al. Adaptive immune responses triggered by oxidative stress contribute to hepatic inflammation in NASH. *Hepatology*. 2014;59(3):886-897.

58. Gambino R, Musso G, Cassader M. Redox balance in the pathogenesis of nonalcoholic fatty liver disease: mechanisms and therapeutic opportunities. *Antioxid Redox Signal*. 2011;15(5):1325-1365.

59. Ahmed MH, Byrne CD. Modulation of sterol regulatory element binding proteins (SREBPs) as potential treatments for non-alcoholic fatty liver disease (NAFLD). *Drug Discov Today*. 2007;12(17-18):740-747.

60. Paruk IM, Pirie FJ, Motala AA. Non-alcoholic fatty liver disease in Africa: a hidden danger. *Glob Heal Epidemiol genomics*. 2019;4.

61. Kruger FC, Daniels C, Kidd M, et al. Non-alcoholic fatty liver disease (NAFLD) in the Western Cape: a descriptive analysis. *SAMJ South African Med J*. 2010;100(3):168-171.

62. Jain MR, Giri SR, Bhoi B, et al. Dual PPAR α/γ agonist Saroglitazar improves liver histopathology and biochemistry in experimental NASH models. *Liver Int*. 2018;38(6):1084-1094.

63. Berlanga A, Guiu-Jurado E, Porras JA, Auguet T. Molecular pathways in non-alcoholic fatty liver disease. *Clin Exp Gastroenterol*. 2014;7:221.

64. Byrne CD, Targher G. NAFLD: a multisystem disease. *J Hepatol*. 2015;62(1):S47-S64.

65. Rocio G, Morales-Garza LA, Martin-Estal I, Castilla-Cortazar I. Insulin-like growth factor-1 deficiency and cirrhosis establishment. *J Clin Med Res*. 2017;9(4):233.

66. Huang Y, Adams LA, Joseph J, Bulsara MK, Jeffrey GP. The ability of Hepascore to predict liver fibrosis in chronic liver disease: a meta-analysis. *Liver Int*. 2017;37(1):121-131.

67. Ekstedt M, Hagström H, Nasr P, et al. Fibrosis stage is the strongest predictor for disease-specific mortality in NAFLD after up to 33 years of follow-up. *Hepatology*. 2015;61(5):1547-1554.

68. Shetty K, Chen J, Shin J, Jogunoori W, Mishra L. Pathogenesis of hepatocellular carcinoma development in non-alcoholic fatty liver disease. *Curr Hepatol reports*. 2015;14(2):119-127.

69. Shimomura I, Bashmakov Y, Horton JD. Increased levels of nuclear SREBP-1c associated with fatty livers in two mouse models of diabetes mellitus. *J Biol Chem*. 1999;274(42):30028-30032.

70. Newton JL. Systemic symptoms in non-alcoholic fatty liver disease. *Dig Dis*. 2010;28(1):214-219.

71. Yahagi N, Shimano H, Hasty AH, et al. Absence of sterol regulatory element-binding protein-1 (srebp-1) ameliorates fatty livers but not obesity or insulin resistance inlep ob/lep ob mice. *J Biol Chem*. 2002;277(22):19353-19357.

72. Knebel B, Göddeke S, Hartwig S, et al. Alteration of liver peroxisomal and mitochondrial functionality in the NZO mouse model of metabolic syndrome. *PROTEOMICS–Clinical Appl*. 2018;12(1):1700028.

73. Unger RH, Clark GO, Scherer PE, Orci L. Lipid homeostasis, lipotoxicity and the metabolic syndrome. *Biochim Biophys Acta (BBA)-Molecular Cell Biol Lipids*. 2010;1801(3):209-214.

74. Lodhi IJ, Semenkovich CF. Peroxisomes: a nexus for lipid metabolism and cellular signaling. *Cell Metab*. 2014;19(3):380-392.

75. Knebel B, Fahlbusch P, Dille M, et al. Fatty Liver Due to Increased de novo Lipogenesis: Alterations in the Hepatic Peroxisomal Proteome. *Front Cell Dev Biol*. 2019;7:248. doi:10.3389/fcell.2019.00248

76. Brown MS, Goldstein JL. The SREBP pathway: regulation of cholesterol metabolism by proteolysis of a membrane-bound transcription factor. *Cell*. 1997;89(3):331-340.

77. Horton JD, Goldstein JL, Brown MS. SREBPs: activators of the complete program of cholesterol and fatty acid synthesis in the liver. *J Clin Invest*. 2002;109(9):1125-1131.

78. Lee WJ, Kim M, Park H-S, et al. AMPK activation increases fatty acid oxidation in skeletal muscle by activating PPARα and PGC-1. *Biochem Biophys Res Commun*. 2006;340(1):291-295.

79. Zong H, Ren JM, Young LH, et al. AMP kinase is required for mitochondrial biogenesis in skeletal muscle in response to chronic energy deprivation. *Proc Natl Acad Sci*. 2002;99(25):15983-15987.

80. Han H-S, Kang G, Kim JS, Choi BH, Koo S-H. Regulation of glucose metabolism from a liver-centric perspective. *Exp Mol Med*. 2016;48(3):e218-e218.

81. Masarone M, Rosato V, Dallio M, et al. Role of Oxidative Stress in Pathophysiology of Nonalcoholic Fatty Liver Disease. *Oxid Med Cell Longev*. 2018;2018:9547613. doi:10.1155/2018/9547613

82. Silva MFB, Aires CCP, Luis PBM, et al. Valproic acid metabolism and its effects on mitochondrial fatty acid oxidation: a review. *J Inherit Metab Dis*. 2008;31(2):205-216.

83. Davidzon G, Mancuso M, Ferraris S, et al. POLG mutations and Alpers syndrome. *Ann Neurol Off J Am Neurol Assoc Child Neurol Soc*. 2005;57(6):921-923.

84. Aubert J, Begriche K, Knockaert L, Robin M-A, Fromenty B. Increased expression of cytochrome P450 2E1 in nonalcoholic fatty liver disease: mechanisms and pathophysiological role. *Clin Res Hepatol Gastroenterol*. 2011;35(10):630-637.

85. Naik A, Košir R, Rozman D. Genomic aspects of NAFLD pathogenesis. *Genomics*. 2013;102(2):84-95. doi:10.1016/j.ygeno.2013.03.007

86. Nobili V, Parola M, Alisi A, et al. Oxidative stress parameters in paediatric non-alcoholic fatty liver disease. *Int J Mol Med*. 2010;26(4):471-476.

87. Irie M, Sohda T, Iwata K, et al. Levels of the oxidative stress marker γ-glutamyltranspeptidase at different stages of nonalcoholic fatty liver disease. *J Int Med Res*. 2012;40(3):924-933.

88. Jorge ASB, Andrade JMO, Paraíso AF, et al. Body mass index and the visceral adipose tissue expression of IL-6 and TNF-alpha are associated with the morphological severity of non-alcoholic fatty liver disease in individuals with class III obesity. *Obes Res Clin Pract*. 2018;12(1):1-8. doi:10.1016/j.orcp.2016.03.009

89. Faheem S, Saeed N, El-naga R, Azab S. Non alcoholic fatty liver disease: pathogenesis, role of (TNF-α, IL-6) in hepatic inflammation and future potential nutraceutical treatment. *Arch Pharm Sci Ain Shams Univ*. 2019;3(2):154-169. doi:10.21608/aps.2019.17201.1012

90. Utzschneider KM, Largajolli A, Bertoldo A, et al. Serum ferritin is associated with non-alcoholic fatty liver disease and decreased B-cell function in non-diabetic men and women. *J Diabetes Complications*. 2014;28(2):177-184. doi:https://doi.org/10.1016/j.jdiacomp.2013.11.007

91. Buzzetti E, Pinzani M, Tsochatzis EA. The multiple-hit pathogenesis of non-alcoholic fatty liver disease (NAFLD). *Metabolism*. 2016;65(8):1038-1048. doi:https://doi.org/10.1016/j.metabol.2015.12.012

92. Gamberi T, Magherini F, Modesti A, Fiaschi T. Adiponectin Signaling Pathways in Liver Diseases. *Biomedicines*. 2018;6(2):52. https://www.mdpi.com/2227-9059/6/2/52

93. Day CP. From Fat to Inflammation. *Gastroenterology*. 2006;130(1):207-210. doi:10.1053/j.gastro.2005.11.017

94. Joza N, Susin SA, Daugas E, et al. Essential role of the mitochondrial apoptosis-inducing factor in programmed cell death. *Nature*. 2001;410(6828):549-554.

95. Fan Y, Bergmann A. Apoptosis-induced compensatory proliferation. The Cell is dead. Long live the Cell! *Trends Cell Biol*. 2008;18(10):467-473.

96. Rysavy NM, Shimoda LMN, Dixon AM, et al. Beyond apoptosis: the mechanism and function of phosphatidylserine asymmetry in the membrane of activating mast cells. *Bioarchitecture*. 2014;4(4-5):127-137.

97. Alkhouri N, Carter-Kent C, Feldstein AE. Apoptosis in nonalcoholic fatty liver disease: diagnostic and therapeutic implications. *Expert Rev Gastroenterol Hepatol*. 2011;5(2):201-212.

98. Siebler J, Schuchmann M, Strand S, Lehr HA, Neurath MF, Galle PR. Enhanced sensitivity to CD95-induced apoptosis in ob/ob mice. *Dig Dis Sci*. 2007;52(9):2396-2402.

99. Ferreira DMS, Castro RE, Machado M V, et al. Apoptosis and insulin resistance in liver

and peripheral tissues of morbidly obese patients is associated with different stages of non-alcoholic fatty liver disease. *Diabetologia*. 2011;54(7):1788-1798.

100. Malhi H, Bronk SF, Werneburg NW, Gores GJ. Free fatty acids induce JNK-dependent hepatocyte lipoapoptosis. *J Biol Chem*. 2006;281(17):12093-12101. doi:10.1074/jbc.M510660200

101. Caldwell SH, Chang CY, Nakamoto RK, Krugner-Higby L. Mitochondria in nonalcoholic fatty liver disease. *Clin Liver Dis*. 2004;8(3):595-617, x. doi:10.1016/j.cld.2004.04.009

102. Byrne CD, Targher G. Ectopic Fat, Insulin Resistance, and Nonalcoholic Fatty Liver Disease. *Arterioscler Thromb Vasc Biol*. 2014;34(6):1155-1161. doi:10.1161/atvbaha.114.303034

103. Hui JM, Hodge A, Farrell GC, Kench JG, Kriketos A, George J. Beyond insulin resistance in NASH: TNF-α or adiponectin? *Hepatology*. 2004;40(1):46-54.

104. Wong VW-S, Wong GL-H, Choi PC-L, et al. Disease progression of non-alcoholic fatty liver disease: a prospective study with paired liver biopsies at 3 years. *Gut*. 2010;59(7):969-974.

105. Zelber-Sagi S, Lotan R, Shlomai A, et al. Predictors for incidence and remission of NAFLD in the general population during a seven-year prospective follow-up. *J Hepatol*. 2012;56(5):1145-1151.

106. Polyzos SA, Kountouras J, Zavos C. Nonlinear distribution of adiponectin in patients with nonalcoholic fatty liver disease limits its use in linear regression analysis. *J Clin Gastroenterol*. 2010;44(3):229-230.

107. Shargorodsky M, Omelchenko E, Matas Z, Boaz M, Gavish D. Relation between augmentation index and adiponectin during one-year metformin treatment for nonalcoholic steatohepatosis: effects beyond glucose lowering? *Cardiovasc Diabetol*. 2012;11(1):61.

108. Chruściel P, Sahebkar A, Rembek-Wieliczko M, et al. Impact of statin therapy on plasma adiponectin concentrations: a systematic review and meta-analysis of 43 randomized controlled trial arms. *Atherosclerosis*. 2016;253:194-208.

109. Chaudhury A, Duvoor C, Reddy Dendi VS, et al. Clinical Review of Antidiabetic Drugs: Implications for Type 2 Diabetes Mellitus Management. *Front Endocrinol (Lausanne)*. 2017;8. doi:10.3389/fendo.2017.00006

110. Ibrahim SH, Kohli R, Gores GJ. Mechanisms of lipotoxicity in NAFLD and clinical implications. *J Pediatr Gastroenterol Nutr*. 2011;53(2):131-140. doi:10.1097/MPG.0b013e31822578db

111. Ahmadian M, Suh JM, Hah N, et al. PPARγ signaling and metabolism: the good, the bad and the future. *Nat Med*. 2013;19(5):557-566. doi:10.1038/nm.3159

112. Laurencikiene J, Rydén M. Liver X receptors and fat cell metabolism. *Int J Obes*. 2012;36(12):1494-1502.

113. Lee C-H, Olson P, Evans RM. Minireview: lipid metabolism, metabolic diseases, and peroxisome proliferator-activated receptors. *Endocrinology*. 2003;144(6):2201-2207.

114. Phielix E, Szendroedi J, Roden M. The role of metformin and thiazolidinediones in the regulation of hepatic glucose metabolism and its clinical impact. *Trends Pharmacol Sci*. 2011;32(10):607-616.

115. Bell LN, Wang J, Muralidharan S, et al. Relationship between adipose tissue insulin resistance and liver histology in nonalcoholic steatohepatitis: a pioglitazone versus vitamin E versus placebo for the treatment of nondiabetic patients with nonalcoholic steatohepatitis trial follow-up study. *Hepatology*. 2012;56(4):1311-1318.

116. Nordling L. Rooibos tea profits will be shared with Indigenous communities in landmark agreement. *Nature*. 2019;575(7781):19.

117. Schloms L, Storbeck K-H, Swart P, Gelderblom WCA, Swart AC. The influence of Aspalathus linearis (Rooibos) and dihydrochalcones on adrenal steroidogenesis: quantification of steroid intermediates and end products in H295R cells. *J Steroid Biochem Mol Biol*. 2012;128(3-5):128-138.

118. Choo CY, Sulong NY, Man F, Wong TW. Vitexin and isovitexin from the leaves of Ficus deltoidea with in-vivo α-glucosidase inhibition. *J Ethnopharmacol*. 2012;142(3):776-781.

119. Choi JS, Islam MN, Ali MY, Kim EJ, Kim YM, Jung HA. Effects of C-glycosylation

on anti-diabetic, anti-Alzheimer's disease and anti-inflammatory potential of apigenin. *Food Chem Toxicol*. 2014;64:27-33.

120. Muller CJF, Joubert E, De Beer D, et al. Acute assessment of an aspalathin-enriched green rooibos (Aspalathus linearis) extract with hypoglycemic potential. *Phytomedicine*. 2012;20(1):32-39.

121. Liu J, Ma Y, Wang Y, Du Z, Shen J, Peng H. Reduction of lipid accumulation in HepG2 cells by luteolin is associated with activation of AMPK and mitigation of oxidative stress. *Phyther Res*. 2011;25(4):588-596.

122. Ajuwon OR, Katengua-Thamahane E, Van Rooyen J, Oguntibeju OO, Marnewick JL. Protective effects of rooibos (Aspalathus linearis) and/or red palm oil (Elaeis guineensis) supplementation on tert-butyl hydroperoxide-induced oxidative hepatotoxicity in Wistar rats. *Evidence-Based Complement Altern Med*. 2013;2013.

123. Pandey KB, Rizvi SI. Plant polyphenols as dietary antioxidants in human health and disease. *Oxid Med Cell Longev*. 2009;2(5):270-278.

124. Rein MJ, Renouf M, Cruz-Hernandez C, Actis-Goretta L, Thakkar SK, da Silva Pinto M. Bioavailability of bioactive food compounds: a challenging journey to bioefficacy. *Br J Clin Pharmacol*. 2013;75(3):588-602.

125. Courts FL, Williamson G. The occurrence, fate and biological activities of C-glycosyl flavonoids in the human diet. *Crit Rev Food Sci Nutr*. 2015;55(10):1352-1367.

126. Kreuz S, Joubert E, Waldmann K-H, Ternes W. Aspalathin, a flavonoid in Aspalathus linearis (rooibos), is absorbed by pig intestine as a C-glycoside. *Nutr Res*. 2008;28(10):690-701.

127. Orlando P, Chellan N, Muller CJF, et al. Green rooibos extract improves plasma lipid profile and oxidative status in diabetic non-human primates. *Free Radic Biol Med*. 2017;108:S97.

128. Cicero AFG, Colletti A, Bajraktari G, et al. Lipid-lowering nutraceuticals in clinical practice: position paper from an International Lipid Expert Panel. *Nutr Rev*. 2017;75(9):731-767.

129. Fraga CG, Galleano M, Verstraeten S V, Oteiza PI. Basic biochemical mechanisms

behind the health benefits of polyphenols. *Mol Aspects Med*. 2010;31(6):435-445.

130. Johnson R, de Beer D, Dludla P V, Ferreira D, Muller CJF, Joubert E. Aspalathin from rooibos (Aspalathus linearis): a bioactive C-glucosyl dihydrochalcone with potential to target the metabolic syndrome. *Planta Med*. 2018;84(09/10):568-583.

131. Beltrán-Debón R, Rull A, Rodríguez-Sanabria F, et al. Continuous administration of polyphenols from aqueous rooibos (Aspalathus linearis) extract ameliorates dietary-induced metabolic disturbances in hyperlipidemic mice. *Phytomedicine*. 2011;18(5):414-424.

132. Patel O, Muller C, Joubert E, et al. Pharmacokinetic interaction of green rooibos extract with atorvastatin and metformin in rats. *Front Pharmacol*. 2019;10:1243.

133. Calitz C, Du Plessis L, Gouws C, et al. Herbal hepatotoxicity: current status, examples, and challenges. *Expert Opin Drug Metab Toxicol*. 2015;11(10):1551-1565.

134. Sun S, Zhang H, Xue B, et al. Protective effect of glutathione against lipopolysaccharide-induced inflammation and mortality in rats. *Inflamm Res*. 2006;55(11):504-510.

135. South-African-Rooibos-Council. No Title. Published 2013. https://sarooibos.co.za

136. Nakamura A, Terauchi Y. Lessons from mouse models of high-fat diet-induced NAFLD. *Int J Mol Sci*. 2013;14(11):21240-21257.

137. Kanuri G, Bergheim I. In vitro and in vivo models of non-alcoholic fatty liver disease (NAFLD). *Int J Mol Sci*. 2013;14(6):11963-11980. doi:10.3390/ijms140611963

138. Vergani L. Fatty acids and effects on in vitro and in vivo models of liver steatosis. *Curr Med Chem*. 2019;26(19):3439-3456.

139. C Chavez-Tapia N, Rosso N, Tiribelli C. In vitro models for the study of non-alcoholic fatty liver disease. *Curr Med Chem*. 2011;18(7):1079-1084.

140. Araya J, Rodrigo R, Videla LA, et al. Increase in long-chain polyunsaturated fatty acid n− 6/n− 3 ratio in relation to hepatic steatosis in patients with non-alcoholic fatty liver disease. *Clin Sci*. 2004;106(6):635-643.

141. Rogue A, Anthérieu S, Vluggens A, et al. PPAR agonists reduce steatosis in oleic acid-

overloaded HepaRG cells. *Toxicol Appl Pharmacol*. 2014;276(1):73-81.

142. Niklas J, Bonin A, Mangin S, et al. Central energy metabolism remains robust in acute steatotic hepatocytes challenged by a high free fatty acid load. *BMB Rep*. 2012;45(7):396-401.

143. Moravcova A, Cervinkova Z, Kucera O, Mezera V, Rychtrmoc D, Lotkova H. The effect of oleic and palmitic acid on induction of steatosis and cytotoxicity on rat hepatocytes in primary culture. *Physiol Res*. 2015;64:S627.

144. Mazibuko SE. In vitro and in vivo effect of Aspalathus linearis and its major polyphenols on carbohydrate and lipid metabolism in insulin resistant models. Published online 2014.

145. Alkhatatbeh MJ, Lincz LF, Thorne RF. Low simvastatin concentrations reduce oleic acid-induced steatosis in HepG2 cells: An in vitro model of non-alcoholic fatty liver disease. *Exp Ther Med*. 2016;11(4):1487-1492. doi:10.3892/etm.2016.3069

146. Mosmann T. Rapid colorimetric assay for cellular growth and survival: application to proliferation and cytotoxicity assays. *J Immunol Methods*. 1983;65(1-2):55-63.

147. Mehlem A, Hagberg CE, Muhl L, Eriksson U, Falkevall A. Imaging of neutral lipids by oil red O for analyzing the metabolic status in health and disease. *Nat Protoc*. 2013;8(6):1149-1154.

148. Reers M, Smith TW, Chen LB. J-aggregate formation of a carbocyanine as a quantitative fluorescent indicator of membrane potential. *Biochemistry*. 1991;30(18):4480-4486.

149. Sivandzade F, Bhalerao A, Cucullo L. Analysis of the mitochondrial membrane potential using the cationic JC-1 dye as a sensitive fluorescent probe. *Bio-protocol*. 2019;9(1).

150. Ishida H, Takizawa M, Ozawa S, et al. Pioglitazone improves insulin secretory capacity and prevents the loss of β-cell mass in obese diabetic db/db mice: possible protection of β cells from oxidative stress. *Metabolism*. 2004;53(4):488-494.

151. Reagan-Shaw S, Nihal M, Ahmad N. Dose translation from animal to human studies revisited. *FASEB J*. 2008;22(3):659-661. doi:10.1096/fj.07-9574LSF

152. Trak-Smayra V, Paradis V, Massart J, Nasser S, Jebara V, Fromenty B. Pathology of the liver in obese and diabetic ob/ob and db/db mice fed a standard or high-calorie diet. *Int J Exp Pathol*. 2011;92(6):413-421.

153. Johnson R, Dludla P, Joubert E, et al. Aspalathin, a dihydrochalcone C-glucoside, protects H9c2 cardiomyocytes against high glucose induced shifts in substrate preference and apoptosis. *Mol Nutr Food Res*. 2016;60(4):922-934.

154. Laemmli UK. Cleavage of Structural Proteins during the Assembly of the Head of Bacteriophage T4. *Nature*. 1970;227(5259):680-685. doi:10.1038/227680a0

155. Pacheco BS, dos Santos MAZ, Schultze E, et al. Cytotoxic activity of fatty acids from antarctic macroalgae on the growth of human breast cancer cells. *Front Bioeng Biotechnol*. 2018;6:185.

156. Jeong H-S, Cho Y-H, Kim K-H, et al. Anti-lipoapoptotic effects of Alisma orientalis extract on non-esterified fatty acid-induced HepG2 cells. *BMC Complement Altern Med*. 2016;16(1):1-11.

157. Xu X, So J-S, Park J-G, Lee A-H. Transcriptional control of hepatic lipid metabolism by SREBP and ChREBP. In: *Seminars in Liver Disease*. Vol 33. NIH Public Access; 2013:301.

158. Iizuka K. The transcription factor carbohydrate-response element-binding protein (ChREBP): A possible link between metabolic disease and cancer. *Biochim Biophys Acta (BBA)-Molecular Basis Dis*. 2017;1863(2):474-485.

159. Sanderson M, Mazibuko SE, Joubert E, et al. Effects of fermented rooibos (Aspalathus linearis) on adipocyte differentiation. *Phytomedicine*. 2014;21(2):109-117.

160. Aghamohammadzadeh N, Niafar M, Dalir Abdolahinia E, et al. The effect of pioglitazone on weight, lipid profile and liver enzymes in type 2 diabetic patients. *Ther Adv Endocrinol Metab*. 2015;6(2):56-60.

161. Hsiao PJ, Chiou HC, Jiang HJ, Lee MY, Hsieh TJ, Kuo KK. Pioglitazone Enhances Cytosolic Lipolysis, beta-oxidation and Autophagy to Ameliorate Hepatic Steatosis. *Sci Rep*. 2017;7(1):9030. doi:10.1038/s41598-017-09702-3

162. Trösemeier J-H, Rudorf S, Loessner H, et al. Optimizing the dynamics of protein

expression. *Sci Rep*. 2019;9(1):1-15.

163. Smith GC, Turner N. FOX01 Is the Headline Akt Regulating Hepatic Glucose Metabolism. *Endocrinology*. 2017;158(8):2436-2438.

164. Mazibuko-Mbeje SE, Dludla P V, Roux C, et al. Aspalathin-enriched green rooibos extract reduces hepatic insulin resistance by modulating PI3K/AKT and AMPK pathways. *Int J Mol Sci*. 2019;20(3):633.

165. An J, Muoio DM, Shiota M, et al. Hepatic expression of malonyl-CoA decarboxylase reverses muscle, liver and whole-animal insulin resistance. *Nat Med*. 2004;10(3):268-274.

166. Chakravarthy M V, Neuschwander-Tetri BA. The metabolic basis of nonalcoholic steatohepatitis. *Endocrinol Diabetes Metab*.:e00112.

167. SIlva A., Favaro R., Furuya D., et al. Liver overexpression of GLUT2 and Slc2a2 are associated with nonalcoholic steatohepatitis in obese diabetic mice. Published 2013. https://www.easd.org/virtualmeeting/home.html#!resources/liver-overexpression-of-glut2-and-slc2a2-are-associated-with-nonalcoholic-steatohepatitis-in-obese-diabetic-mice--2

168. Lei K-J, Shelly LL, Pan C-J, Sidbury JB, Chou JY. Mutations in the glucose-6-phosphatase gene that cause glycogen storage disease type 1a. *Science (80-)*. 1993;262(5133):580-583.

169. Huang X, Liu G, Guo J, Su Z. The PI3K/AKT pathway in obesity and type 2 diabetes. *Int J Biol Sci*. 2018;14(11):1483.

170. Honma M, Sawada S, Ueno Y, et al. Selective insulin resistance with differential expressions of IRS-1 and IRS-2 in human NAFLD livers. *Int J Obes*. 2018;42(9):1544-1555.

171. Gross DN, Wan M, Birnbaum MJ. The role of FOXO in the regulation of metabolism. *Curr Diab Rep*. 2009;9(3):208-214.

172. Saltiel AR, Kahn CR. Insulin signalling and the regulation of glucose and lipid metabolism. *Nature*. 2001;414(6865):799-806.

173. Burke SJ, Batdorf HM, Burk DH, et al. db/db mice exhibit features of human type 2 diabetes that are not present in weight-matched C57BL/6J mice fed a western diet. *J Diabetes Res*. 2017;2017.

174. Berger J, Moller DE. The mechanisms of action of PPARs. *Annu Rev Med*. 2002;53(1):409-435.

175. Yan H, Meng F, Jia H, Guo X, Xu B. The identification and oxidative stress response of a zeta class glutathione S-transferase (GSTZ1) gene from Apis cerana cerana. *J Insect Physiol*. 2012;58(6):782-791.

176. Ceriello A, dello Russo P, Amstad P, Cerutti P. High glucose induces antioxidant enzymes in human endothelial cells in culture: evidence linking hyperglycemia and oxidative stress. *Diabetes*. 1996;45(4):471-477.

177. García-Ruiz I, Solís-Muñoz P, Fernández-Moreira D, Muñoz-Yagüe T, Solís-Herruzo JA. In vitro treatment of HepG2 cells with saturated fatty acids reproduces mitochondrial dysfunction found in nonalcoholic steatohepatitis. *Dis Model Mech*. 2015;8(2):183-191.

178. Jiang W, Guo M-H, Hai X. Hepatoprotective and antioxidant effects of lycopene on non-alcoholic fatty liver disease in rat. *World J Gastroenterol*. 2016;22(46):10180.

179. Flanagan L, Meyer M, Fay J, et al. Low levels of Caspase-3 predict favourable response to 5FU-based chemotherapy in advanced colorectal cancer: Caspase-3 inhibition as a therapeutic approach. *Cell Death Dis*. 2016;7(2):e2087-e2087.

9. Appendix

9.1 Ethical approval (SAMRC-ECRA REF.05/17):

ETHICS COMMITTEE FOR RESEARCH ON ANIMALS (ECRA)

29 March 2017

Miss Y Ntamo
BRIP
MEDICAL RESEARCH COUNCIL

Dear Miss Ntamo,

CERTIFICATE OF FINAL APPROVAL – REF. 05/17 "Amelioration of the longer term effects of diabetes on pancreatic beta cells and hepatotoxicity by *Aspalathus linearis* (Rooibos) in db/db mice"

The ECRA Committee reviewed your corrected Application and it was final approved.

Attached herewith please find your Certificate of Approval for the period 30 March 2017 – 31 July 2-18. Should this study period not be long enough, please write a letter to the ECRA Committee requested an extension on the study.

Should you encounter any difficulties duties your study or sudden death of the animals, please do not hesitate to inform the ECRA thereof as well as the reason for the death. You will need to submit every 6 months an interim report on the study to the ECRA Committee. The secretariat will inform you thereof in time.

Kind regards.

PROF D DU TOIT

Animal Ethics Approval Certificate

Decision of the Animal Ethics Committee for the use of living vertebrates for research, diagnostic procedures and product development

APPROVAL PERIOD: 30 March 2017 – 31 July 2018

PROJECT NUMBER:	05/17			
PROJECT TITLE:	**"Amelioration of the longer term effects of diabetes on pancreatic beta cells and hepatotoxicity by *Asapalthus linearis* (Rooibos) in db/db mice"**			
PROJECT LEADER:	Miss Yonela Ntamo			
DIVISION:	Biomedical Research and Innovation Platform (BRIP)			
CATEGORY:	Diabetes			
SPECIES OF ANIMAL:	Mouse BKS.Cg-Dock7 (m)	+/+ Lepr (db)/J	6 week old males 30gr	
NUMBER OF ANIMALS:	200			
NOT APPROVED:	n/a			
APPROVED:	29 March 2017			

PLEASE NOTE: Should the number or species of animal(s) required, or the experimental procedure(s) change, please submit a revised animal ethics clearance form to the animal ethics committee for approval before commencing with the experiment

PROF D DU TOIT **DATE** **29 March 2017**

CHAIRPERSON ANIMAL ETHICS COMMITTEE

9.2 Ethical approval (UZREC 171110-030):

UNIVERSITY OF ZULULAND
RESEARCH ETHICS COMMITTEE
(Reg No: UZREC 171110-030)

RESEARCH & INNOVATION
Website: http://www.unizulu.ac.za
Private Bag X1001
KwaDlangezwa 3886
Tel: 035 902 6731
Fax: 035 902 6222
Email: DlaminJA@unizulu.ac.za

ETHICAL CLEARANCE CERTIFICATE

Certificate Number	**UZREC 171110-030 PGM 2017/479**							
Project Title	**A STUDY OF THE PROTECTIVE EFFECTS OF AN ASPALATHIN ENRICHED GREEN EXTRACT ON EXPERIMENTALLY-INDUCED HEPATIC STEATOSIS**							
Principal Researcher/ Investigator	NT Khuboni							
Supervisor and Co-supervisor	Prof AP Kappo Dr K Gabuza		Prof C Muller Dr R Mosa					
Department	Biochemistry and Microbiology							
Faculty	SCIENCE AND AGRICULTURE							
Type of Risk	Low Risk– Data collection from animals							
Nature of Project	Honours/4th Year		Master's	x	Doctoral		Departmental	

The University of Zululand's Research Ethics Committee (UZREC) hereby gives ethical approval in respect of the undertakings contained in the above-mentioned project. The Researcher may therefore commence with data collection as from the date of this Certificate, using the certificate number indicated above.

Special conditions:

(1) This certificate is valid for 3 years from the date of issue.
(2) Principal researcher must provide an annual report to the UZREC in the prescribed format [due date-30 April 2018]
(3) Principal researcher must submit a report at the end of project in respect of ethical compliance.
(4) The UZREC must be informed immediately of any material change in the conditions or undertakings mentioned in the documents that were presented to the meeting.

The UZREC wishes the researcher well in conducting research.

Professor Gideon De Wet
Chairperson: University Research Ethics Committee
Deputy Vice-Chancellor: Research & Innovation
08 March 2018

CHAIRPERSON
UNIVERSITY OF ZULULAND RESEARCH
ETHICS COMMITTEE (UZREC)
REG NO: UZREC 171110-30
09 -03- 2018
RESEARCH & INNOVATION OFFICE

9.3 Ethical approval (ACU-2020-14382):

UNIVERSITEIT
STELLENBOSCH
UNIVERSITY

Animal Tissue Use Approval

30 April 2020

PI: Mr Thendo Mabuda

REC: ACU Reference #: ACU-2020-14382

Title: Effect of rooibos treatment on inflammatory and oxidative stress genes in in vitro and in vivo models of NAFLD.

Dear Mr Thendo Mabuda

Your application with reference number #ACU-2020-14382, was reviewed on 29 April 2020 by the Research Ethics Committee: Animal Care and Use via committee review procedures and was approved. Please note that this clearance is valid for a period of five years. A new application must be submitted when the source of the material changes.

Applicants are reminded that they are expected to comply with accepted standards for the use of animals in research and teaching as reflected in the South African National Standards 10386: 2008. The SANS 10386: 2008 document is available on the Division for Research Developments website www.sun.ac.za/research.

As provided for in the Veterinary and Para-Veterinary Professions Act, 1982. It is the principal investigator's responsibility to ensure that all study participants are registered with or have been authorised by the South African Veterinary Council (SAVC) to perform the procedures on animals, or will be performing the procedures under the direct and continuous supervision of a SAVC-registered veterinary professional or SAVC-registered para-veterinary professional, who are acting within the scope of practice for their profession.

Please remember to use your REC: ACU reference number: # ACU-2020-14382 on any documents or correspondence with the REC: ACU concerning your research protocol.

If you have any questions or need further help, please contact the REC: ACU office at 021 808 9003.

Visit the Division for Research Developments website www.sun.ac.za/research for documentation on REC: ACU policy and procedures.

Sincerely,

Mr Winston Beukes

Coordinator: Research Ethics (Animal Care and Use)

9.4 List of materials

Table 9.1 List of materials and suppliers.

Product	**Supplier/Company**
(ca 12%) Aspalathin-rich Afriplex GRT	Afriplex, Paarl, Western Cape, RSA
1.5ml centrifuge tubes	Sigma-Aldrich, Saint Louis, USA
10x Tris/Glycine/SDS	Bio-Rad, Berkeley, California, USA
12% Mini-PROTEAN® TGX™ Stain-free FastCast Acrylamide kit	Bio-Rad, Berkeley, California, USA
15ml Centrifuge tubes	NEST Biotechnology Co. LTD, Jiangsu, China
2ml Cryo-vials	Corning, MA, USA
2ml Safe-lock tubes	Eppendorf, Hamburg, Germany
50ml Centrifuge tubes	NEST Biotechnology Co. LTD, Jiangsu, China
5x TransBlot® Turbo Transfer Buffer, RTA Transfer Kit, LF PVDF	Bio-Rad, Berkeley, California, USA
Bovine serum albumin (BSA) – fatty-acid free	Capricorn scientific Auf der Lette 13A, Ebsdorfergrund, Germany
C3A human liver cells	American Type Culture Collection, Manassas, USA
Calcium chloride ($CaCl_2$)	Sigma-Aldrich, Saint Louis, USA
Carbon dioxide (CO_2)	Air Products, Centurion, Gauteng, RSA
Cell counting chamber slides	Life Technologies Corporation, Carlsbad, CA, USA
Citric acid monohydrate	Sigma-Aldrich, Saint Louis, USA
Clarity™ Western C ECL Substrate	Bio-Rad, Berkeley, California, USA
Corning® 500ml Bottle Top Vacuum Filter	Corning Inc, New York, USA
Crystal violet	Merck, Whitehouse Station, NJ, USA
Dexamethasone	Sigma-Aldrich, Saint Louis, USA
Dimethyl Sulfoxide (DMSO)	Sigma-Aldrich, Saint Louis, USA
Dithiothreitol	Sigma-Aldrich, Saint Louis, USA
Dulbecco's phosphate saline buffer (DPBS)	Lonza, Walkersville, MD, USA
Eagle's Minimum Essential Medium (EMEM)	Lonza, Walkersville, MD, USA
Ethyl alcohol	Sigma-Aldrich, Saint Louis, USA
Ethylenediaminetetraacetic acid disodium salt dihydrate (EDTA)	Sigma-Aldrich, Saint Louis, USA
Foetal bovine serum (FBS)	Lonza, Walkersville, MD, USA
Glass Pasteur Pipettes	Lasec, Marienfeld, Germany
Glucose Standard 1	Wako Chemicals, Osaka, Japan
Glucose Standard 2	Wako Chemicals, Osaka, Japan
Horse-serum	Highveld biological, Johannesburg, Gauteng, RSA
Invitrogen™ MTT (3-(4,5-Dimethylthiazol-2-yl)-2,5-Diphenyltetrazolium Bromide)	Thermo Fisher Scientific™, Johannesburg, Gauteng, RSA
Isopropanol	Sigma-Aldrich, Saint Louis, USA
L-Glutamine	Lonza, Walkersville, MD, USA
Low fat free milk powder	Clover, Johannesburg, Gauteng, RSA

LumiGLO Chemiluminescent Substrate Kit	Cell Signaling Technology, Boston, USA
Magnesium chloride (MgCl2)	Sigma-Aldrich, Saint Louis, USA
Methanol	VWR Chemicals, Fontenay-sous-Bois, France
Millex-GP syringe filter unit	Millipore PES membrane, Merck
NON-CELLBIND -96 well plates	Corning, MA, USA
NON-CELLBIND -6 well plates	Corning, MA, USA
Oil O Red	Sigma-Aldrich, Saint Louis, USA
p-Nitrophenyl phosphate disodium salt hexahydrate	Sigma-Aldrich, Saint Louis, USA
Pierce™ BCA Protein Assay Kit	Thermo Fisher Scientific™, Johannesburg, Gauteng, RSA
Ponceau S Stain	Sigma-Aldrich, Saint Louis, USA
Potassium Chloride (KCl)	Sigma-Aldrich, Saint Louis, USA
Precision Protein™ StrepTactin-HRP Conjugate	Bio-Rad, Berkeley, California, USA
Protease Inhibitors	Roche, Basel, Switzerland
Restore Plus Western blot stripping buffer	Thermo Fisher Scientific™, Johannesburg, Gauteng, RSA
Scintillation vials	CJ Labs, Johannesburg, Gauteng, RSA
Serological pipettes -2ml	Corning, MA, USA
Serological pipettes-10ml	Corning, MA, USA
Serological pipettes-25ml	Corning, MA, USA
Serological pipettes-50ml	Corning, MA, USA
Sodium bicarbonate (NaHCO3)	Sigma-Aldrich, Saint Louis, USA
Sodium chloride (NaCl)	Sigma-Aldrich, Saint Louis, USA
Sodium citrate tribasic dihydrate	Sigma-Aldrich, Saint Louis, USA
Sodium dodecyl sulphate (SDS)	Sigma-Aldrich, Saint Louis, USA
Sodium hydroxide (NaOH)	Sigma-Aldrich, Saint Louis, USA
Stainless steel beads	Qiagen, Hilden, Germany
Sterile TC water	Lonza, Walkersville, MD, USA
T75 (75cm^2) Flasks	Greiner bio-one, Frickenhausen, Germany
TissueLyser	Qiagen, Hilden, Germany
Trizma® base	Sigma-Aldrich, Saint Louis, USA
Trypan blue	Invitrogen, Carlsbad, CA, USA
Trypsin-versene	Lonza, Walkersville, MD, USA
Tween-20	Sigma-Aldrich, Saint Louis, USA
β-mercaptoethanol	Sigma-Aldrich, Saint Louis, USA

9.5 Preparation of buffers and reagents:

1 x Transfer buffer for Semi-dry Western blot: A 1 x transfer buffer was prepared by mixing 200 ml of 5 x TransBlot® Turbo Transfer Buffer with 600 ml distilled water and 200 ml absolute ethanol.

1 x Tris-buffered saline Tween-20 (TBST): A 1 L solution of TBST was prepared by mixing 100 ml 10 x TBS with 900 ml distilled water and 1 ml Tween-20. The buffer was kept at 4°C.

10 x Tris-buffered saline (TBS) pH 7.6: To make 2 L of a 10 x TBS buffer, 48.44 g of 2-Amino-2-(hydroxymethyl)-1,3-propanediol (Trizma® base) (Mw 121.14 g/mol) and 160.12 g of NaCl (Mw 58.44 g/mol) were dissolved in 2000 ml distilled water. The pH was adjusted to 7.6 using concentrated hydrochloric acid. The buffer was kept at 4 °C.

Crystal Violet solution: A 2 % (w/v) crystal violet stock solution was prepared by dissolving 2 g of crystal violet powder with 100 ml distilled water. Thereafter, a 0.5 % (v/v) working solution was prepared by mixing 250 µl of the 2 % stock solution with 50 ml distilled water.

Laemmli Buffer: A 2 x Laemmli Buffer is composed of 4 % SDS, 20 % glycerol, 10 % 2-mercaptoethanol, 0.004 % bromphenol blue and 0.125 M Tris HCl at pH 6.8. The buffer was kept at 23 °C.

MTT Reagent: A 2 mg/ml MTT reagent was prepared by dissolving 90 mg MTT in 45 ml PBS. The reagent was kept at 4 °C.

Oil Red O (ORO) solution: A 1 % (w/v) ORO (Sigma-Aldrich, Saint Louis, USA) stock solution was prepared by dissolving 1 g ORO powder in 100 ml isopropanol. From the 1 % stock solution a 0,7 % (v/v) ORO working solution was prepared by mixing 7 ml ORO stock solution with 3 ml distilled water. The working solution was prepared fresh on the day of the assay and filtered using filter paper (pore size: 11 µl)

Sorensons Buffer: Glycine (0,1 M) and NaCl (0,1 M) were dissolved in 100 ml cell culture water and the pH set to 10.5 using 1 M NaOH (Mw 40.00 g/mol). The buffer was kept at 4°C.

Table 9.2 Preparation of RIPA buffer.

Reagents	**Final Volume**
50 mM Tris (pH7.5)	2.5 µl
1 mM DTT	0.008 g
50 mM NaF	0.104 g
100 µM Na_3VO_4	500 µl
1% NP40	500 µl
1% Triton X 144	500 µl
25 µg/ml RNase	125 µl
Protease inhibitor tablets	2 tablets
Phosho inhibiting tablets	5 tablets

Table 9.3 Preparation of 1.5 mm Bio-Rad (Hercules, USA) TGX Stain-free FastCast Acrylamide gel.

	Stacking Gel				**Resolving Gel**			
	x2	**x3**	**x4**	**x6**	**x2**	**x3**	**x4**	**x6**
Gel %	**4%**				**12%**			
Solution A	2 ml	3 ml	4 ml	6 ml	6 ml	9 ml	12 ml	18 ml
Solution B	2 ml	3 ml	4 ml	6 ml	6 ml	9 ml	12 ml	18 ml
10% APS	20 µl	30 µl	40 µl	60 µl	60 µl	90 µl	120 µl	180 µl
TEMED	4 µl	6 µl	8 µl	12 µl	6 µl	9 µl	12 µl	18 µl
Total Volume	4 ml	6 ml	8 ml	12 ml	12 ml	18 ml	24 ml	36 ml

9.6 *In vitro* dose-dependent response to pioglitazone

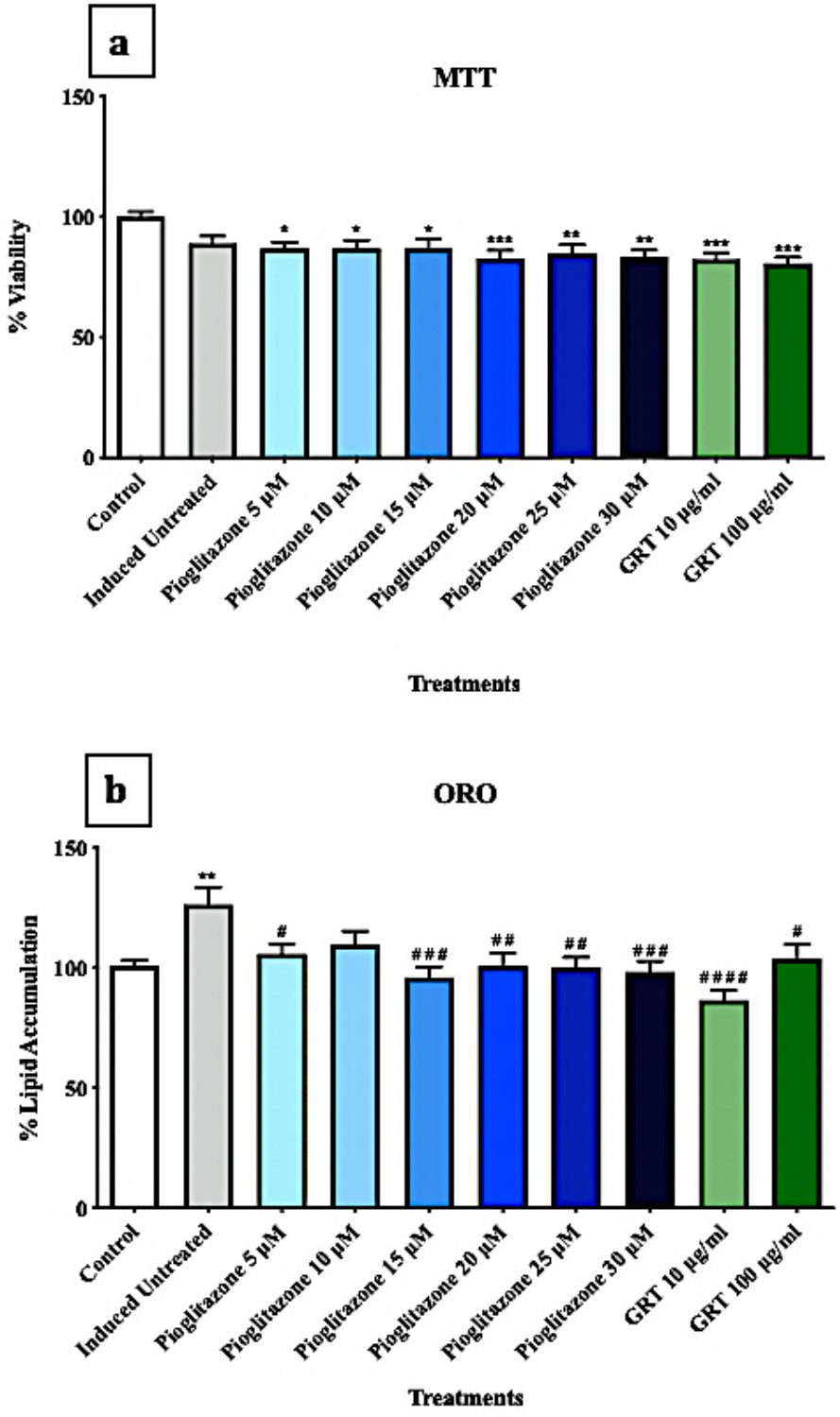

Figure 9.1 (**a**) MTT and (**b**) ORO assay showing the effects of steatosis induction [1mM oleic acid] along with the effects of anti-steatotic treatment using a range of pioglitazone treatments or Afriplex GRT (GRT), on cell viability and lipid accumulation. Data represents Mean ± SEM (n = 3), where *P < 0.05, **P < 0.01 and ***P < 0.001, when compared to the normal control; $^{\#}$P < 0.05, $^{\#\#}$P < 0.01, $^{\#\#\#}$P < 0.001 and $^{\#\#\#\#}$P < 0.0001 when compared to the induced control respectively.

Treatment with pioglitazone showed a significant decrease in mitochondrial activity in a dose-dependent manner when compared to the normal control, with the exception of pioglitazone at 20 µM. The data, although significant, showed no cytotoxicity with any treatment dose and this is evident as the mitochondrial activity of the C3A cells was above 70% throughout the various treatment concentrations. The same was observed when the cells were treated with Afriplex GRT.

An Oil red O assay (Figure 8.1 (**b**)), expectedly showed a significant increase when comparing the normal control to cells which were treated with just 1 mM oleic acid (induced control). Subsequent treatment with pioglitazone showed a significant decrease in lipid accumulation when compared to the induced control, with the exception of pioglitazone at 10 µM. Interestingly lipid accumulation was most substantially reduced when the cells were treated with pioglitazone at 15 and 30 µM. Treatment with Afriplex GRT also showed a significant reduction, with GRT 10 µg/ml the more significant.

9.7 Permission to use copyrighted information in the thesis

Copyright Clearance Center Marketplace™

Springer Nature BV - License Terms and Conditions

This is a License Agreement between Thendo Mabuda ("You") and Springer Nature BV ("Publisher") provided by Copyright Clearance Center ("CCC"). The license consists of your order details, the terms and conditions provided by Springer Nature BV, and the CCC terms and conditions.

All payments must be made in full to CCC.

Order Date	22-Jun-2020	Type of Use	Republish in a thesis/dissertation
Order license ID	1043428-1		
ISSN	1476-4687	Publisher	Nature Publishing Group
		Portion	Image/photo/illustration

LICENSED CONTENT

Publication Title	Nature	Publication Type	e-Journal
Article Title	Rooibos tea profits will be shared with Indigenous communities in landmark agreement.	Start Page	19
		End Page	20
		Issue	7781
Date	01/01/1995	Volume	575
Language	English	URL	http://www.nature.com/nature/
Country	United States of America		
Rightsholder	Springer Nature BV		

REQUEST DETAILS

Portion Type	Image/photo/illustration	Distribution	Other territories and/or countries
Number of images / photos / illustrations	1	Enter territories/countries	Republic of South Africa
Format (select all that apply)	Print, Electronic	Translation	Original language of publication
Who will republish the content?	Academic institution	Copies for the disabled?	No
Duration of Use	Life of current edition	Minor editing privileges?	No
Lifetime Unit Quantity	Up to 19,999	Incidental promotional use?	No
Rights Requested	Main product	Currency	USD

NEW WORK DETAILS

Title	Effect of rooibos treatment on inflammatory and oxidative stress genes in in vitro and in vivo models of NAFLD	Institution name	Stellenbosch University
		Expected presentation date	2020-12-01

WOLTERS KLUWER HEALTH, INC. LICENSE
TERMS AND CONDITIONS

Dec 08, 2020

This Agreement between Stellenbosch University / SAMRC -- Thendo Mabuda ("You") and Wolters Kluwer Health, Inc. ("Wolters Kluwer Health, Inc.") consists of your license details and the terms and conditions provided by Wolters Kluwer Health, Inc. and Copyright Clearance Center.

The publisher has provided special terms related to this request that can be found at the end of the Publisher's Terms and Conditions.

License Number	4860420619288
License date	Jul 01, 2020
Licensed Content Publisher	Wolters Kluwer Health, Inc.
Licensed Content Publication	ATVB
Licensed Content Title	Ectopic Fat, Insulin Resistance, and Nonalcoholic Fatty Liver Disease
Licensed Content Author	Christopher D. Byrne, Giovanni Targher
Licensed Content Date	Apr 17, 2014
Licensed Content Volume	34
Licensed Content Issue	6

ELSEVIER LICENSE
TERMS AND CONDITIONS

Dec 08, 2020

This Agreement between Stellenbosch University / SAMRC -- Thendo Mabuda ("You") and Elsevier ("Elsevier") consists of your license details and the terms and conditions provided by Elsevier and Copyright Clearance Center.

License Number	4851310327626
License date	Jun 17, 2020
Licensed Content Publisher	Elsevier
Licensed Content Publication	Trends in Endocrinology & Metabolism
Licensed Content Title	Insulin resistance, inflammation, and non-alcoholic fatty liver disease
Licensed Content Author	Herbert Tilg,Alexander R. Moschen
Licensed Content Date	Dec 1, 2008
Licensed Content Volume	19
Licensed Content Issue	10
Licensed Content Pages	9
Start Page	371

ELSEVIER LICENSE
TERMS AND CONDITIONS

Dec 08, 2020

This Agreement between Stellenbosch University / SAMRC -- Thendo Mabuda ("You") and Elsevier ("Elsevier") consists of your license details and the terms and conditions provided by Elsevier and Copyright Clearance Center.

License Number	4851301391825
License date	Jun 17, 2020
Licensed Content Publisher	Elsevier
Licensed Content Publication	The Lancet
Licensed Content Title	Non-alcoholic steatohepatitis: another disease of affluence
Licensed Content Author	*Oliver James,Christopher Day
Licensed Content Date	May 15, 1999
Licensed Content Volume	353
Licensed Content Issue	9165
Licensed Content Pages	3
Start Page	1634

JOHN WILEY AND SONS LICENSE
TERMS AND CONDITIONS

Dec 08, 2020

This Agreement between Stellenbosch University / SAMRC -- Thendo Mabuda ("You") and John Wiley and Sons ("John Wiley and Sons") consists of your license details and the terms and conditions provided by John Wiley and Sons and Copyright Clearance Center.

License Number	4851301016954
License date	Jun 17, 2020
Licensed Content Publisher	John Wiley and Sons
Licensed Content Publication	Hepatology
Licensed Content Title	The diagnosis and management of nonalcoholic fatty liver disease: Practice guidance from the American Association for the Study of Liver Diseases
Licensed Content Author	Arun J. Sanyal, Elizabeth M. Brunt, Stephen A. Harrison, et al
Licensed Content Date	Sep 29, 2017
Licensed Content Volume	67

9.8 Turnitin Report

Thendo Mabuda

ORIGINALITY REPORT

23%	17%	13%	8%
SIMILARITY INDEX	INTERNET SOURCES	PUBLICATIONS	STUDENT PAPERS

PRIMARY SOURCES

1	Submitted to University of the Western Cape Student Paper	3%
2	worldwidescience.org Internet Source	1%
3	www.mdpi.com Internet Source	1%
4	hdl.handle.net Internet Source	1%
5	Submitted to University of Zululand Student Paper	1%
6	www.frontiersin.org Internet Source	1%
7	ilc-congress.eu Internet Source	1%
8	www.laser-therapy.us Internet Source	1%
9	www.physoc.org Internet Source	<1%